BEDSIDE VISUAL IMAGE TECHNOLOGIES FOR RESPIRATORY AND CIRCULATORY MANAGEMENT IN INTENSIVE CARE SETTINGS

EDITED BY: Huaiwu He, Zhanqi Zhao, Knut Moeller and Yun Long

PUBLISHED IN: Frontiers in Medicine

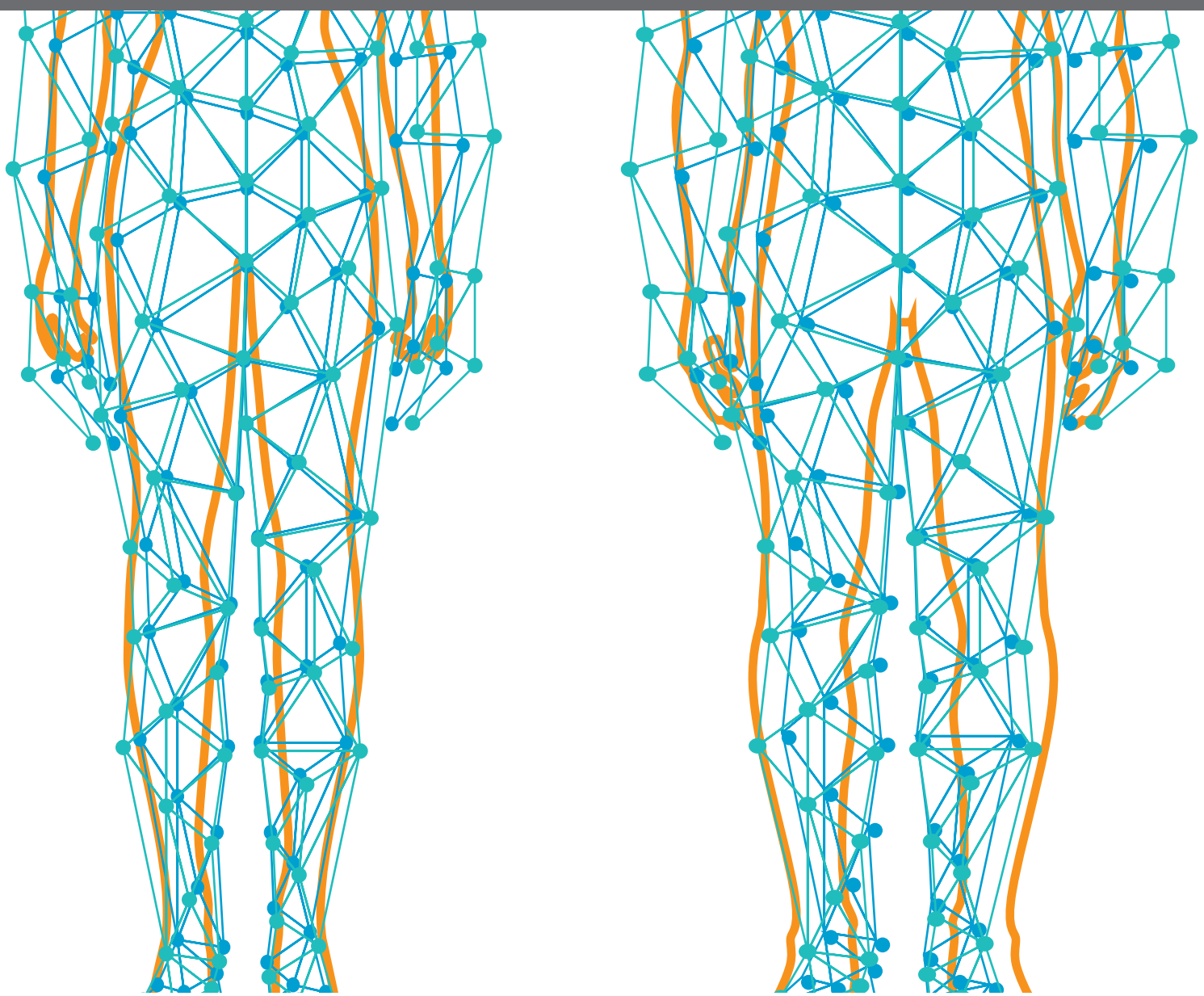

frontiers Research Topics

frontiers

ISSN 1664-8714
ISBN 978-2-88976-772-4
DOI 10.3389/978-2-88976-772-4

About Frontiers

Frontiers is more than just an open-access publisher of scholarly articles: it is a pioneering approach to the world of academia, radically improving the way scholarly research is managed. The grand vision of Frontiers is a world where all people have an equal opportunity to seek, share and generate knowledge. Frontiers provides immediate and permanent online open access to all its publications, but this alone is not enough to realize our grand goals.

Frontiers Journal Series

The Frontiers Journal Series is a multi-tier and interdisciplinary set of open-access, online journals, promising a paradigm shift from the current review, selection and dissemination processes in academic publishing. All Frontiers journals are driven by researchers for researchers; therefore, they constitute a service to the scholarly community. At the same time, the Frontiers Journal Series operates on a revolutionary invention, the tiered publishing system, initially addressing specific communities of scholars, and gradually climbing up to broader public understanding, thus serving the interests of the lay society, too.

Dedication to Quality

Each Frontiers article is a landmark of the highest quality, thanks to genuinely collaborative interactions between authors and review editors, who include some of the world's best academicians. Research must be certified by peers before entering a stream of knowledge that may eventually reach the public - and shape society; therefore, Frontiers only applies the most rigorous and unbiased reviews.
Frontiers revolutionizes research publishing by freely delivering the most outstanding research, evaluated with no bias from both the academic and social point of view. By applying the most advanced information technologies, Frontiers is catapulting scholarly publishing into a new generation.

What are Frontiers Research Topics?

Frontiers Research Topics are very popular trademarks of the Frontiers Journals Series: they are collections of at least ten articles, all centered on a particular subject. With their unique mix of varied contributions from Original Research to Review Articles, Frontiers Research Topics unify the most influential researchers, the latest key findings and historical advances in a hot research area! Find out more on how to host your own Frontiers Research Topic or contribute to one as an author by contacting the Frontiers Editorial Office: frontiersin.org/about/contact

BEDSIDE VISUAL IMAGE TECHNOLOGIES FOR RESPIRATORY AND CIRCULATORY MANAGEMENT IN INTENSIVE CARE SETTINGS

Topic Editors:
Huaiwu He, Peking Union Medical College Hospital (CAMS), China
Zhanqi Zhao, Furtwangen University, Germany
Knut Moeller, Furtwangen University, Germany
Yun Long, Peking Union Medical College Hospital (CAMS), China

Citation: He, H., Zhao, Z., Moeller, K., Long, Y., eds. (2022). Bedside Visual Image Technologies for Respiratory and Circulatory Management in Intensive Care Settings. Lausanne: Frontiers Media SA. doi: 10.3389/978-2-88976-772-4

Table of Contents

frontiers | Frontiers in Medicine

TYPE Editorial
PUBLISHED 18 July 2022
DOI 10.3389/fmed.2022.973679

OPEN ACCESS

EDITED AND REVIEWED BY
Zhongheng Zhang,
Sir Run Run Shaw Hospital, China

*CORRESPONDENCE
Huaiwu He
hehuaiwu@pumch.cn
Zhanqi Zhao
zhanqi.zhao@hs-furtwangen.de

SPECIALTY SECTION
This article was submitted to Intensive Care Medicine and Anesthesiology, a section of the journal Frontiers in Medicine

RECEIVED 20 June 2022
ACCEPTED 04 July 2022
PUBLISHED 18 July 2022

CITATION
He H, Long Y, Möller K and Zhao Z (2022) Editorial: Bedside visual image technologies for respiratory and circulatory management in intensive care settings. *Front. Med.* 9:973679. doi: 10.3389/fmed.2022.973679

Editorial: Bedside visual image technologies for respiratory and circulatory management in intensive care settings

Huaiwu He[1]*, Yun Long[1], Knut Möller[2] and Zhanqi Zhao[2,3]*

[1]State Key Laboratory of Complex Severe and Rare Disease, Department of Critical Care Medicine, Peking Union Medical College Hospital, Peking Union Medical College, Chinese Academy of Medical Sciences, Beijing, China, [2]Institute of Technical Medicine, Furtwangen University, Villingen-Schwenningen, Germany, [3]Department of Biomedical Engineering, Fourth Military Medical University, Xi'an, China

KEYWORDS

critical EIT, critical ultrasound, lung ventilation, lung perfusion, respiratory and circulatory management

Editorial on the Research Topic
Bedside Visual Image Technologies for Respiratory and Circulatory Management in Intensive Care Settings

Cardiovascular and pulmonary systems are the major systems that suffer from critical diseases and injuries among patients. Accessible and accurate tools providing diagnosis and monitoring information are warranted to assist individualized therapy and decision making. Up-to-date, novel imaging techniques emerge thanks to the advancement in the field, including novel imaging modalities that have not been widely used in clinical practice. Bedside visual image technologies, including electrical impedance tomography (EIT) for ventilation and perfusion, and critical care ultrasound for alveolar atelectasis and cardiac output assessments, have gained great attentions in ICU/operating theater. In the current Research Topic, we are happy to collect one review, two case reports, one simulation, and five clinical studies investigated in more than 250 subjects to update our knowledge in the field.

Interactions among cardiovascular, pulmonary and other systems are often complicated. Many diseases could lead to multiple-organ failure. One example is hepatopulmonary syndrome, which causes pulmonary vascular dysfunction secondary to liver cirrhosis (1). Evidence of intrapulmonary vascular dilatation is one of the diagnostic criteria for hepatopulmonary syndrome. Therefore, imaging examination could be one of the critical measures to identify pulmonary vasodilatation. In the current Research Topic, Luo and Du reviewed the recent advance diagnostic imaging techniques for hepatopulmonary syndrome, including ultrasound, dynamic pulmonary perfusion imaging, pulmonary angiography, and computed tomography. They discussed the pros and cons of the current techniques and pointed out the need and room for further development of imaging techniques.

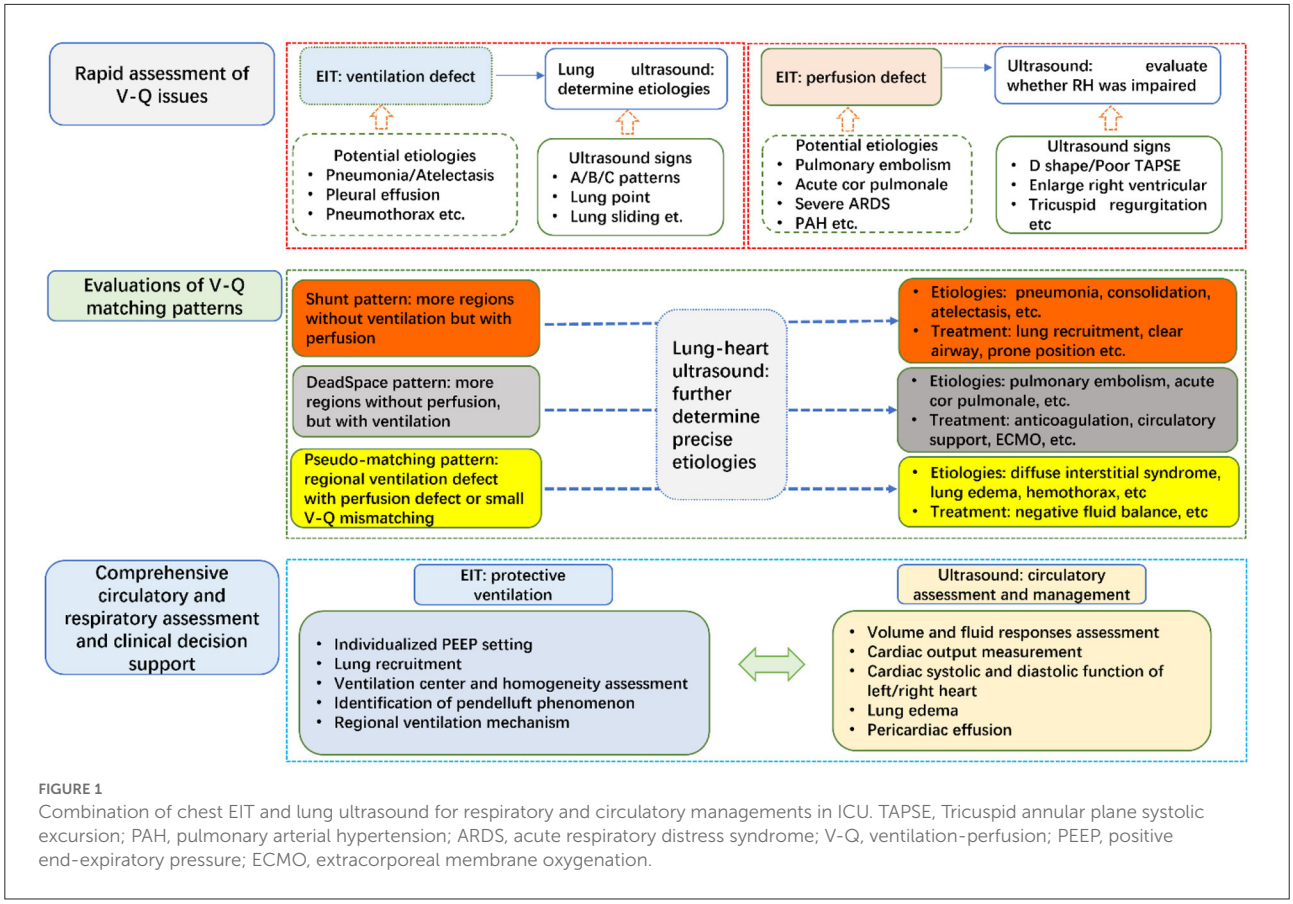

FIGURE 1
Combination of chest EIT and lung ultrasound for respiratory and circulatory managements in ICU. TAPSE, Tricuspid annular plane systolic excursion; PAH, pulmonary arterial hypertension; ARDS, acute respiratory distress syndrome; V-Q, ventilation-perfusion; PEEP, positive end-expiratory pressure; ECMO, extracorporeal membrane oxygenation.

In addition to the multiple-organ interactions, treatment of cardiopulmonary diseases may introduce some psychological impairments (2). Some studies indicated that revisiting the ICU treatment period could be helpful *via* providing patients with necessary information (3). Vlake et al. demonstrated in a patient recovered from COVID-19 that virtual reality intervention provided a valuable adjunct to improve patient's psychological status. The development and application of the virtual reality module require an interdisciplinary cooperation. To increase the effectiveness, the module might need to be constructed individually to meet the experience of the patient groups. Therefore, it is a promising field that requires further investigation.

The rest of the papers in the Research Topic are either ultrasound or EIT related, which implicates rapid development in these two imaging modalities. The use of medical ultrasound for cardiovascular system can date back to 1960s (4). To date, ultrasound is used as a diagnostic tool as well as guiding tool for certain maneuvers. To evaluate the right ventricle filling state, Zhao et al. used echocardiography to dynamically monitor central venous pressure and the size of right ventricle. They were able to clarify the correlation between left ventricle stroke volume and negative fluid balance in 71 patients with elevated central venous pressure *via* comparing hemodynamic and echo parameters at baseline and after negative fluid balance. Ultrasound-guided catheterization has been used for a decade but the success rate may depend on arterial depth (5). Tian et al. retrospectively analyzed 119 patients and demonstrated a potential correlation between first-attempt success and arterial depth.

EIT is a novel non-invasive bedside imaging modality (6). EIT can be used to monitor the ventilation distributions during the entire ventilation support period. A recently important milestone is the evidence from two randomized-controlled trials that EIT-guided positive end-expiratory pressure (PEEP) settings may improve outcomes (length of hospital stay, mortality etc.) in patients with acute respiratory distress syndrome (ARDS) (7, 8). Li et al. evaluated the possibility to predict weaning outcome in patients with delayed upper abdominal surgery. Another team tested the ability of EIT to predict outcome of high flow nasal cannula therapy. These studies broadened the use of EIT to support the respiratory management in ICU. Lung perfusion assessed with EIT helps physicians to understand the ventilation-perfusion matching status and identify the potential reasons for respiratory failure (9). Hypertonic saline bolus is injected *via* central venous catheter to augment the impedance signal. Wang et al. shared their experience in managing a patient with high-risk pulmonary

embolism. Not only adult patients can benefit from EIT. Ren et al. compared PEEP titration with global and regional compliance calculated with EIT data in pediatric ARDS. We believe more and more EIT applications in pediatric patients may be published when the device manufactures provide EIT for such patient group. Various requirements need to be considered for different applications and different patient groups, such as electrode size, position, noise suppression, baseline drift and moving artifacts. Yang et al. presented mathematical method to overcome some of the issues during practical EIT measurements. Although the effectiveness was only validated in limited patient data but the results were promising.

Although medical ultrasound has been reported since several decades, due to the lack of bedside tools, lung ultrasound became one of the hot topics in recent years (10, 11). Lung and heart ultrasound provides different information compared to EIT: ultrasound could provide morphology information of cardiopulmonary lesions, cardiac systolic and diastolic function, special signs of etiologies, whereas EIT could make a rapid functional assessment of regional lung ventilation, perfusion and the corresponding matching. Development of personalized medicine and clinical decision may benefit from the information of both bedside techniques. In clinical practice, we propose to combine these two techniques to manage patients with cardiopulmonary dysfunctions (Figure 1). By combining EIT and ultrasound, we can make a holistic management for the circulatory and respiratory failure. Further studies are warranted to examine whether the proposed workflow can improve patient outcomes.

Author contributions

HH and ZZ drafted the manuscript. YL and KM critically revised the manuscript. All authors have approved the final version.

Conflict of interest

The authors declare that the research was conducted in the absence of any commercial or financial relationships that could be construed as a potential conflict of interest.

Publisher's note

References

1. Kennedy TC, Knudson RJ. Exercise-aggravated hypoxemia and orthodeoxia in cirrhosis. *Chest.* (1977) 72:305–9. doi: 10.1378/chest.72.3.305

2. Bienvenu OJ, Friedman LA, Colantuoni E, Dinglas VD, Sepulveda KA, et al. Psychiatric symptoms after acute respiratory distress syndrome: a 5-year longitudinal study. *Intensive Care Med.* (2017) 44:38–47. doi: 10.1007/s00134-017-5009-4

3. Vlake JH, van Genderen ME, Schut A, Verkade M, Wils E-J, et al. (2020) Patients suffering from psychological impairments following critical illness are in need of information. *J Intensive Care* 8. doi: 10.1186/s40560-019-0422-0

4. Gramiak R, Shah PM. Echocardiography of the aortic root. *Invest Radiol.* (1968) 3:356–66. doi: 10.1097/00004424-196809000-00011

5. Nakayama Y, Nakajima Y, Sessler DI, Ishii S, Shibasaki M, et al. A novel method for ultrasound-guided radial arterial catheterization in pediatric patients. *Anesthesia Analgesia.* (2014) 118:1019–26. doi: 10.1213/ANE.0000000000000164

6. Frerichs I, Amato MB, van Kaam AH, Tingay DG, Zhao Z, et al. Chest electrical impedance tomography examination, data analysis, terminology, clinical use and recommendations: consensus statement of the TRanslational EIT developmeNt stuDy group. *Thorax.* (2017) 72:83–93. doi: 10.1136/thoraxjnl-2016-208357

7. He H, Chi Y, Yang Y, Yuan S, Long Y, et al. Early individualized positive end-expiratory pressure guided by electrical impedance tomography in acute respiratory distress syndrome: a randomized controlled clinical trial. *Crit Care.* (2021) 25:230. doi: 10.1186/s13054-021-03645-y

8. Hsu HJ, Chang HT, Zhao Z, Wang PH, Zhang JH, et al. Positive end-expiratory pressure titration with electrical impedance tomography pressure-volume curve: a randomized trial in moderate to severe ARDS. *Physiol Meas.* (2021) 42:014002. doi: 10.1088/1361-6579/abd679

9. He H, Chi Y, Long Y, Yuan S, Zhang R, et al. Three broad classifications of acute respiratory failure etiologies based on regional ventilation and perfusion by electrical impedance tomography: a hypothesis-generating study. *Ann Intensive Care.* (2021) 11:134. doi: 10.1186/s13613-021-00921-6

10. Blanco PA, Cianciulli TF. Pulmonary edema assessed by ultrasound: impact in cardiology and intensive care practice. *Echocardiography.* (2016) 33:778–87. doi: 10.1111/echo.13182

11. Brogi E, Gargani L, Bignami E, Barbariol F, Marra A, et al. Thoracic ultrasound for pleural effusion in the intensive care unit: a narrative review from diagnosis to treatment. *Crit Care.* (2017) 21:325. doi: 10.1186/s13054-017-1897-5

frontiers in Medicine

BRIEF RESEARCH REPORT
published: 05 February 2021
doi: 10.3389/fmed.2020.629086

Intensive Care Unit-Specific Virtual Reality for Psychological Recovery After ICU Treatment for COVID-19; A Brief Case Report

Johan H. Vlake[1,2], *Jasper van Bommel*[1], *Merel E. Hellemons*[3], *Evert-Jan Wils*[2], *Diederik Gommers*[1] *and Michel E. van Genderen*[1,2]*

[1] Department of Intensive Care, Erasmus MC, Rotterdam, Netherlands, [2] Department of Intensive Care, Franciscus Gasthuis & Vlietland, Rotterdam, Netherlands, [3] Department of Pulmonology, Erasmus MC, Rotterdam, Netherlands

A substantial number of ICU survivors are expected due to the SARS-CoV-2 outbreak, who are at risk for psychological impairments, such as post-traumatic stress disorder (PTSD), anxiety, and depression. We designed a COVID-19 intensive care unit-specific virtual reality (ICU-VR) intervention and tested it on one of our COVID-19 patients. The impact of event scale-revised and the hospital anxiety and depression scale showed that this patient suffered from PTSD, anxiety, and depression on the day of the intervention. One week after receiving ICU-VR, levels of PTSD, anxiety and depression had normalized, and stayed normalized until 6 months after discharge. In conclusion, innovative technologies, such as VR, have the potential to improve psychological rehabilitation, and should therefore be considered by clinicians for the treatment of ICU-related psychological sequelae after COVID-19.

Keywords: COVID-19, post-intensive care syndrome, critical care, virtual reality, post-traumatic stress disorder, anxiety, depression

OPEN ACCESS

Edited by:
Marcelo Arruda Nakazone, Faculty of Medicine of São José Do Rio Preto, Brazil

Reviewed by:
Marco Di Nicola, Catholic University of the Sacred Heart, Italy
Oscar Joseph Bienvenu, Johns Hopkins Medicine, United States
Leslie Hoffman, University of Pittsburgh, United States

***Correspondence:**
Michel E. van Genderen
m.vangenderen@erasmusmc.nl

Specialty section:
This article was submitted to Intensive Care Medicine and Anesthesiology, a section of the journal Frontiers in Medicine

Received: *13 November 2020*
Accepted: *29 December 2020*
Published: *05 February 2021*

Citation:
Vlake JH, van Bommel J, Hellemons ME, Wils E-J, Gommers D and van Genderen ME (2021) Intensive Care Unit-Specific Virtual Reality for Psychological Recovery After ICU Treatment for COVID-19; A Brief Case Report. Front. Med. 7:629086. doi: 10.3389/fmed.2020.629086

INTRODUCTION

In December 2019, a novel coronavirus, SARS-CoV-2, was first found in Wuhan, China, and rapidly spread around the world. The outbreak has officially been declared a pandemic by the World Health Organization in March 2020 (1). ICU-admission rates were reported as high as 16% (2). Because a majority of patients treated in the ICU for COVID-19 survive (survival rate in our ICU: 76%), a large group of ICU survivors can be anticipated.

One-third of general ICU survivors develop psychological impairments, such as post-traumatic stress disorder (PTSD), anxiety, and depression, due to their ICU stay (3, 4). These impairments are part of the post-intensive care syndrome (PICS), and cause a decrease in health-related quality of life and a patient's ability to return to their former life. Known risk factors for these impairments are prolonged mechanical ventilation, benzodiazepines, and a prolonged ICU stay (5). These factors were all present during COVID-19 ICU treatment, and clinicians must therefore be prepared for an increase in the incidence of COVID-19 stress-related psychopathological sequelae (6). Due to the large number of COVID-19 ICU-survivors, a uniform, low-time-consuming and easy-to-implement treatment modality is needed.

Virtual reality (VR) is a relatively new technique that has been proven to be effective for treating several psychological impairments, including PTSD and anxiety disorders (7–10). VR has three major advances; first, it represents a means of addressing the limitations of imaginal exposure

and overcomes the inability to engage in sufficient detail and affective magnitude to recreate the traumatic event, a significant hurdle of imaginal exposure; second, it is an appropriate tool for patient information delivery, and can thus be used to provide additional treatment information, of which post-ICU patients are in need; and third, using VR, one can truthfully reconstruct phases of ICU treatment to replace and adjust possible delusional memories, the largest contributor to psychological distress (11–13). As such, Virtual Reality could be a valuable adjunct to improve psychological recovery and health-related quality of life after ICU treatment for COVID-19 (13, 14). Here, we describe the effect of an intensive care unit-specific VR intervention in the first patient that visited our COVID-19 outpatient clinic.

MATERIALS AND METHODS

We developed a COVID-19 intensive care unit-specific virtual reality (ICU-VR) intervention based on previous findings. A similar VR-module was tested safe in healthy volunteers and demonstrated beneficial effects in sepsis survivors (15, 16). In short, the content of ICU-VR was determined by an interdisciplinary team of ICU physicians and nurses, a psychologist, a psychiatrist, and a post-ICU patient. We adapted this module suitable for COVID-19 ICU survivors by adding additional COVID-19 specific aspects of ICU treatment (i.e., mechanical ventilation in prone position, tracheostomy and isolation measures) and information regarding SARS-CoV-2. The COVID-19 ICU-VR intervention thereby consists of six scenes; (1) the ICU physician and nurse welcome the patient in front of the ICU, where the patient is virtually installed in an ICU bed. After being brought to and installed in the ICU room, explanation is given (2) about the surveillance monitor, medication pumps, intubation (including tracheal tube suction), mechanical ventilation, and prone positioning; (3) about the peripheral drip, central line, arterial line, gastric tube, and tracheotomy, including its procedures; (4) about the treatment team and their responsibilities, (5) about isolation measures and personal protection equipment, and (6) about SARS-CoV-2 and COVID-19 (**Figures 1A–F**).

We tested the module in a COVID-19 patient after ICU treatment. Seven days after hospital discharge, he underwent the ICU-VR intervention twice during his visit to the outpatient clinic. After the first VR session, the patient directly asked to see the VR module for a second time. Hereafter he was given the opportunity to ask questions and to discuss the experience.

The hospital anxiety and depression scale (HADS) and impact of event scale-revised (IES-R) were used to assess anxiety-, depression-, and post-traumatic stress-related symptoms on the day of the COVID-19 outpatient clinic visit, directly prior to receiving the intervention, and 7 days and 6 months after hospital discharge (17, 18).

RESULTS

The patient was male, 57 years old, known with non-insulin dependent diabetes type 2, severe obstructive apnea syndrome, and no psychiatric history. He was initially admitted for respiratory insufficiency caused by a diffuse bilateral COVID-19 pneumonia, after being ill for 5 days. After 2 days of ICU treatment including deep sedation and ventilation in prone positioning, he deteriorated and was transferred to our hospital. After a consecutive treatment of 20 days in our ICU, he underwent a tracheostomy for weaning failure and started weaning in combination with intensive physiotherapy. The patient was eventually discharged from the ICU after 39 days and from the hospital after 54 days.

Seven days after discharge, he received the ICU-VR intervention twice. Prior to receiving ICU-VR, the IES-R sum score was 56, indicating severe PTSD, and the HADS depression and anxiety score were 9 and 13, indicating clinically relevant depression and anxiety, respectively. One week after receiving the COVID-19 specific ICU-VR, the IES-R score was 24, indicating none to mild PTSD, the HADS depression score was one, and the HADS anxiety score was three, indicating neither clinically relevant anxiety nor depression. More importantly, the patient stated that ICU-VR had helped him to better grasp ICU treatment, helped him to put his delusional memories into perspective, and thereby helped him to better cope with ICU-related psychological sequelae. He experienced the intervention as an enervating treatment modality and would recommend it to all patients treated for COVID-19 in the ICU.

Six months after hospital discharge, the patient suffered from critical illness polyneuropathy, had some pulmonary residual abnormalities on CT, but no decline in pulmonary function (FVC: 4.24, 82%; FEV1: 3.09, 78%). He did not suffer from psychological impairments with a still normalized IES-R score and HADS anxiety and depression scores. He partially started working again.

DISCUSSION

This is the first report of intensive care unit-specific virtual reality to reduce psychological distress and improve health-related quality of life after ICU treatment for COVID-19. The patient described showed a considerable decrease in post-traumatic stress disorder-, anxiety-, and depression-related symptomatology, shortly after seeing the VR module. Moreover, he reported that the intervention had helped him put his delusional memories into perspective and make sense of what happened to him during ICU treatment.

In the psychology field, VR is becoming an accepted treatment modality for several non-ICU-related psychological disorders (10). Although we are aware that the current report does not provide empirical evidence, it suggests that, especially during the current demand of care, an innovative technique, such as VR, can be considered to improve psychological well-being after ICU treatment. A larger, formally powered, randomized controlled trial should definitely demonstrate the effectiveness of our COVID-19 ICU-VR intervention. We are currently performing such a trial (Netherlands Trial Register, http://www.trialregister.nl/, identifier: NL8835).

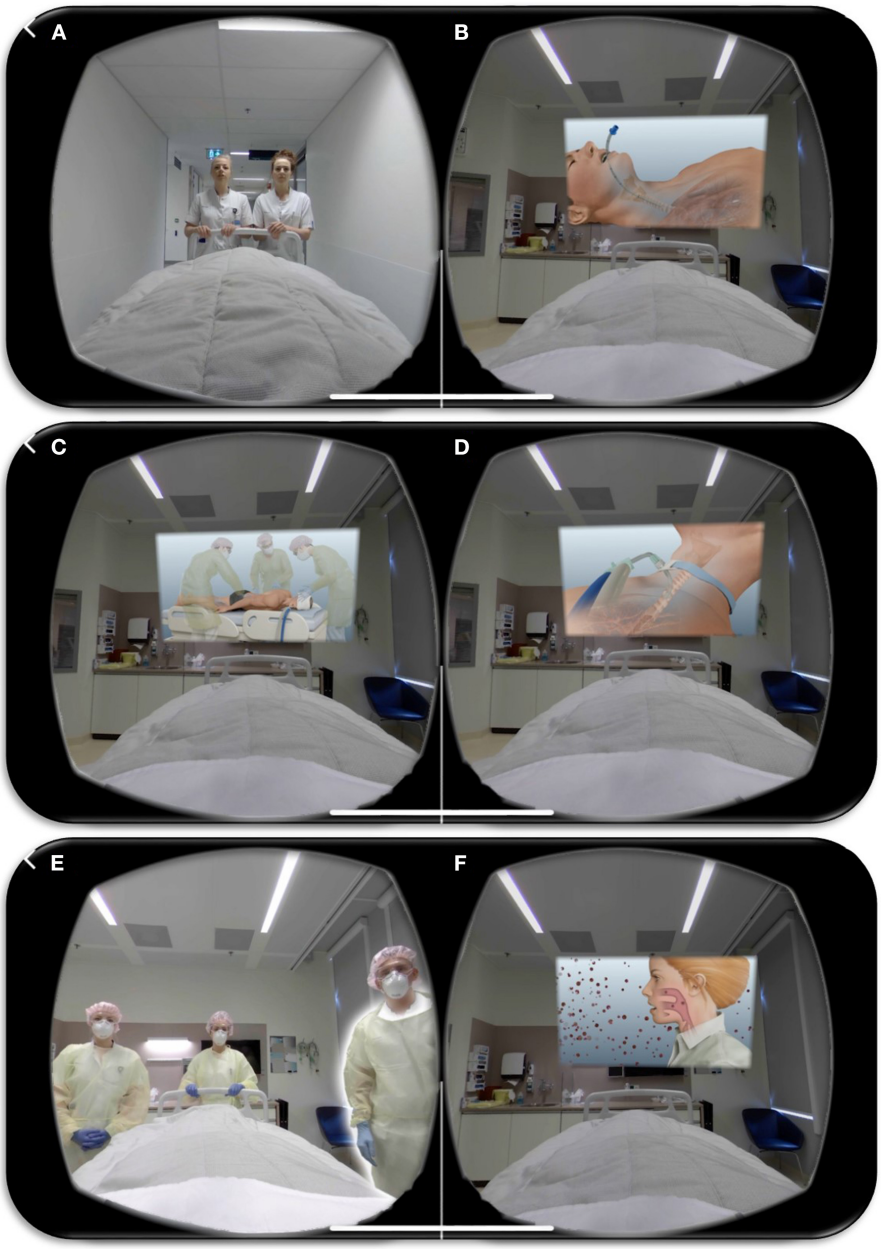

FIGURE 1 | Impression of the COVID-19 Intensive Care Unit-specific Virtual Reality intervention. Screenshots of the COVID-19 Intensive Care Unit-specific Virtual Reality intervention; (1) the ICU physician and nurse welcome the patient in front of the ICU **(A)**, where the patient is virtually installed in an ICU bed. After being brought to and installed in the ICU room, explanation is given about (2) the surveillance monitor, medication pumps, intubation (including trachea tube suction) **(B)**, mechanical ventilation, and prone positioning **(C)**; (3) about the peripheral drip, central line, arterial line, gastric tube, and tracheotomy, including its procedures **(D)**; (4) about the treatment team and their responsibilities, (5) about isolation measures and personal protection equipment **(E)**, and (6) about SARS-CoV-2 and COVID-19 **(F)**.

Anxiety- and stress-related disorders are common in ICU survivors, and literature suggests that these are predominantly caused by delusional memories, sensory overload, and amnesia (19–21). A recent study by Di Nicola et al. added important knowledge and suggested a role of serum 25-hydroxyvitamine D levels and suggested a role of serum 25-hydroxyvitamine D levels in the development of symptoms of psychological stress (22). Although the role of serum 25-hydroxyvitamine D in the development of psychological sequelae after ICU treatment has not previously been examined, it could be hypothesized that low serum levels during ICU treatment could influence psychological outcomes. Future studies should examine this hypothesis, and the possibility to prevent psychological PICS by normalizing serum levels of vitamin D.

It should be acknowledged that we used self-reported questionnaires to assess the patient's psychological well-being. These questionnaires are commonly used in, and accepted for, patients after critical illness and are as such validated in critical care survivors (23, 24). One should however take into account that formal assessment of psychological disorders requires a consultation with a psychologist or psychiatrist. Additionally, although the decrease in psychological distress was substantial and can therefore be expected to be at least partially explained by the intervention, we were unable to formally rule out that other factors may have influenced the decrease in psychological sequelae.

In conclusion, innovative technologies, such as VR, have the potential to improve psychological rehabilitation, and should therefore be considered by clinicians for the treatment of ICU-related psychological sequelae after COVID-19.

DATA AVAILABILITY STATEMENT

The original contributions presented in the study are included in the article/supplementary material, further inquiries can be directed to the corresponding author/s.

ETHICS STATEMENT

Written informed consent was obtained from the individual(s) for the publication of any potentially identifiable images or data included in this article.

AUTHOR CONTRIBUTIONS

JV, JvB, E-JW, and MvG designed the intensive care unit specific virtual reality film. JV, MvG, and MH recruited the patient. JV and MG wrote the first draft of the manuscript. JvB, MH, E-JW, and DG helped drafting the manuscript. All authors reviewed and approved the final version of the manuscript.

FUNDING

This project was funded by BeterKeten (foundation), Stichting Coolsingel (foundation), DSW, Stichting Thea (foundation), and Stichting SGS (foundation). The funding sources had no role in writing this manuscript.

REFERENCES

1. Wang C, Horby PW, Hayden FG, Gao GF. A novel coronavirus outbreak of global health concern. *Lancet.* (2020) 395:470–3. doi: 10.1016/S0140-6736(20)30185-9
2. Grasselli G, Pesenti A, Cecconi M. Critical care utilization for the COVID-19 outbreak in lombardy, italy: early experience and forecast during an emergency response. *JAMA*. (2020) 323:1545–6. doi: 10.1001/jama.2020.4031
3. Needham DM, Davidson J, Cohen H, Hopkins RO, Weinert C, Wunsch H, et al. Improving long-term outcomes after discharge from intensive care unit: report from a stakeholders' conference. *Crit. Care Med.* (2012) 40:502–9. doi: 10.1097/CCM.0b013e318232da75
4. Bienvenu OJ, Friedman LA, Colantuoni E, Dinglas VD, Sepulveda KA, Mendez-Tellez P, et al. Psychiatric symptoms after acute respiratory distress syndrome: a 5-year longitudinal study. *Intensive Care Med.* (2018) 44:38–47. doi: 10.1007/s00134-017-5009-4
5. Sivanathan L, Wunsch H, Vigod S, Hill A, Pinto R, Scales DC. Mental illness after admission to an intensive care unit. *Intensive Care Med.* (2019) 45:1550–8. doi: 10.1007/s00134-019-05752-5
6. Rogers JP, Chesney E, Oliver D, Pollak TA, McGuire P, Fusar-Poli P, et al. Psychiatric and neuropsychiatric presentations associated with severe coronavirus infections: a systematic review and meta-analysis with comparison to the COVID-19 pandemic. *Lancet Psychiatry.* (2020) 7:611–27. doi: 10.1016/S2215-0366(20)30203-0
7. Kothgassner OD, Goreis A, Kafka JX, Van Eickels RL, Plener PL, Felnhofer A. Virtual reality exposure therapy for posttraumatic stress disorder (PTSD): a meta-analysis. *Eur J Psychotraumatol.* (2019) 10:1654782. doi: 10.1080/20008198.2019.1654782
8. Wechsler TF, Kumpers F, Muhlberger A. Inferiority or even superiority of virtual reality exposure therapy in phobias?-a systematic review and quantitative meta-analysis on randomized controlled trials specifically comparing the efficacy of virtual reality exposure to gold standard in vivo exposure in agoraphobia, specific phobia, social phobia. *Front. Psychol.* (2019) 10:1758. doi: 10.3389/fpsyg.2019.01758
9. Deng W, Hu D, Xu S, Liu X, Zhao J, Chen Q, et al. The efficacy of virtual reality exposure therapy for PTSD symptoms: A systematic review and meta-analysis. *J Affect Disord.* (2019) 257:698–709. doi: 10.1016/j.jad.2019.07.086
10. Park MJ, Kim DJ, Lee U, Na EJ, Jeon HJ. A literature overview of virtual reality (VR) in treatment of psychiatric disorders: recent advances and limitations. *Front Psychiatry.* (2019) 10:505. doi: 10.3389/fpsyt.2019.00505
11. Bekelis K, Calnan D, Simmons N, MacKenzie TA, Kakoulides G. Effect of an immersive preoperative virtual reality experience on patient reported outcomes: a randomized controlled trial. *Ann. Surg.* (2017) 265:1068–73. doi: 10.1097/SLA.0000000000002094
12. Peri T, Gofman M. Narrative Reconstruction: An integrative intervention module for intrusive symptoms in PTSD patients. *Psychol Trauma.* (2014) 6:176. doi: 10.1037/a0031965
13. Vlake JH, van Genderen ME, Schut A, Verkade M, E-Wils, Gommers D, et al. Patients suffering from psychological impairments following critical illness are in need of information. *J. Intens. Care.* (2020) 8:6. doi: 10.1186/s40560-019-0422-0
14. Singh RP, Javaid M, Kataria R, Tyagi M, Haleem A, Suman R. Significant applications of virtual reality for COVID-19 pandemic. *Diabetes Metab. Syndr.* (2020) 14:661–4. doi: 10.1016/j.dsx.2020.05.011
15. Vlake JH, Wils EJ, Van Bommel J TI.Korevaar MG, Diederik, Van Genderen. ME, Intensive Care Specific Virtual Reality Exposure Therapy is immersive, feasible and safe to treat psychological post-ICU sequelae; a healthy adult study. *ICMx.* (2019) 7:162–3. doi: 10.1186/s40635-019-0265-y
16. Vlake JH, E-Wils J, Van Bommel JT, Korevaar IM, Gommers D, Van Genderen. ME. Intensive care specific virtual reality (ICU-VR) to improve post-intensive care syndrome-related psychological sequelae in survivors of critical illness. *ICMx.* (2020) 8:63. doi: 10.1186/s40560-020-00354-8
17. Zigmond AS, Snaith RP. The hospital anxiety and depression scale. *Acta Psychiatr Scand.* (1983) 67:361–70. doi: 10.1111/j.1600-0447.1983.tb09716.x
18. Weiss DS. *The Impact of Event Scale: Revised, Cross-Cultural Assessment of Psychological Trauma and PTSD.* Springer (2007). p. 219–38. doi: 10.1007/978-0-387-70990-1_10
19. Askari Hosseini SM, Arab M, Karzari Z, Razban F. Post-traumatic stress disorder in critical illness survivors and its relation to memories of ICU. *Nurs Crit Care.* (2020) 1–7. doi: 10.1111/nicc.12532
20. Doig L, Solverson K. Wanting to forget: intrusive and delusional memories from critical illness. *Case Rep Crit Care.* (2020) 2020:7324185. doi: 10.1155/2020/7324185
21. Granja C, Gomes E, Amaro A, Ribeiro O, Jones C, Carneiro A, et al. Understanding posttraumatic stress disorder-related symptoms after critical

care: the early illness amnesia hypothesis. *Crit. Care Med.* (2008) 36:2801–9. doi: 10.1097/CCM.0b013e318186a3e7

22. Di Nicola M, Dattoli L, Moccia L, Pepe M, Janiri D, Fiorillo A, et al. Serum 25-hydroxyvitamin D levels and psychological distress symptoms in patients with affective disorders during the COVID-19 pandemic. *Psychoneuroendocrinology.* (2020) 122:104869. doi: 10.1016/j.psyneuen.2020.104869
23. Sukantarat KT, Williamson RC, Brett SJ. Psychological assessment of ICU survivors: a comparison between the hospital anxiety and depression scale and the depression, anxiety and stress scale. *Anaesthesia.* (2007) 62:239–43. doi: 10.1111/j.1365-2044.2006.04948.x
24. Bienvenu OJ, Williams JB, Yang A, Hopkins RO, Needham DM. Posttraumatic stress disorder in survivors of acute lung injury: evaluating the Impact of Event Scale-Revised. *Chest.* (2013) 144:24–31. doi: 10.1378/chest.12-0908

Conflict of Interest: The authors declare that the research was conducted in the absence of any commercial or financial relationships that could be construed as a potential conflict of interest.

frontiers in Medicine

ORIGINAL RESEARCH
published: 31 August 2021
doi: 10.3389/fmed.2021.715099

High Central Venous Pressure and Right Ventricle Size Are Related to Non-decreased Left Ventricle Stroke Volume After Negative Fluid Balance in Critically Ill Patients: A Single Prospective Observational Study

Zhao Hua, Ding Xin, Wang Xiaoting and Liu Dawei* on behalf of the Critical Ultrasound Study Group (CCUSG)*

Department of Critical Care Medicine, Peking Union Medical College Hospital, Peking Union Medical College, Chinese Academy of Medical Sciences, Beijing, China

OPEN ACCESS

Edited by:
Zhanqi Zhao,
Furtwangen University, Germany

Reviewed by:
Yi Yang,
Southeast University, China
Jiapeng Huang,
University of Louisville, United States

***Correspondence:**
Wang Xiaoting
wangxiaoting@pumch.cn
Liu Dawei
dwliu98@163.com

Specialty section:
This article was submitted to Intensive Care Medicine and Anesthesiology, a section of the journal Frontiers in Medicine

Received: *26 May 2021*
Accepted: *29 July 2021*
Published: *31 August 2021*

Citation:
Hua Z, Xin D, Xiaoting W and Dawei L (2021) High Central Venous Pressure and Right Ventricle Size Are Related to Non-decreased Left Ventricle Stroke Volume After Negative Fluid Balance in Critically Ill Patients: A Single Prospective Observational Study. Front. Med. 8:715099. doi: 10.3389/fmed.2021.715099

Background: Optimal adjustment of cardiac preload is essential for improving left ventricle stroke volume (LVSV) and tissue perfusion. Changes in LVSV caused by central venous pressure (CVP) are the most important concerns in the treatment of critically ill patients.

Objectives: This study aimed to clarify the changes in LVSV after negative fluid balance in patients with elevated CVP, and to elucidate the relationship between the parameters of right ventricle (RV) filling state and LVSV changes.

Methods: This prospective cohort study included patients with high central venous pressure (CVP) (≥8 mmHg) within 24 h of ICU admission in the Critical Medicine Department of Peking Union Medical College Hospital. Patients were classified into two groups based on the LVSV changes after negative fluid balance. The cutoff value was 10%. The hemodynamic and echo parameters of the two groups were recorded at baseline and after negative fluid balance.

Results: A total of 71 patients included in this study. Forty in VI Group (LVOT VTI increased ≥10%) and 31 in VNI Group (LVOT VTI increased <10%). Of all patients, 56.3% showed increased LVSV after negative fluid balance. In terms of hemodynamic parameters at T0, patients in VI Group had a higher CVP ($p < 0.001$) and P(v-a)CO_2 ($p < 0.001$) and lower $ScVO_2$ ($p < 0.001$) relative to VNI Group, regarding the echo parameters at T0, the RV_D/LV_D ratio ($p < 0.001$), $DIVC_{end-expiratory}$ ($p < 0.001$), and ΔLVOT VTI ($p < 0.001$) were higher, while T0 LVOT VTI ($p < 0.001$) was lower, in VI Group patients. The multifactor logistic regression analysis suggested that a high CVP and RV_D/LV_D ratio ≥0.6 were significant associated with LVSV increase after negative fluid balance in critically patients. The AUC of CVP was 0.894. A CVP >10.5 mmHg provided a sensitivity of 87.5% and a specificity of 77.4%. The AUC of CVP combined with the RV_D/LV_D ratio ≥0.6 was 0.926, which provided a sensitivity of 92.6% and a specificity of 80.4%.

Conclusion: High CVP and RV_D/LV_D ratio ≥0.6 were significant associated with RV stressed in critically patients. Negative fluid balance will not always lead to a decrease, even an increase, in LVSV in these patients.

Keywords: central venous pressure, fluid management, echocardiography, right ventricle size, right ventricle filling

INTRODUCTION

In the management of hemodynamic instability, optimal adjustment of cardiac preload is essential for improving stroke volume (SV) and tissue perfusion. Fluid management in critical patients is crucial for prognosis, as both inadequate fluid or fluid overload can lead to negative outcomes (1). In particular, fluid overload and high CVP are associated with poor outcomes in critically ill patients (2). Some studies have concluded that elevated CVP is associated with increased mortality in critically ill patients (3). Conversely, early reductions in CVP during treatment may help maintain good organ function and result in a higher survival rate (4). Negative fluid balance is the most common clinical intervention to reduce CVP. Based on the Frank-Starling mechanism and venous return theory proposed by Guyton, venous return should match cardiac output (CO) as determined by the mean systemic filling pressure (MSFP) and the CVP gradient (5, 6). Changes in CO due to CVP are important concerns for the treatment of critically ill patients. The trend of changes between CVP and CO is not consistent in different conditions. Nevertheless, increases in CO with decreases in CVP occur in routine clinical work, which are indicative of improvement of heart function and pulmonary circulation, especially right heart function.

Right heart function is essential for venous return (7, 8). The healthy human RV fills at or below its unstressed volume, such that RV end-diastolic volume changes occur without any changes in RV diastolic wall stretch. With increased volume loading of the RV, right ventricular end-diastolic pressure (RVEDP) and LVSV both increased. When RV reaches the flat part of the pressure-volume curve, the RV further increases in size will lead a leftward ventricular septal (VS) shift (9). VS shift can result in decreased LVSV, leading to a phenomenon colloquially termed "falling off the Starling curve" (7).

According to the understanding of fluid responsiveness (FR), assessing the filling state of the RV is key to judging the volume status. However, evaluation of the filling state remains a challenge. Dynamic monitoring of CVP and assessment of RV size via echocardiography are currently used as indices of RV filling state (10–13). In our previous retrospective study, the patients with increased cardiac output (CO) and decreased CVP achieved negative fluid balance, but the effect of cardiotonic drugs couldn't be rule out (14). The changes of LVSV after negative fluid balance is still unknown in patients with high CVP. CVP has been used as a surrogate of right ventricle filling pressure, but CVP as a single measure is highly questionable: (1) It remains unclear what level of CVP is deleterious and may be considered a trigger for intervention; (2) The effect of varying intrathoracic pressure in mechanically ventilated patients, and might not reflect preload directly. Several studies have reported that fluid overload can increase RV size [the right to left ventricular end-diastolic dimensions (RV_D/LV_D) ratio is ≥0.6] (15–17). Furthermore, the relationship between hemodynamic parameters and LVSV changes after negative fluid balance is unclear. We therefore aimed to assess the changes of LVSV after negative fluid management and to elucidate the relationship between the parameters of right ventricle (RV) filling state and LVSV changes.

MATERIALS AND METHODS

Study Design and Patient Enrollment

This is a *post-hoc* analysis of data collected during a prospective cohort study at the Critical Care Department of Peking Union Medical College Hospital. All patients with abnormally high CVP (i.e., outside the normal range of 0–7 mmHg) within 24 h of ICU admission from July 2017 to December 2017 were included in the study. All the patients authorized us to use their clinical data. The research protocol was reviewed and approved by Ethics Committee of Peking Union Medical College Hospital (PUMCH-S617).

Inclusion and Exclusion Criteria

The inclusion criteria were (1) CVP ≥8 mmHg and (2) age >18 years. The exclusion criteria were (1) negative balance therapy was not performed; (2) non-curative goals of therapy, (3) a history of cardiac disease, pulmonary hypertension, or precaval malformations, and (4) abdominal hypertension.

Study Protocol

All patients were treated as follows:

All enrolled patients underwent the routine procedures of the Critical Care Department of Peking Union Medical College Hospital. Arterial and venous lines were inserted. Time 0 (T0) is defined as the time of patient enrollment, and Time 1 (T1) is defined as a negative fluid balance of 500 ml. Central venous and arterial blood gases analysis were performed at T0 and T1. Patients were divided into two groups according to the LVOT VTI changes after negative fluid balance: VI Group comprised patients with ΔLVOT VTI(T1-T0)/T0 LVOT VTI ≥10% (VI) and VNI Group comprised patients with ΔLVOT VTI(T1-T0) /T0 LVOT VTI <10%(VNI).

- *Hemodynamic monitoring methods*: The lines of central venous and arterial were inserted, CVP, central venous oxygen saturation ($ScVO_2$), central venous-arterial carbon dioxide difference [$P(v\text{-}a)CO_2$], and serum lactate levels (lac) were

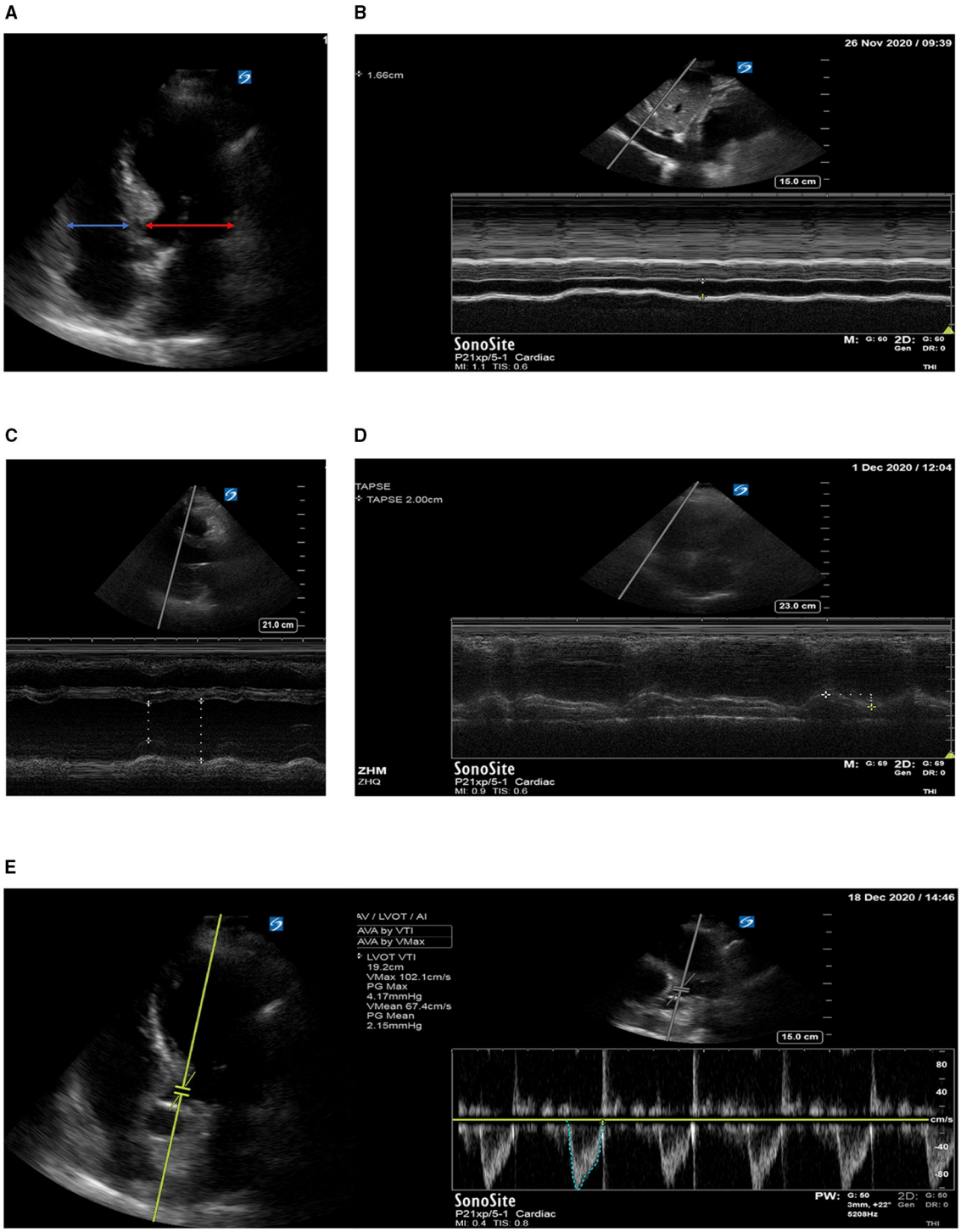

FIGURE 1 | (A) Right to left ventricular diastolic dimensions ratio (RV_D/LV_D ratio); **(B)** diameter of the inferior vena cava; **(C)** left ventricular eject fraction EF; **(D)** tricuspid annular plane systolic excursion TPASE; **(E)** left ventricular outflow tract velocity time integral VTI.

tested (detailed were showed in **Supplementary Material 1**). Bladder pressure was used as a surrogate of intra-abdominal pressure (IAP), IAP $\geq$12 mmHg is defined as abdominal hypertension.

- *Echocardiography*: Echocardiography was also performed at T0 and T1 by competent attending physicians or fellows, who had at least 3 years of experience in echocardiography performance and interpretation. An ultrasound system

equipped with an array probe (X-Porte, Sonosite, Bothell, WA, USA) was used. At least five standard views (acoustic windows) were obtained and recorded for each scan (**Figure 1**) (detailed were showed in **Supplementary Material 1**). All the reviews were confirmed by two competent attending physicians.

- *Clinical treatment*: The method of negative fluid balance (application of diuretic drugs or continuous renal replacement therapy) was determined by the physician. No changes were made that may cause changes in CVP. In the case of patient hypoxia, the inhaled oxygen concentration was adjusted to ensure SPO_2 >95%, PaO_2 >60 mmHg.

Data Collection

Clinical data were extracted from the ICU computerized database and medical records, including patients' socio-demographic data, biometric parameters, comorbidities, respiratory support mode, and Acute Physiology and Chronic Health Evaluation II score, SOFA score. Hemodynamic parameters [heart rate, mean arterial blood pressure, CVP, $ScVO_2$, P(v-a)CO_2, and lac] and echo parameters [such as tricuspid annular plane systolic excursion (TAPSE), diameter of the inferior vena cava (DIVC $_{end-expiratory}$), left ventricular eject fraction (LVEF), RV_D/LV_D ratio, left ventricle outflow tract velocity-time integral (LVOT VTI), mitral annular plane systolic excursion (MAPSE), mitral diastolic filling Eatly (Em), mitral diastolic filling Atrial (A m), and early diastolic velocity of the mitral annulus Ea m] were recorded at T0 and T1, were also recorded at the same time. The primary outcome of the study was to clarify LVOT VTI changes after negative fluid management in patients with high CVP. The secondary outcome was to evaluate the relationship between the relationship between the parameters of RV filling state and LVOT VTI changes after negative fluid management.

Statistical Analysis

Statistical analysis was performed using SPSS software version 20.0 for Windows (IBM, Armonk, NY). Considering this is a *post-hoc* analysis of data, sample size was calculated through events per variable (EPV) method. EPV of 5–10 is usually used to estimate sample size in the literature. At most 6 candidate variables could be included in the multivariate modeling process when half of patients will present positive result. The data distribution test and the homogeneity of variance test were performed on the data. Results for continuous variables with a normal distribution (e.g., age, Acute Physiology and Chronic Health Evaluation II score) are reported as the mean ± standard deviation. Student's *t*-test was used to compare means between two groups. Results for continuous variables that were not normally distributed are reported as the median (25th and 75th percentiles) and compared using non-parametric tests. Qualitative data were expressed as proportions; testing for differences was performed using a chi-square test or Fisher's exact test. The paired sample *t*-test was used for comparisons between groups before and after treatment. The correlation between RV variables and LVOT VTI changes was analyzed using Pearson correlation analysis. Risk factors associated with VI were identified in univariate and multivariate logistic regression analysis, variables with a $P < 0.2$ were subjected to a multivariate analysis with backward stepwise models to measure the odd risk (OR) and 95% confidence intervals (CIs). Receiver operating characteristic (ROC) curves were used to determine the ability of the indices to predict LVOT VTI increase >10% after negative fluid balance. The areas under the ROC curves (AUCs) were compared using DeLong's test. The AUC, sensitivity, and specificity are expressed as values with 95% CI. A $p < 0.05$ was considered to be statistically significant.

RESULTS

Demographic and Clinical Characteristics of Patients

During the study period, a total of 154 patients were admitted with CVP ≥8 mmHg. Of these, 65 did not meet the study criteria (28 didn't undergo negative fluid management, 26 had underlying heart disease, 5 had abdominal hypertension, 6 with non-curative goals of therapy). In addition, 9 were excluded due to poor TT image quality or incomplete image acquisition; 6 were excluded due to inconsistent judgments of the ultrasound results by the two physicians; and 3 were excluded due to new tachyarrhythmia during the trial. Thus, the final sample for analysis comprised 71 patients (33 males, 38 females) (**Figure 2**). Overall, 40 (56.3%) patients were grouped to VI Group, 31 (43.7%) patients were grouped to VNI Group. The demographical and clinical characteristics of all patients are shown in **Table 1**. Except for the P/F ratio ($p < 0.05$), there were no significant differences in other demographic characteristics between the two groups. In terms of hemodynamic parameters at T0, patients in VI Group had a higher CVP and P(v-a)CO_2 and lower $ScVO_2$ relative to VNI Group (all $p < 0.05$). No group differences were observed for HR, MAP, or lactate levels. Regarding the echo parameters at T0, the RV_D/LV_D ratio ≥0.6, DIVC $_{end-expiratory}$, ΔLVOT VTI were higher, while T0 LVOT VTI was lower, in VI Group (all $p < 0.05$). There were no group differences in LV systolic and diastolic function, RV systolic fuction, and tricuspid regurgitation as shown in **Table 2**.

Comparison of Hemodynamic Parameters at T0 and T1 Between Patients With Rv Dilation or Not

The analysis showed there was a significant difference in proportion of RV_D/LV_D ratio ≥0.6 (RV dilation) between the two groups. We compared the hemodynamic parameters at T0 and T1 between patients with RV_D/LV_D ratio ≥0.6 (RV dilation) or not (non-RV dilation).

As shown in **Figure 3**, CVP, DIVC $_{end-expiratory,}$ and RV_D/LV_D ratio decreased significantly in both groups after negative fluid management ($p < 0.05$). None of the patients in our study experienced tissue perfusion insufficiency. Flow related parameters [LVOT VTI, P(v-a)CO_2, $ScVO_2$] improved in patients with RV_D/LV_D ratio ≥0.6 ($p < 0.05$), and the lactate level decreased

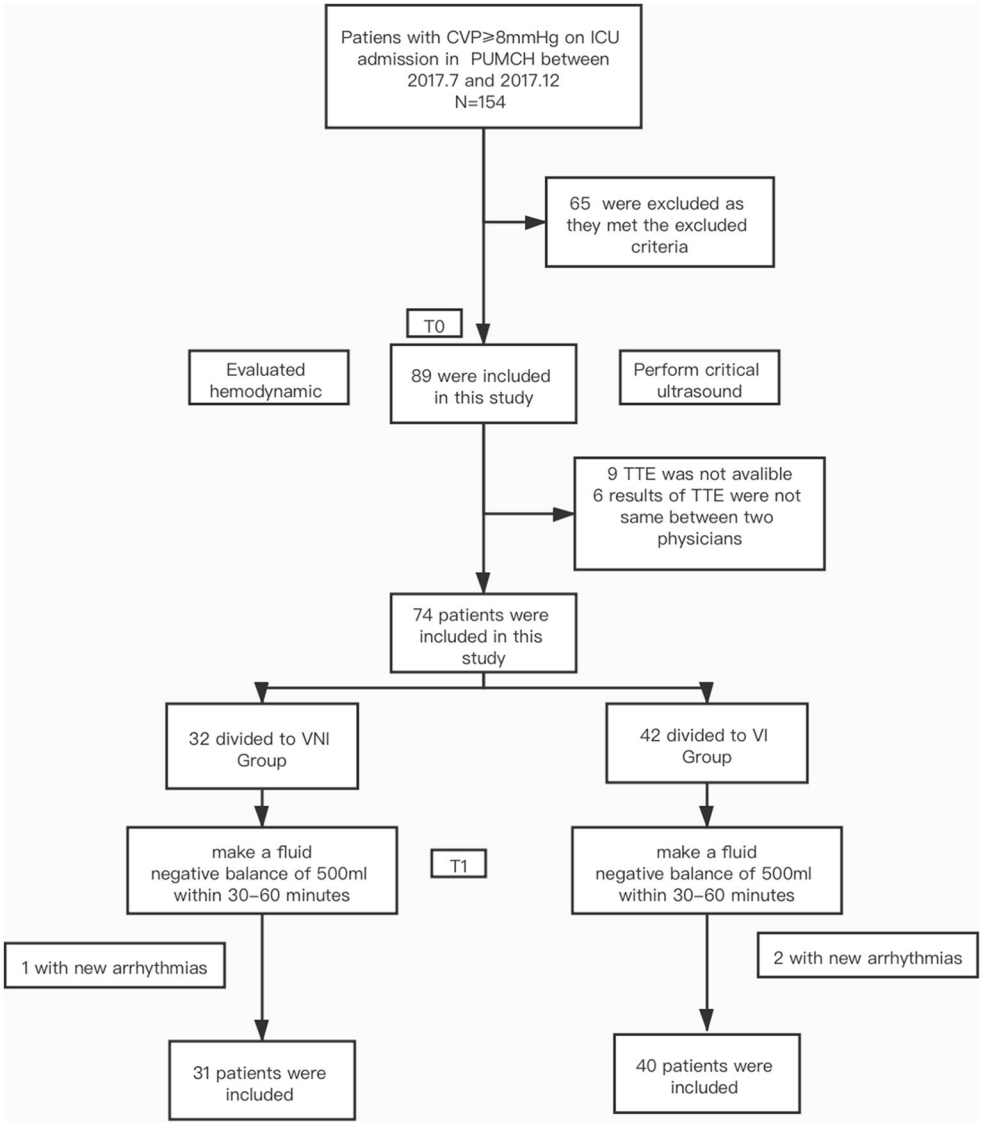

FIGURE 2 | Flow chart.

in patients with RV_D/LV_D ratio <0.6 ($p < 0.05$). In addition, the P/F ratio increased significantly in both groups ($p < 0.05$).

Correlation Between RV Parameters and Δ LVOT VTI/T0 LVOT VTI

Figure 4 presents the individual parameter values for RV and Δ LVOT VTI/T0 LVOT VTI among all patients. CVP, RV_D/LV_D ratio, and DIVC $_{end-expiratory}$ were significantly correlated with Δ LVOT VTI/T0 LVOT VTI [$r = 0.64$ ($p < 0.05$), 0.64 ($p < 0.053$), and 0.59 ($p < 0.05$), respectively]. By contrast, no relationship was observed between LV systolic and diastolic functions, RV systolic function and tricuspid regurgitation and Δ LVOT VTI/T0 LVOT VTI.

Risk Factors for a LVOT VTI Increase ≥10% at T1

The multifactor logistic regression analysis was used to examine possible risk factors for the changes of LVOT VTI after negative fluid management. All relevant variables were taken into account (including demographics and clinical characteristics, hemodynamic and ECHO findings). P(v-a) CO_2 and $ScVO_2$ were excluded, as they are derived variables of LVOT VTI, P/F was exclude as it was consequence variables of RV stressed. The results of univariate analysis suggested that the *P*-value of CVP, RV_D/LV_D ratio, LVOT VTI, DIVC $_{end-expiratory}$ and E m

TABLE 1 | The demographic and clinical characteristics of the patients included in this study at T0.

Variable	All patients (*N* = 71)	VI group (*N* = 40)	VNI group (*N* = 31)	*P*-value
Gender (male/female)	71 (33/38)	40 (18/22)	31 (15/16)	0.321
Age (years)	49 ± 16	48 ± 16	50 ± 14	0.334
SOFA Score (mean ± SD)	9.1 ± 4.5	9.2 ± 4.5	8.9 ± 4.4	0.384
APACHE II Score (mean ± SD)	16 ± 5	17 ± 5	15 ± 5	0.173
Underlying disease *n* (%)				
Coronary artery disease	13 (18.3)	7 (17.5)	6 (19.4)	0.540
Hypertension	28 (39.4)	17 (42.5)	11 (35.5)	0.362
Diabetes mellitus	24 (33.8)	16 (40)	8 (25.8)	0.158
Choric renal failure	12 (16.9)	8 (20)	4 (12.9)	0.218
Choric liver failure	4 (5.6)	3 (7.5)	1 (3.2)	0.409
Stroke	8 (11.3)	4 (10)	4 (12.9)	0.493
Cancer	6 (8.5)	4 (10)	2 (6.5)	0.466
Primary disease *n* (%)				
Sepsis	34 (47.9)	20 (50)	14 (45.1)	0.435
gastrointestinal bleeding	3 (4.2)	2 (5)	1 (3.2)	0.596
Traumatic brain injuries	3 (4.2)	2 (5)	1 (3.2)	0.596
Acute coronary syndrome	9 (12.7)	5 (12.5)	4 (12.9)	0.616
Post-operative of gastrointestinal tumors	5 (7.0)	3 (7.5)	2 (6.5)	0.621
Post-operative of urinary system	10 (14.1)	4 (10)	6 (19.4)	0.217
Post-operative of gynecologic cancer	7 (9.9)	4 (10)	3 (9.7)	0.642
RASS Score	−2.33 ± 1.16	−2.45 ± 1.23	−2.37 ± 1.19	0.674
Proportion of organ failure				
PaO_2/FiO_2 (mmHg)	240.62 ± 46.19	214.10 ± 39.63	274.84 ± 28.09	<0.001
Acute kidney injury *n* (%)	16 (22.5)	9 (22.5)	7 (22.5)	0.607
Acute myocardial injury *n* (%)	10 (14.1)	6 (15)	4 (12.9)	0.541
Acute liver injury *n* (%)	4 (5.6)	3 (7.5)	1 (3.2)	0.409
Interventions				
CRRT (*n* %)	8 (11.3)	5 (12.5)	3 (9.7)	0.507
Ventilation modes *n* (%)				
Non-invasive ventilation	13 (18.3)	8 (20)	5 (23.8)	0.256
Invasive ventilation	58 (81.7)	32 (80)	26 (74.2)	0.354
Vasoactive drugs (*n* %)	36 (50.7)	20 (50.0)	16 (51.6)	0.542
Fluid input (T0–T1) (ml)	86 ± 15	85 ± 14	87 ± 16	0.482
T1–T0 time (minute)	63 ± 14	58 ± 15	64 ± 16	0.275

Quantitative data are expressed as the mean ± SD or median interquartile (25–75) %. Qualitative data are expressed as n (%). APACHE II, Acute Physiology and Chronic Health Evaluation II; Sofa Score, Sequential Organ Failure Assessment Score; PaO_2, arterial oxygen pressure; FiO_2, fraction of inspiration oxygen; CRRT, continue renal replacement therapy; RASS Score, Richmond Agitation-Sedation Scale Score.

was <0.2 (**Table 3**). Then these variables were subjected to the multivariate logistic regression analysis with backward stepwise model. The results suggested that a high CVP and RV_D/LV_D ratio were significant associated with LVSV increase after negative fluid balance in critically patients ($p < 0.05$). The OR of CVP and RV_D/LV_D ratio were 2.425 (95% CI, 1.458–4.003) and 8.588 (95% CI, 1.947–37.887), respectively (**Table 3**).

Effect of Risk Parameters for Predicting a LVOT VTI Increase >10% at T1

The AUC of CVP for predicting a LVOT VTI increase >10% at T1 was 0.883 (95% CI 0.804–0.902). The best diagnostic threshold was 10.5 mmHg, which provided a sensitivity of 87.5% and a specificity of 77.4% (**Figure 5**).

The regression equation for all of the risk parameters is:

Logit (P) = −10.474 + CVP * 0.886 + RV_D/LV_D ratio * 2.854 (≥0.6 = 1, <0.6 = 0).

The AUC of CVP combined with RV_D/LV_D ratio for predicting a LVOT VTI increase >10% at T1 was 0.926 (95% CI 0.866–0.96). The best diagnostic threshold was 0.3689, which provided a sensitivity of 92.5% and a specificity of 80.6% (**Figure 5**).

DISCUSSION

The main findings of our study are as follows: (1) Negative fluid balance will not always lead to a decrease, even an increase, in patients with high CVP, especially combined with

TABLE 2 | The hemodynamic and echo characteristics of all the included patients at T0.

Variable	All patients (*N* = 71)	VI group (*N* = 40)	VNI group (*N* = 31)	*P*-value
Hemodynamic parameters				
Central venous pressure CVP (mmHg)	11.42 ± 2.27	12.74 ± 1.98	9.74 ± 1.32	<0.001
Mean arterial blood pressure MAP (mmHg)	75.70 ± 8.724	75.72 ± 8.48	75.68 ± 8.06	0.981
Heart rate HR (bpm)	94.06 ± 15.86	95.83 ± 16.28	91.77 ± 15.24	0.289
P(v-a)CO_2 (mmHg)	5.42 ± 1.98	6.43 ± 1.63	4.11 ± 1.59	<0.001
$ScVO_2$ %	68.44 ± 7.71	64.32 ± 5.45	73.76 ± 6.94	<0.001
Arterial blood lactate level lac (mmol/l)	3.23 ± 0.79	3.30 ± 0.83	3.13 ± 0.73	0.353
Echo parameters				
LVOT VTI (T0)	18.38 ± 2.72	16.94 ± 1.59	20.23 ± 2.76	<0.001
Left ventricular eject fraction EF %	62.08 ± 5.04	62.13 ± 4.99	62.03 ± 5.17	0.939
MAPSE (cm)	1.34 ± 0.28	1.33 ± 0.21	1.36 ± 0.37	0.428
E/A m	1.12 ± 0.36	1.21 ± 0.57	1.08 ± 0.29	0.539
E m (cm/s)	68 ± 19	71 ± 19	65 ± 11	0.029
A m (cm/s)	62 ± 20	63 ± 22	61 ± 18	0.673
E/Ea m	10.52 ± 2.19	11.74 ± 1.36	10.09 ± 3.27	0.126
Tricuspid vale regurgitation (TVR) *n* (%)	29 (40.4)	19 (47.5)	10 (32.3)	0.167
$+^{*}$ *n* (%)	26 (36.6)	17 (42.5)	9 (29.0)	0.094
$++^{*}$ *n* (%)	3 (4.2)	2 (5)	1 (3.2)	0.243
DIVC $_{end-expiratory}$ (cm)	1.93 ± 0.28	2.08 ± 0.25	1.75 ± 0.21	<0.001
TAPSE (cm)	2.16 ± 0.26	2.15 ± 0.28	2.18 ± 0.25	0.765
RV_D/LV_D ratio ≥0.6 *n* (%)	35 (49.3)	29 (72.5)	6 (20)	<0.001

P(v-a)CO_2, central venous-arterial carbon dioxide difference; $ScVO_2$, central venous oxygen saturation; MAPSE, mitral annular plane systolic excursion; DIVC $_{end-expiratory}$, diameter of the inferior vena cava; TPASE, tricuspid annular plane systolic excursion; LVOT VTI, T0 left ventricle outflow tract velocity time integral T0; RV_D/LV_D ratio, right to left ventricular end-diastolic dimensions ratio; Em, mitral diastolic filling Eatly; A m, mitral diastolic filling Atrial; Ea m, early diastolic velocity of the mitral annulus.

*TVR <2.8 m/s.

$^{+*}$TVR ≥2.8 m/s.

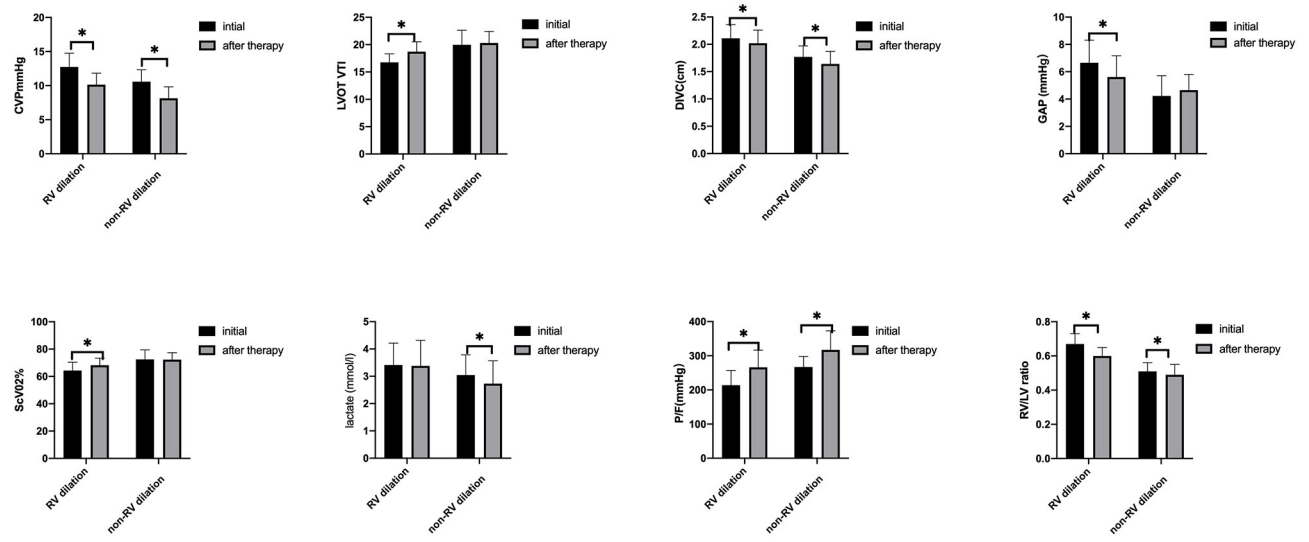

FIGURE 3 | Hemodynamic parameters between T0 and T1 in the two groups, *indicates a $p < 0.05$ between the two groups. CVP, central venous pressure; LVOT VTI, left ventricular outflow tract velocity time integral; DIVC $_{end-expiratory}$, diameter of the inferior vena cava; P(V-A)CO_2, central venous-arterial carbon dioxide difference; ScVO2, central venous oxygen saturation; P/F, arterial partial pressure of oxygen to fractional concentration of inspired oxygen; RV_D/LV_D ratio, right to left ventricular diastolic dimensions ratio.

RV_D/LV_D ratio ≥0.6. (2) The underling mechanism may be related to the filling state of RV. Our results suggested high CVP and RV_D/LV_D ratio (≥0.6) were significantly associated with RV stressed, CVP ≥10.5 combined with RV_D/LV_D ratio ≥0.6 can predict higher LVSV derived from negative fluid balance. (3) We found that the patients with high CVP can benefit

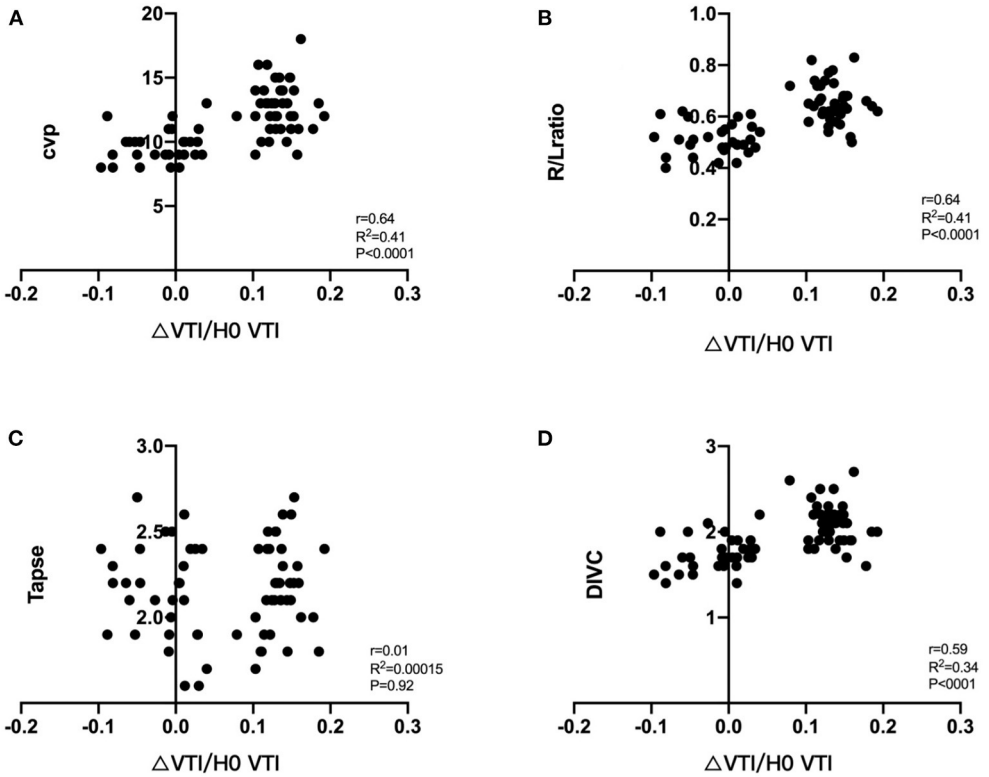

FIGURE 4 | Correlation between ΔLVOT VTI/T0 LVOT VTI and RV parameters, ΔLVOT VTI/T0LVOT VTI = T1LVOT VTI-T0 LVOT VTI/T0LVOT VTI, its relationship with CVP **(A)**, RV_D/LV_D ratio **(B)**, TAPSE **(C)**, DIVC $_{end-expiratory}$ **(D)**. VTI, velocity time integral; CVP, central venous pressure; TPASE, tricuspid annular plane systolic excursion; RV_D/LV_D ratio, right to left ventricular diastolic dimensions ratio; DIVC $_{end-expiratory,}$ diameter of the inferior vena cava.

from oxygenation index improvement through dehydration treatment, CVP can be used as a clinical safety mechanism to avoid fluid overload.

In our study, the intervention was performed in a short period of time (63 ± 14 min), while other factors affecting CVP were unchanged. Notably, 56.3% of our patients showed increased VTI after negative fluid balance, 43.7% showed decreased or unchanged VTI, which is not exactly the same as the comment cognition. As the Starling curve does not have descending branches, it cannot explain the increase in LVSV after negative fluid management. Thus, we assume that patients experienced RV stressed. A negative fluid balance can reduce RV volume, resulting in a rightward VS shift, an increase in left ventricular end-diastolic volume, and an increase in LVSV.

In terms of the hemodynamic and echo parameters in our cohort, CVP, $P(v\text{-}a)CO_2$, ScVO2, RV_D/LV_D ratio, LVOT VTI, and DIVC $_{end-expiratory}$ differed significantly between the two groups at T0. A high CVP value and RV_D/LV_D ratio ≥0.6 were significantly associated with RV stressed. Antoine Vieillard-Baron also found RV failure was frequent (42% of cases) when defined by the association of RV dilatation (RV/LV EDA ≥0.6) with systemic congestion (CVP ≥8 mmHg) in septic shock patients, and only 20–30% patients responded to fluid (18, 19). Due to its geometrical complexity, assessment of RV volume is a very difficult task. Although quantitative validation is lacking, RV_D/LV_D ratio has prognostic value in multiple patient populations, including acute pulmonary embolism, idiopathic pulmonary arterial hypertension, and post-left ventricular assist device implantation, the correlation of RV linear dimensions with RV end-diastolic volumes appears to worsen with increased preload (20–22). RV_D/LV_D ratio has been shown to be an indicator of RV size, and can thus provide reliable information about RV shape and size. A ratio ≥0.6, regardless of whether RV is within the normal reference limits, may relate to certain conditions such as RV stressed (20). Our results are similar to those of previous studies (23). Our measurement method is more clinically operable and repeatable. However, in patients with pulmonary embolism and chronic pulmonary hypertension, only RVEDA/LVEDA >1 indicates RV stressed (24, 25). When R/V ratio is applied clinically, it should be considered in combination with the patient's underlying disease and ventricular septal morphology. We also identified high CVP was significantly associated with RV stressed. The gold standard for evaluating RV filling pressure is invasive monitoring using a centrally placed venous catheter (26). Since the filling pressure and LVSV of the RV do not have a linear relationship, it has recently been acknowledged that CVP is ineffective for evaluating a patient's fluid responsiveness (27–29). While the absolute value of CVP

TABLE 3 | Logistic regression analysis for possible risk factors of LVOT VTI increased ≥10% after negative fluid balance.

Variables	Univariate logistic regression analysis				Univariate logistic regression analysis			
	OR	95% CI for OR		*P* value	OR	95% CI for OR		*P* value
		Lower	Upper			Lower	Upper	
Central venous pressure CVP (mmHg)	2.920	1.813	4.703	<0.001	2.425	1.458	4.033	0.001
RV_D/LV_D ratio ≥0.6	23.250	6.427	84.112	<0.001	8.588	1.947	37.887	0.005
$DIVC_{end-expiratory}$ (cm)	860.978	34.924	21225.283	<0.001	1.846	0.012	294.155	0.813
TAPSE (cm)	1.320	0.221	7.902	0.761				
LVOTs VTI T0	0.495	0.351	0.697	<0.001	0.689	0.452	1.051	0.084
LVEF (%)	1.004	0.914	1.102	0.938				
MAPSE (cm)	1.123	0.879	1.105	0.687				
E m (cm/s)	1.049	1.003	1.098	0.036	1.019	0.953	1.090	0.574
Am (cm/s)	1.006	0.846	1.423	0.635				
E/Ea	0.987	0.684	1.256	0.578				
Tricuspid vale regurgitation (TVR)								
+	0.553	0.204	1.500	0.245				
++	0.633	0.055	7.323	0.715				
Mean arterial blood pressure MAP (mmHg)	1.001	0.945	1.060	0.981				
Heart rate HR (bpm)	1.017	0.986	1.049	0.286				
Arterial blood lactate level lac (mmol/l)	1.337	0.728	2.455	0.348				
Demographics and clinical characteristics								
SOFA Score	1.012	0.910	1.126	0.821				
APACHE II Score	0.941	0.856	1.034	0.209				
Primary disease								
Sepsis/septic shock	0.824	0.322	2.109	0.824				
Acute coronary syndrome	1.037	0.254	4.236	0.960				
Traumatic brain injuries	0.633	0.055	7.323	0.715				
Gastrointestinal bleeding	0.633	0.055	7.323	0.715				

MAPSE, mitral annular plane systolic excursion; $DIVC_{end-expiratory}$, diameter of the inferior vena cava; TPASE, tricuspid annular plane systolic excursion; LVOT VTI T0, left ventricle outflow tract velocity time integral T0; RV_D/LV_D ratio, right to left ventricular end-diastolic dimensions ratio; Em, mitral diastolic filling Eatly; A m, mitral diastolic filling Atrial; Ea m, early diastolic velocity of the mitral annulus; APACHE II, Acute Physiology and Chronic Health Evaluation II; Sofa Score, Sequential Organ Failure Assessment Score.

alone cannot predict fluid responsiveness, it is necessary to understand that CVP is a marker of pressure and a regulating factor of venous return. Thus, an increase in CVP can be used as a clinical safety mechanism to avoid fluid overload and high RV filling pressure (30). In the present study, we found that a high CVP may reflect that the RV volume load has exceeded the normal range; failure to appreciate this limit may result in a VS rightward shift and reduced LVSV. It has been proposed that, once CVP has exceeded 10–14 mm Hg in non-intubated patients with acute RV myocardial infarction, further volume loading is detrimental. A mean CVP >14 mmHg is almost always associated with a reduced RVSWI (31, 32). Garcia-Montilla et al. (33) reported that the optimal RV filling pressure in patients with acute respiratory distress syndrome (ARDS) is 13 ± 2 mm Hg. Furthermore, they demonstrated that once CVP reaches 15 mmHg, further increments in filling pressure did not increase RVSPG; rather, due to overstretching of myocardial fibers, RVSPG decreased. These values may be considered the optimal RV filling pressure in patients with acute RV infarction or ARDS. Our results suggest that CVP >10.5 mmHg can predict whether VTI increases after a negative fluid balance in patients without underlying cardiac disease with high sensitivity but low specificity, when combined with RV_D/LV_D ratio ≥0.6 the predictive ability improved.

Notably, none of our patients experienced tissue perfusion insufficiency after negative fluid balance. However, the oxygenation index improved in both groups—especially VI Group. It is well-known that fluid overload may lead to pulmonary edema and failure of weaning from mechanical ventilation. A milestone study by National Heart, Lung, and Blood Institute Acute Respiratory Distress Syndrome (ARDS) Clinical Trials Network et al. (34) showed that a conservative fluid management protocol aimed to lower CVP resulted in a major reduction in net fluid balance, improving lung function and shortening the duration of mechanical ventilation. Clinicians should be alert to high CVP as it may indicate increased RV tension and leftward VS, potentially leading to increased left ventricular filling pressure and pulmonary edema.

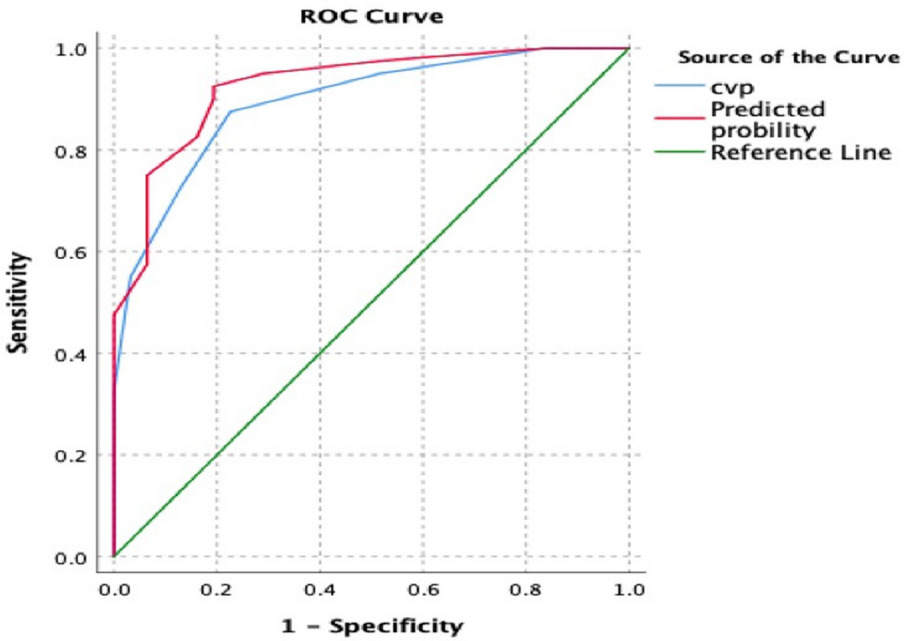

FIGURE 5 | The receiver operating characteristic (ROC) curves and the area under the ROC curve (AUC) for prediction of VTI increase after negative fluid balance. The "red model" included CVP and RV_D/LV_D ratio, while the "blue model" only included CVP. The AUC was 0.926 and 0.894, respectively. VTI, velocity time integral; CVP, central venous pressure; RV_D/LV_D ratio, right to left ventricular diastolic dimensions ratio.

Accurate fluid therapy for patients with high CVP (systemic congestion) will not lead to hypoperfusion, but will be beneficial for other organs.

This study has some limitations. First, it was a single- center, prospective cohort study. In addition, the sample size is limited, and may have thus systematically excluded some participant groups. As a pragmatic study, this population had similar characteristics to previous clinical audits using the same inclusion criteria. Although RV_D/LV_D ratio entered to the equation and the $P < 0.05$, but the range of 95% CI for OR was widely. A study with larger sample size is needed to confirm our findings. Secondly, although we excluded patients with any pre-existing heart disease based on clinical records or echocardiography, some patients might have developed subclinical heart disease after their last echocardiography. Thirdly, the determination of RV volume load may be imperfect, more accurate RV volume measurement should be performed in the future study. Fourthly, as all the participants were enrolled within 24 h of entering the ICU, the treatments prior to inclusion were implemented in other departments, the detailed information could not be obtained accurately, we will pay more attention to the collection of relevant information in future studies.

CONCLUSION

In general, this study challenges traditional fluid resuscitation, which is frequently used in everyday practice. We found negative fluid balance will not always lead to a decrease, even an increase, in LVSV in patients with high CVP ($\geq$8 mmHg) especially combined with RV_D/LV_D ratio $\geq$0.6. The underling mechanism may be related to the filling state of RV. High CVP value and RV_D/LV_D ratio $\geq$0.6 were significantly associated with RV stressed. Further studies of whether precise fluid management can improve patients' 28-day mortality, shorten ICU stay, or shorten the duration of mechanical ventilation are required.

DATA AVAILABILITY STATEMENT

The raw data supporting the conclusions of this article will be made available by the authors, without undue reservation.

ETHICS STATEMENT

The research protocol was reviewed and approved by Ethics Committee of Peking Union Medical College Hospital (PUMCH-S617). The patients/participants provided their written informed consent to participate in this study.

AUTHOR CONTRIBUTIONS

LD and WX: conception and design, review, and revision of the manuscript. DX and ZH: data extraction. ZH: statistical analysis, interpretation of data, and writing. All authors contributed to the article and approved the submitted version.

FUNDING

This work was supported by capital clinic research and demonstration application of diagnosis and treatment project (No. Z201100005520038).

SUPPLEMENTARY MATERIAL

The Supplementary Material for this article can be found online at: https://www.frontiersin.org/articles/10.3389/fmed.2021.715099/full#supplementary-material

REFERENCES

1. Rivers E, Nguyen B, Havstad S, Ressler J, Muzzin A, Knoblich B, et al. Early goal-directed therapy in the treatment of severe sepsis and septic shock. *N Engl J Med.* (2001) 345:1368–77. doi: 10.1056/NEJMoa010307
2. Boyd JH, Forbes J, Nakada TA, Walley KR, Russell JA. Fluid resuscitation in septic shock: a positive fluid balance and elevated central venous pressure are associated with increased mortality. *Crit Care Med.* (2011) 39:259–65. doi: 10.1097/CCM.0b013e3181feeb15
3. Acheampong A, Vincent JL. A positive fluid balance is an independent prognostic factor in patients with sepsis. *Crit Care.* (2015) 19:251. doi: 10.1186/s13054-015-0970-1
4. Wang XT, Yao B, Liu DW, Zhang HM. Central venous pressure dropped early is associated with organ function and prognosis in septic shock patients: a retrospective observational study. *Shock.* (2015) 44:426–30. doi: 10.1097/SHK.0000000000000445
5. Berlin DA, Bakker J. Starling curves and central venous pressure. *Crit Care.* (2015) 19:55. doi: 10.1186/s13054-015-0776-1
6. Magder S. Bench-to-bedside review: an approach to hemodynamic monitoring–Guyton at the bedside. *Crit Care.* (2012) 16:236. doi: 10.1186/cc11395
7. Pinsky MR. The right ventricle: interaction with the pulmonary circulation. *Crit Care.* (2016) 20:266. doi: 10.1186/s13054-016-1524-x
8. Takata M, Harasawa Y, Beloucif S, Robotham JL. Coupled vs. uncoupled pericardial constraint: effects on cardiac chamber interactions. *J Appl Physiol.* (1985) (1997) 83:1799–813. doi: 10.1152/jappl.1997.83.6.1799
9. Funk DJ, Jacobsohn E, Kumar A. The role of venous return in critical illness and shock-part I: physiology. *Crit Care Med.* (2013) 41:255–62. doi: 10.1097/CCM.0b013e3182772ab6
10. Martyn JA, Snider MT, Farago LF, Burke JF. Thermodilution right ventricular volume: a novel and better predictor of volume replacement in acute thermal injury. *J Trauma.* (1981) 21:619–26. doi: 10.1097/00005373-198108000-00005
11. Krishnan S, Schmidt GA. Acute right ventricular dysfunction: real-time management with echocardiography. *Chest.* (2015) 147:835–46. doi: 10.1378/chest.14-1335
12. Puchalski MD, Williams RV, Askovich B, Minich LL, Mart C, Tani LY. Assessment of right ventricular size and function: echo versus magnetic resonance imaging. *Congenit Heart Dis.* (2007) 2:27–31. doi: 10.1111/j.1747-0803.2007.00068.x
13. Dandel M, Hetzer R. Evaluation of the right ventricle by echocardiography: particularities and major challenges. *Expert Rev Cardiovasc Ther.* (2018) 16:259–75. doi: 10.1080/14779072.2018.1449646
14. Su L, Pan P, Li D, Zhang Q, Zhou X, Long Y, et al. Central venous pressure (CVP) reduction associated with higher cardiac output (CO) favors good prognosis of circulatory shock: a single-center, retrospective cohort study. *Front Med.* (2019) 6:216. doi: 10.3389/fmed.2019.00216
15. Atherton JJ, Moore TD, Lele SS, Thomson HL, Galbraith AJ, Belenkie I, et al. Diastolic ventricular interaction in chronic heart failure. *Lancet.* (1997) 349:1720–4. doi: 10.1016/S0140-6736(96)05109-4
16. Tyberg JV, Taichman GC, Smith ER, Douglas NW, Smiseth OA, Keon WJ. The relationship between pericardial pressure and right atrial pressure: an intraoperative study. *Circulation.* (1986) 73:428–32. doi: 10.1161/01.CIR.73.3.428
17. Rudski LG, Lai WW, Afilalo J, Hua L, Handschumacher MD, Chandrasekaran K, et al. Guidelines for the echocardiographic assessment of the right heart in adults: a report from the American Society of Echocardiography endorsed by the European Association of Echocardiography, a registered branch of the European Society of Cardiology, and the Canadian Society of Echocardiography. *J Am Soc Echocardiogr.* (2010) 23:685–713; quiz: 786–8. doi: 10.1016/j.echo.2010.05.010
18. Abou-Arab O, Moussa MD, Beyls C, Mahjoub Y. Comments on "right ventricular failure in septic shock: characterization, incidence and impact on fluid responsiveness": which parameter to assess right ventricular failure and venous congestion? *Crit Care.* (2021) 25:136. doi: 10.1186/s13054-021-03473-0
19. Vieillard-Baron A, Prigent A, Repesse X, Goudelin M, Prat G, Evrard B, et al. Right ventricular failure in septic shock: characterization, incidence and impact on fluid responsiveness. *Crit Care.* (2020) 24:630. doi: 10.1186/s13054-020-03345-z
20. Lai WW, Gauvreau K, Rivera ES, Saleeb S, Powell AJ, Geva T. Accuracy of guideline recommendations for two-dimensional quantification of the right ventricle by echocardiography. *Int J Cardiovasc Imaging.* (2008) 24:691–8. doi: 10.1007/s10554-008-9314-4
21. Haddad F, Hunt SA, Rosenthal DN, Murphy DJ. Right ventricular function in cardiovascular disease, part I: anatomy, physiology, aging, and functional assessment of the right ventricle. *Circulation.* (2008) 117:1436–48. doi: 10.1161/CIRCULATIONAHA.107.653576
22. Meyer G, Vieillard-Baron A, Planquette B. Recent advances in the management of pulmonary embolism: focus on the critically ill patients. *Ann Intensive Care.* (2016) 6:19. doi: 10.1186/s13613-016-0122-z
23. Wiesenack C, Fiegl C, Keyser A, Laule S, Prasser C, Keyl C. Continuously assessed right ventricular end-diastolic volume as a marker of cardiac preload and fluid responsiveness in mechanically ventilated cardiac surgical patients. *Crit Care.* (2005) 9:R226–33. doi: 10.1186/cc3503
24. Mercat A, Diehl JL, Meyer G, Teboul JL, Sors H. Hemodynamic effects of fluid loading in acute massive pulmonary embolism. *Crit Care Med.* (1999) 27:540–4. doi: 10.1097/00003246-199903000-00032
25. Fremont B, Pacouret G, Jacobi D, Puglisi R, Charbonnier B, de Labriolle A. Prognostic value of echocardiographic right/left ventricular end-diastolic diameter ratio in patients with acute pulmonary embolism: results from a monocenter registry of 1,416 patients. *Chest.* (2008) 133:358–62. doi: 10.1378/chest.07-1231
26. Beigel R, Cercek B, Luo H, Siegel RJ. Noninvasive evaluation of right atrial pressure. *J Am Soc Echocardiogr.* (2013) 26:1033–42. doi: 10.1016/j.echo.2013.06.004
27. Eskesen TG, Wetterslev M, Perner A. Systematic review including re-analyses of 1148 individual data sets of central venous pressure as a predictor of fluid responsiveness. *Intensive Care Med.* (2016) 42:324–32. doi: 10.1007/s00134-015-4168-4
28. Cecconi M, Hofer C, Teboul JL, Pettila V, Wilkman E, Molnar Z, et al. Fluid challenges in intensive care: the FENICE study: a global inception cohort

study. *Intensive Care Med.* (2015) 41:1529–37. doi: 10.1007/s00134-015-3850-x
29. Osman D, Ridel C, Ray P, Monnet X, Anguel N, Richard C, et al. Cardiac filling pressures are not appropriate to predict hemodynamic response to volume challenge. *Crit Care Med.* (2007) 35:64–8. doi: 10.1097/01.CCM.0000249851.94101.4F
30. Sondergaard S, Parkin G, Aneman A. Central venous pressure: we need to bring clinical use into physiological context. *Acta Anaesthesiol Scand.* (2015) 59:552–60. doi: 10.1111/aas.12490
31. Greyson CR. Pathophysiology of right ventricular failure. *Crit Care Med.* (2008) 36:S57–65. doi: 10.1097/01.CCM.0000296265.52518.70
32. Berisha S, Kastrati A, Goda A, Popa Y. Optimal value of filling pressure in the right side of the heart in acute right ventricular infarction. *Br Heart J.* (1990) 63:98–102. doi: 10.1136/hrt.63.2.98
33. Garcia-Montilla R, Imam F, Miao M, Stinson K, Khan A, Heitner S. Optimal right heart filling pressure in acute respiratory distress syndrome determined by strain echocardiography. *Echocardiography.* (2017) 34:851–61. doi: 10.1111/echo.13546
34. National Heart, Lung, and Blood Institute Acute Respiratory Distress Syndrome (ARDS) Clinical Trials Network, Wiedemann HP, Wheeler AP, Bernard GR, Thompson BT, Hayden D, et al. Comparison of two fluid-management strategies in acute lung injury. *N Engl J Med.* (2006) 354:2564–75. doi: 10.1056/NEJMoa062200

Conflict of Interest: The authors declare that the research was conducted in the absence of any commercial or financial relationships that could be construed as a potential conflict of interest.

Publisher's Note: All claims expressed in this article are solely those of the authors and do not necessarily represent those of their affiliated organizations, or those of the publisher, the editors and the reviewers. Any product that may be evaluated in this article, or claim that may be made by its manufacturer, is not guaranteed or endorsed by the publisher.

frontiers in Medicine

ORIGINAL RESEARCH
published: 08 October 2021
doi: 10.3389/fmed.2021.737810

First Attempt at Using Electrical Impedance Tomography to Predict High Flow Nasal Cannula Therapy Outcomes at an Early Phase

Zhe Li[1†], Zhiyun Zhang[1†], Qian Xia[1], Danling Xu[1], Shaojie Qin[1], Meng Dai[2], Feng Fu[2], Yuan Gao[1] and Zhanqi Zhao[2,3*]*

[1] Department of Critical Care Medicine, Renji Hospital, School of Medicine, Shanghai Jiao Tong University, Shanghai, China, [2] Department of Biomedical Engineering, Fourth Military Medical University, Xi'an, China, [3] Institute of Technical Medicine, Furtwangen University, Villingen-Schwenningen, Germany

OPEN ACCESS

Edited by:
Savino Spadaro,
University of Ferrara, Italy

Reviewed by:
Gaetano Scaramuzzo,
University of Ferrara, Italy
Elena Spinelli,
IRCCS Ca 'Granda Foundation Maggiore Policlinico Hospital, Italy

***Correspondence:**
Yuan Gao
rj_gaoyuan@163.com
Zhanqi Zhao
zhanqi.zhao@hs-furtwangen.de

[†] These authors have contributed equally to this work

Specialty section:
This article was submitted to Intensive Care Medicine and Anesthesiology, a section of the journal Frontiers in Medicine

Received: 07 July 2021
Accepted: 07 September 2021
Published: 08 October 2021

Citation:
Li Z, Zhang Z, Xia Q, Xu D, Qin S, Dai M, Fu F, Gao Y and Zhao Z (2021) First Attempt at Using Electrical Impedance Tomography to Predict High Flow Nasal Cannula Therapy Outcomes at an Early Phase. Front. Med. 8:737810. doi: 10.3389/fmed.2021.737810

Objective: Spatial and temporal ventilation distributions in patients with acute respiratory failure during high flow nasal cannula (HFNC) therapy were previously studied with electrical impedance tomography (EIT). The aim of the study was to explore the possibility of predicting HFNC failure based on various EIT-derived parameters.

Methods: High flow nasal cannula failure was defined reintubation within 48 h after HFNC. EIT was performed with the patients spontaneously breathing in the supine position at the start of HFNC. EIT-based indices (comprising the global inhomogeneity index, center of ventilation, ventilation delay, rapid shallow breathing index, minute volume, and inspiration to expiration time) were explored and evaluated at three time points (prior to HFNC, T1; 30 min after HFNC started, T2; and 1 h after, T3).

Results: A total of 46 subjects were included in the final analysis. Eleven subjects had failed HFNC. The time to failure was 27.8 ± 12.4 h. The ROX index (defined as SpO_2/FiO_2/respiratory rate) for HFNC success patients was 8.3 ± 2.7 and for HFNC failure patients, 6.2 ± 1.8 ($p = 0.23$). None of the investigated EIT-based parameters showed significant differences between subjects with HFNC failure and success. Further subgroup analysis indicated that a significant difference in ventilation inhomogeneity was found between ARDS and non-ARDS [0.54 (0.37) vs. 0.46 (0.28) as evaluated with *GI*, $p < 0.01$]. Ventilation homogeneity significantly improved in ARDS after 60-min HFNC treatment [0.59 (0.20) vs 0.57 (0.19), T1 vs. T3, $p < 0.05$].

Conclusion: Spatial and temporal ventilation distributions were slightly but insignificantly different between the HFNC success and failure groups. HFNC failure could not be predicted by changes in EIT temporal and spatial indexes of ventilation distribution within the first hour. Further studies are required to predict the outcomes of HFNC.

Keywords: high flow nasal cannula, electrical impedance tomography, acute respiratory failure, ventilation distribution, outcome prediction

INTRODUCTION

High flow nasal cannula therapy may help avoid invasive mechanical ventilation in patients with hypoxemia (1). Recent studies have indicated that a high flow nasal cannula (HFNC) improves respiratory drive and lung mechanics and enhances CO_2 removal (2, 3). HFNC introduces low levels of airway pressure, which increase end-expiratory lung volume and improve oxygenation and regional lung aeration (4). However, in cases of HFNC failure, a delay in mechanical ventilation may result in deterioration in patient outcomes. Therefore, early prediction of HFNC outcomes is important in order for clinicians to decide the need for mechanical ventilation. Higher simplified acute physiology score II, the severity of hypoxemia, and C-reactive protein level may be correlated with HFNC failure (5, 6). A simple index calculated as the ratio of SpO_2/FiO_2 to respiratory rate may be able to identify HFNC failure after a 12-h trial (7). This index does not directly reflect ventilation status and may, therefore, require a longer period to identify the HFNC failure.

Electrical impedance tomography (EIT) is a novel noninvasive, radiation-free, bedside method for monitoring ventilation changes related to different lung conditions. These include lung regional recruitment and overdistension during positive end-expiratory pressure (PEEP) titration in patients with acute respiratory distress syndrome (8–11). Various EIT-based parameters were proposed to evaluate the status of ventilation in patients with spontaneous breathing (12, 13). In addition, previous studies have shown that EIT can be used to assess the effect of HFNC on regional ventilation (14, 15).

This study aimed to describe the evolution of spatial and temporal ventilation distributions in patients with acute respiratory failure (ARF) during the first hour of HFNC. Furthermore, we examined the possibility of predicting HFNC failure based on regional ventilation information derived from the EIT.

METHODS

Subjects and Measurement

The study protocol was approved by the ethics committees of Renji Hospital, School of Medicine, Shanghai Jiao Tong University (KY2021-057-B). Written informed consent was obtained from all the subjects before the study.

Patients who were treated with HFNC after ICU admission from 2021.05.27 to 2021.06.20 were screened. Only patients with acute respiratory failure ARF (respiratory rate >25 breaths/min, $PaO_2/FiO_2 < 300$ mmHg) were included. Exclusion criteria included age <18 years, pregnancy, and lactation period, weaning from the ventilator, intubation required, tracheotomy, bronchoscopy, absence of commitment to pursue full life support, and any contraindication to the use of EIT (pacemaker, automatic implantable cardioverter defibrillator, and implantable pumps).

High flow nasal cannula was performed with Optiflow (Fisher and Paykel Healthcare, East Tamaki, New Zealand) or HFNC module in V300 or V500 (Dräger Medical, Lübeck, Germany). The initial flow setting was 50–60 L/min with heated and humidified oxygen ($FiO_2 = 1$). When peripheral oxygen saturation was over 92%, FiO_2 was reduced gradually. The flow was reduced in the first hour only if the patient felt uncomfortable with the rate. HFNC failure was defined as exacerbation after HFNC, which led to intubation within 48 h. The indications for invasive mechanical ventilation included the level of consciousness (Glasgow coma score < 12), cardiac arrest/arrhythmias and severe hemodynamic instability (norepinephrine > 0.1 μg/kg/min), and a persistent or worsening respiratory condition. This was defined as at least two of the following conditions: failure to achieve correct oxygenation ($PaO_2 < 60$ mmHg despite HFNC flow ≥ 30 L/min and FiO_2 of 1), respiratory acidosis ($PaCO_2 > 50$ mmHg with pH < 7.25), respiratory rate > 30 bpm or inability to clear secretions. The ROX index [defined as SpO_2/FiO_2/respiratory rate (7)] was calculated 1 h after HFNC.

Electrical impedance tomography was performed with the patients spontaneously breathing in the supine position at the start of HFNC. An EIT electrode belt with 16 electrodes was placed around the thorax at the 4th intercostal space, and one reference electrode was placed on the abdomen (PulmoVista 500, Dräger Medical, Lübeck, Germany). Electrical alternating currents were applied in a sequential rotating process. The frequency and the amplitude of the currents were determined automatically according to the background noise of the measurement environment. The resulting surface potential differences between neighboring electrode pairs were measured and recorded at 20 Hz for 1 h. Image reconstruction using this algorithm was performed using the software of the manufacturer (EIT Data Review Tool, Dräger Medical, Lübeck, Germany). The EIT data were analyzed offline with customized software programmed with MATLAB R2015 (The MathWorks Inc., Natick, MA).

EIT Data Analysis

Functional EIT (fEIT)-tidal variation (TV) was calculated by subtracting the end-expiration from the end-inspiration image, representing the variation during tidal breathing. Tidal images of 1 min were averaged to increase the signal-to-noise ratio.

$$TV_i = \frac{1}{N}\sum_{n=1}^{N}\left(Z_{i,Ins,n} - Z_{i,Exp,n}\right) \quad (1)$$

where TV_i is the pixel i in the fEIT image; N is the number of breaths within the analyzed period; and $\Delta Z_{i,Ins}$ and $\Delta Z_{i,Exp}$ are the pixel values in the raw EIT image at end inspiration and end expiration, respectively. When $TV_i < 0$, a value of 0 was assigned to TV_i.

Several EIT-based indices were explored and evaluated at three time points (before HFNC, T1; 30 min after HFNC started, T2; 1 h after, T3). They are explained in detail in the remainder of this section. To investigate the changes from the baseline and treatment, the differences of the EIT indices between the time points were calculated and normalized to the values at T1. The normalized values were denoted as Δ_{T3-T1} and Δ_{T3-T2}, respectively.

The global inhomogeneity (*GI*) index is calculated from the tidal EIT images to summarize the heterogeneity of ventilation (16).

$$GI = \frac{\sum_{l \in lung} \left| TV_l - Median(TV_{lung}) \right|}{\sum_{l \in lung} TV_l} \quad (2)$$

where TV denotes the value of the differential impedance in the tidal images; TV_l is the pixel in the identified lung area; pixel l is considered as a lung region if $TV_l > 10\% \times \max(TV)$. TV_{lung} denotes all pixels representing the lung area. A high-GI index implies high variation among pixel tidal impedance values.

The center of ventilation (CoV) depicts the ventilation distribution influenced by gravity or various lung diseases (relative impedance value weighted with a location in the anteroposterior coordinate) (17):

$$CoV = \frac{\sum (y_i \times TV_i)}{\sum TV_i} \times 100\% \quad (3)$$

where TV_i is the impedance change in the fEIT image for pixel i; y_i is the height of pixel i, and the value is scaled such that the bottom of the image (dorsal) is 100% and the top (ventral) is 0%.

The tidal image was divided into four horizontal, anterior-to-posterior segments of equal height (regions of interest, ROI). The ventilation distributions in these regions were calculated and denoted as *ROIs 1-4*. The regional ventilation delay (RVD) index characterizes the regional ventilation delay as pixel impedance rising time compared to the global impedance curve (18), which may be used to assess tidal recruitment/derecruitment.

$$RVD_l = \frac{t_{l,40\%}}{T_{inspiration,\,global}} \times 100\% \quad (4)$$

where $t_{l,40\%}$ is the time required for pixel l to reach 40% of its maximum inspiratory impedance change. $T_{inspiration,\,global}$ denotes the inspiration time calculated from the global impedance curve.

Besides the conventional EIT-based indices, we constructed further parameters that are relevant to spontaneously breathing patients but are difficult to record without additional devices. The rapid shallow breathing index (RSBI) is defined as the ratio of the respiratory rate to tidal volume. Since the change in tidal volume can be estimated by the measured impedance, $RSBI_{EIT}$ was calculated as the ratio of the respiratory rate to tidal impedance variation in arbitrary units. Similarly, minute volume was estimated as the multiplication of the respiratory rate and tidal impedance variation in arbitrary units (MV_{EIT}). Inspiration time over expiration time (*I:E*) was calculated based on the global impedance—time curves.

Statistical Analysis

Normal distribution was assessed with the Kolmogorov-Smirnov normality test. Normally distributed results were presented as the mean ± SD. Non-normally distributed results were presented as median (interquartile range). The Kruskal–Wallis test was used to compare the parameters at different time points. The Mann–Whitney test was used to compare the EIT parameters between the HFNC success and failure groups. Because EIT can only deliver relative impedance changes, therefore, only the changes in RVD, $RSBI_{EIT}$, and MV_{EIT} were compared between groups. A $p < 0.05$ was considered statistically significant. Bonferroni correction was used to adjust the p-value for multiple comparisons of different time points or ROIs.

RESULTS

A total of 48 subjects were included in the study. Two patients were excluded from the final analysis due to poor EIT data quality (intensive patient movement). The demographics and outcomes of the 46 subjects are summarized in **Table 1**. Totally, 11 patients had failed HFNC. The time to failure was 27.8 ± 12.4 h. The ROX index for HFNC success patients was 8.3 ± 2.7 and for HFNC failure patients, 6.2 ± 1.8 ($p = 0.23$). Twelve patients had a fever (body temperature > 37°C). Two of them were > 38.5°C. Of the HFNC success patients, 21 were not sedated. Of the HFNC failure patients, five were not sedated. No significant differences were found ($p = 0.40$).

Table 2 summarizes the main causes of ARF and the comorbidities of the study subjects. ARF was mainly caused by acute respiratory distress syndrome (ARDS) and pneumonia. Hypertension was the most common comorbidity.

None of the investigated EIT-based parameters showed significant differences between the subjects with HFNC failure and success. **Table 3** summarizes the absolute values of the EIT-derived parameters at different time points (*GI*, *CoV*, and *I:E*). **Figure 1** shows the trends of EIT parameters at different time points. **Figures 2**, **3** compare the EIT-based parameters at different time points between the groups with HFNC failure and success. In the failure group, ventilation was distributed slightly toward the dorsal regions, as indicated by CoV (**Figure 2**, middle; $p > 0.05$). Ventilation delay decreased in both failure and success groups compared to T1, but, as compared to T2, the ventilation delay was worse at T3 in the failure group (**Figure 2**, bottom; $p > 0.05$). Elevated $RSBI_{EIT}$ and shorter inspiration time (lower *I:E*) were found in the failure group at T3 compared to T1 (**Figure 3**, top; $p > 0.05$). MV_{EIT} decreased in the HFNC failure group compared to that in T2, while the median in the success group was higher (**Figure 3** middle; $p > 0.05$).

Further subgroup analysis indicated that significant difference in ventilation inhomogeneity was found between ARDS and non-ARDS [0.54 (0.37) vs. 0.46 (0.28) as evaluated with *GI*, $p < 0.01$]. Ventilation homogeneity significantly improved in ARDS after 60 min HFNC treatment [0.59 (0.20) vs 0.57 (0.19), T1 vs. T3, $p < 0.05$].

DISCUSSION

In the present study, we have examined the ability to predict the outcome of HFNC within the first hour of treatment using EIT. Differences in spatial and temporal ventilation between the HFNC failure and success groups were observed, but they were not statistically significant.

TABLE 1 | Demographics and outcomes of the studied subjects.

Pat. No.	Age	Gender	APACHE II	Height (cm)	Weight (kg)	init. FiO_2	init. PaO_2	ROX	HFNC success	Dead
1	53	F	10	160	56	0.90	72	6.67	1	0
2	39	M	8	172	88	0.80	92	8.95	1	0
3	77	F	12	159	57	0.55	97	5.00	1	0
4	74	M	8	175	68	0.55	78	8.82	0	1
5	82	M	10	177	68	0.80	87	5.94	1	0
6	89	M	16	174	65	0.40	56	6.96	1	0
7	82	M	18	170	68	0.55	68	12.82	1	0
8	67	M	14	173	69	0.70	45	8.67	1	0
9	50	M	8	168	59	0.80	69	7.68	1	0
10	67	M	24	173	68	0.55	82	9.90	1	0
11	35	M	25	170	85	1.00	184	4.44	1	0
12	67	M	20	172	69	0.50	69	5.35	0	0
13	75	M	15	176	64	0.50	47	4.69	0	0
14	72	M	22	178	63	0.60	73	6.94	0	1
15	65	F	15	158	56	1.00	84	4.78	0	0
16	79	M	18	171	59	1.00	64	6.65	0	1
17	76	F	24	158	63	0.60	73	3.07	0	1
18	52	M	24	172	70	0.55	70	6.40	1	0
19	66	M	13	174	69	0.60	51	5.22	1	0
20	72	M	18	175	73	0.60	84	9.26	1	0
21	66	M	21	173	69	0.40	68	4.85	0	0
22	77	M	24	178	65	0.45	61	7.84	1	0
23	83	M	18	169	82	0.80	232	6.94	1	0
24	69	M	24	173	69	1.00	58	6.67	1	0
25	62	M	17	176	68	0.50	65	6.74	1	0
26	66	M	16	174	71	0.50	130	9.26	1	0
27	72	M	18	172	61	0.45	68	8.25	1	0
28	68	M	16	170	58	0.50	100	7.25	1	1
29	77	F	12	155	49	0.50	67	6.27	1	0
30	73	M	17	172	79	0.55	63	6.17	0	1
31	77	M	25	173	72	0.55	83	5.29	1	0
32	51	F	24	155	55	0.60	84	8.98	1	0
33	57	M	25	168	58	0.60	68	7.84	1	0
34	66	F	18	155	57	0.50	65	8.51	1	0
35	66	M	14	173	65	0.50	82	11.70	1	0
36	63	M	17	174	68	0.50	67	8.17	0	1
37	31	F	20	161	56	0.40	57	6.11	1	0
38	54	M	14	175	68	0.50	70	18.46	1	0
39	63	F	13	156	63	0.33	89	10.00	1	0
40	52	M	14	172	65	0.70	153	7.57	1	0
41	82	M	24	172	55	0.50	60	11.53	1	0
42	67	F	17	158	65	0.50	69	8.61	0	0
43	74	M	18	178	59	0.50	62	11.00	1	0
44	52	M	24	169	64	0.50	65	9.51	1	0
45	73	M	24	174	59	0.90	50	8.08	1	0
46	58	F	24	158	51	0.70	83	10.42	1	0
Mean	66	M:F	18	169	65	0.61	80	7.83	s:f	d:a
SD	13	35:11	5	7	8	0.18	34	2.65	35:11	7:39

Pat. No., patient number; SD, standard deviation; M, male; F, female; APACHE II, Acute Physiology and Chronic Health Evaluation II; init, initial; FiO_2, fractional inspired oxygen; PaO_2, arterial oxygen partial pressure; s:f, success vs. failure; d:a, dead vs. alive.

FiO_2 and PaO_2 are values recorded during oxygen therapy before high flow nasal cannula (HFNC).

ROX index, SpO_2/FiO_2/respiratory rate HFNC success was marked 1 and failure marked 0.

Dead marked subjects died in the ICU.

Previous studies indicated that HFNC failure may lead to intubation delay and increase hospitalization time and mortality. Roca et al. showed that the HFNC failure rate in patients with severe pneumonia was up to 28% (19). Rello et al. found that, in patients with confirmed 2009 influenza A/H1N1v infection, the mortality in the HFNC failure group was 27%, whereas the mortality in initially intubated patients was only 20% (20). Kang et al. revealed in a retrospective study that the mortality was significantly higher in patients intubated after 48-h HFNC failure compared with those who were intubated within 48-h HFNC (21). The extubation rate was lower in the HFNC failure after 48 h. Recent studies have indicated that the mortality rate in intubated patients after HFNC failure was around 30–50% (22). When the respiratory drive of the patient was too high, the high-flow rate might induce overdistension (23). EIT has been used to monitor the ventilation during HFNC. A recent study has indicated that EIT can help to identify the overdistension caused by HFNC (15). Besides, EIT can observe pendelluft and diaphragm activities and monitor the corresponding lung injury, which may help to identify the respiratory drive of the patient (24–26).

TABLE 2 | Summary of primary etiology for ARF and the comorbidities.

	HFNC success	HFNC failure
$n = 46$	35	11
Primary etiology for ARF		
ARDS	15	5
Pneumonia	12	5
Cardiogenic pulmonary edema	7	0
Pulmonary embolism	1	1
Comorbidity		
Hypertension	12	7
Congestive heart failure	5	4
Cerebral vascular disease	4	2
Chronic kidney disease	4	3
Chronic pulmonary disease	4	0
Diabetes	7	4

ARF, acute respiratory failure; ARDS, acute respiratory distress syndrome.

TABLE 3 | A summary of the absolute values of electrical impedance tomography (EIT)-derived parameters and the comparison between groups at different time points.

		HFNC success	HFNC falure	*p*
GI	T1	0.48 (0.38–0.68)	0.54 (0.41-0.68)	0.63
	T2	0.48 (0.42–0.71)	0.50 (0.40–0.62)	0.78
	T3	0.50 (0.39–0.71)	0.50 (0.39–0.65)	0.94
CoV (%)	T1	45.4 (42.4–48.8)	44.0 (42.1–46.1)	0.61
	T2	46.8 (41.9–49.8)	44.3 (42.2–46.1)	0.39
	T3	46.6 (41.3–49.8)	45.4 (43.1–46.3)	0.72
I:E	T1	0.64 (0.53–0.71)	0.73 (0.48–0.82)	0.36
	T2	0.58 (0.5–0.68)	0.64 (0.47–0.80)	0.61
	T3	0.61 (0.48–0.70)	0.64 (0.48–0.71)	0.88

In previous studies, EIT has been used mainly as a monitoring tool to demonstrate its superiority over other ventilation modes. For example, HFNC was found to be superior to conventional oxygen therapy or noninvasive ventilation in regard ventilation distribution, end-expiratory lung volume, and respiratory rate, etc., (27, 28). However, the ability to predict the HFNC outcomes has yet to be explored. Previously, the so-called ROX index was proposed (19). The ROX index is relatively easy to obtain and has great potential to predict HFNC outcomes within a few hours after initiating HFNC (7, 19). However, it seems that its effective cutoff value varies depending on the time point of observation and disease. For our study patients (mainly lung healthy subjects after abdominal surgery), the specificity of ROX at 1 h was low (0.36), which is not enough to identify HFNC failure. On the other hand, HFNC results in ventilation redistribution within a brief period as demonstrated in previous studies [e.g., (4, 15)]. Therefore, we took the challenge, attempting to predict the outcome of HFNC within the first hour of treatment. For the selection of EIT-based parameters, we have tested some of the most widely used EIT indices, such as *GI* and *CoV* (29). In addition, the equivalent parameters $RSBI_{EIT}$, MV_{EIT}, and *I:E*

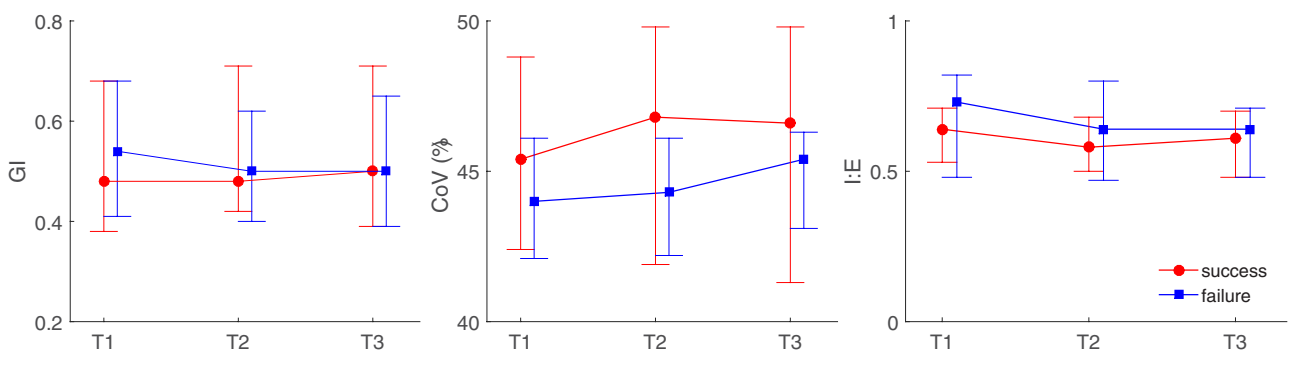

FIGURE 1 | Illustration of electrical impedance tomography (EIT)-derived parameters at different time points between high flow nasal cannula (HFNC) success and failure groups. GI, the global inhomogeneity index; CoV, center of ventilation; I:E, inspiration to the expiration time. T1, before HFNC; T2, 30 min after HFNC started; T3, 1 h after HFNC started.

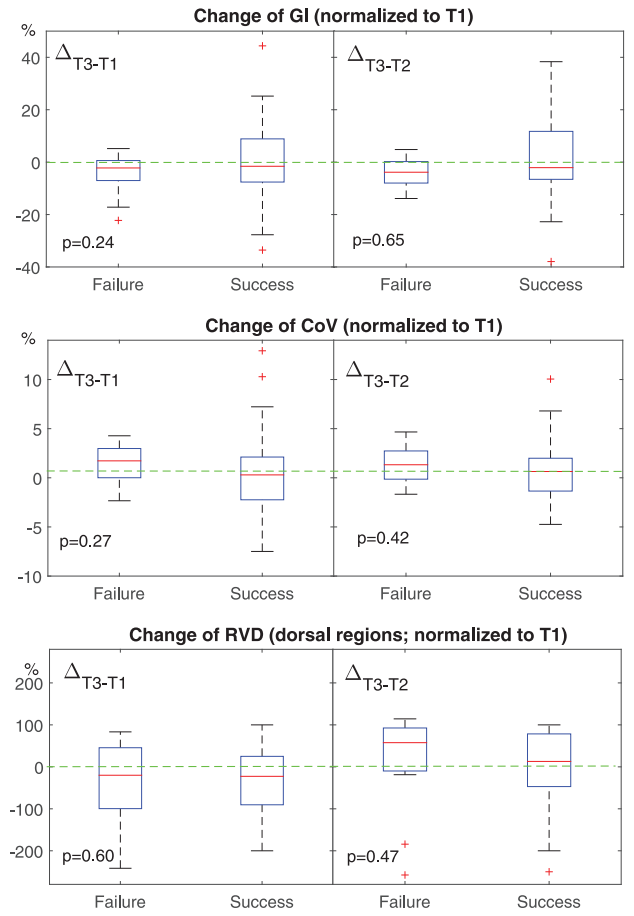

FIGURE 2 | Change of conventional EIT-based parameters at different time points. T1, before HFNC; T2, 30 min after HFNC started; T3, 1 h after HFNC started. All values were normalized to that at T1. The boxes mark the quartiles with median marked red, while the whiskers extend from the box out to the most extreme data value within 1.5* the interquartile range of the sample. The red crosses are outliers. Green dashed lines marked the value of 0. GI, the global inhomogeneity index. Lower than 0 means the ventilation becomes more homogeneous. CoV, the center of ventilation. Higher than 0 means that the ventilation distribution moves toward dorsal regions. RVD, regional ventilation delay. Higher than 0 means the delay is getting worse.

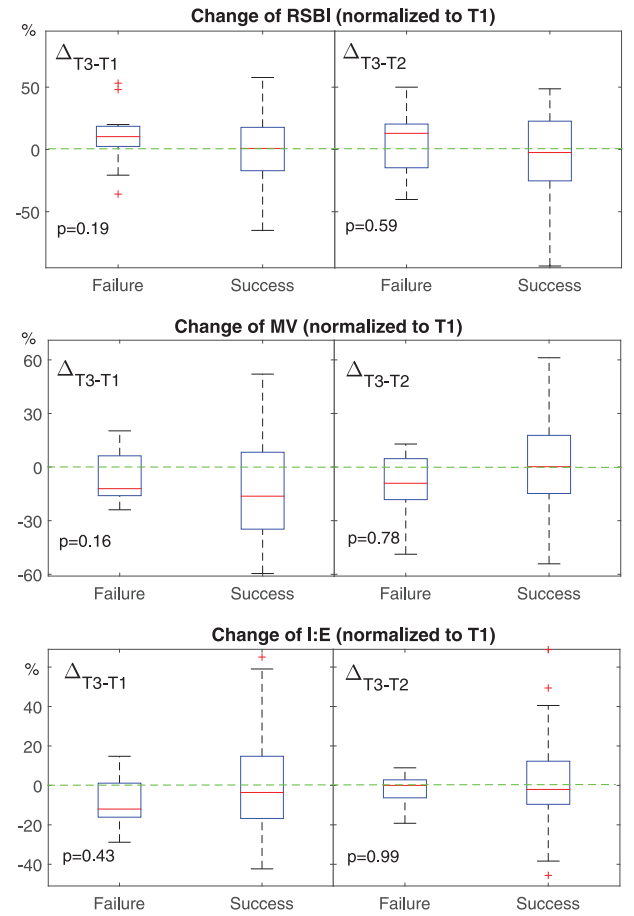

FIGURE 3 | Change of EIT-based parameters for spontaneous breathing at different time points. T1, before HFNC; T2, 30 min after HFNC started; T3, 1 h after HFNC started. All values were normalized to that at T1. The boxes mark the quartiles with median marked red, while the whiskers extend from the box out to the most extreme data value within 1.5* the interquartile range of the sample. The red crosses are outliers. Green dashed lines marked the value of 0. RSBI, rapid shallow breathing index. Higher than 0 means the subject is breathing more rapidly or shallowly. MV, minute volume. Lower than 0 means the minute volume becomes less at T3. I:E, inspiration to the expiration time. Lower than 0 means the inspiration time is getting shorter.

were evaluated because the ventilated volume was not usefully monitored during HFNC.

We found that ventilation was distributed slightly toward the dorsal regions in the failure group (**Figures 1**, **2**, *CoV*). Previous studies suggested that ventilation distribution in the dorsal regions might be associated with diaphragm activity (25). The differences found in *CoV* might indicate an increased respiratory effort in the failure group, which implied an unsatisfactory oxygen delivery. Due to the nature of the study (observational design), we did not include the measurements of transdiaphragmatic pressure or diaphragmatic ultrasound to confirm this speculation. A similar trend of $RSBI_{EIT}$ was observed that might as well support our hypothesis (**Figure 3**, *RSBI*). When the respiratory muscle was fatigued, the inspiration time became shorter and MV decreased at T3 compared to the baseline (**Figure 3**). Ventilation delay at T3 decreased in both failure and success groups compared to T1, but, as compared to T2, it deteriorated in the failure group (**Figure 2** *RVD*). The *RVD* index was initially developed and evaluated during low-flow maneuvers (16). We suspect that, during spontaneous breathing, the inspiration time is too short to have a stable *RVD* value. A recent study has shown that the coefficient of variation for *RVD* in healthy subjects was high (30), which might be the reason why no significant difference could be found in the present study.

Another potential parameter that could be used to evaluate the effect of HFNC is the change in end-expiratory lung impedance

(ΔEELI), which is associated with end-expiratory lung volume. Mauri et al. evaluated the lung mechanics during HFNC in 17 patients with respiratory failure (2). They found that ΔEELI increased and MV decreased with an increasing flow rate during HFNC. We did not explore the parameter ΔEELI for two reasons: (1) As suggested by a previous study (15), HFNC may introduce overdistension as well. Overdistension would lead to an increased EELI but decreased tidal volume, which may explain the finding in the study of Mauri (2). (2) In our study, the impedance value was not normalized to volume so that the ΔEELI was not inter-patient comparable.

Unfortunately, none of the explored EIT-based parameters showed statistical significance when comparing the HFNC success and failure groups. We suspected that a large portion of the included subjects was admitted to ICU after abdominal surgery. Their lung function might be satisfactory, but the pain from the wound might have influenced their respiratory muscles. Moreover, the sample size was small, and only a few patients required intubation. Since this was the first attempt to use EIT to predict an HFNC outcome, no *a priori* information was available to calculate the sample size. The study could be underpowered depending on which parameter was being evaluated. Further studies can be designed based on the current findings. The subject group must be carefully selected. Another limitation of the study design was that only the first hour of EIT data was recorded so that the observation period was very short. It is unclear whether the changes in spatial and temporal ventilation distribution at a later time point could predict the HFNC outcomes.

CONCLUSION

Spatial and temporal ventilation distributions were slightly but insignificantly different for HFNC success and failure groups. HFNC failure could not be predicted by changes in EIT temporal and spatial indexes of ventilation distribution within the first hour. Further studies are required to develop an early indicator to predict the outcome of HFNC.

DATA AVAILABILITY STATEMENT

The original contributions presented in the study are included in the article/supplementary material, further inquiries can be directed to the corresponding author/s.

ETHICS STATEMENT

The studies involving human participants were reviewed and approved by Ethics Committees of Renji Hospital, School of Medicine, Shanghai Jiao Tong University (KY2021-057-B). The patients/participants provided their written informed consent to participate in this study.

AUTHOR CONTRIBUTIONS

ZL, YG, and ZZhao have designed the study. ZZhang, QX, DX, and SQ have performed the measurements and collected the data. ZL, ZZhang, MD, and FF have analyzed the data. ZL, ZZhang, YG, and ZZhao have drafted the manuscript. QX, DX, SQ, MD, and FF have revised the manuscript. All the authors have approved the final version.

FUNDING

This study was supported by Shanghai Jiao Tong University (YG2019ZDB04) and the National Natural Science Foundation of China (52077216).

REFERENCES

1. Yasuda H, Okano H, Mayumi T, Nakane M, Shime N. Association of noninvasive respiratory support with mortality and intubation rates in acute respiratory failure: a systematic review and network meta-analysis. *J Intensive Care.* (2021) 9:32. doi: 10.1186/s40560-021-00539-7
2. Mauri T, Alban L, Turrini C, Cambiaghi B, Carlesso E, Taccone P, et al. Optimum support by high-flow nasal cannula in acute hypoxemic respiratory failure: effects of increasing flow rates. *Intensive Care Med.* (2017) 43:1453–63. doi: 10.1007/s00134-017-4890-1
3. Braunlich J, Beyer D, Mai D, Hammerschmidt S, Seyfarth HJ, Wirtz H. Effects of nasal high flow on ventilation in volunteers, COPD and idiopathic pulmonary fibrosis patients. *Respiration.* (2013) 85:319–25. doi: 10.1159/000342027
4. Mauri T, Turrini C, Eronia N, Grasselli G, Volta CA, Bellani G, et al. Physiologic effects of high-flow nasal cannula in acute hypoxemic respiratory failure. *Am J Respir Crit Care Med.* (2017) 195:1207–15. doi: 10.1164/rccm.201605-0916OC
5. Messika J, Ben Ahmed K, Gaudry S, Miguel-Montanes R, Rafat C, Sztrymf B, et al. Use of high-flow nasal cannula oxygen therapy in subjects with ARDS: a 1-year observational study. *Respir Care.* (2014) 60:162–9. doi: 10.4187/respcare.03423
6. Vianello A, Arcaro G, Molena B, Turato C, Sukthi A, Guarnieri G, et al. High-flow nasal cannula oxygen therapy to treat patients with hypoxemic acute respiratory failure consequent to SARS-CoV-2 infection. *Thorax.* (2020) 75:998–1000. doi: 10.1136/thoraxjnl-2020-214993
7. Roca O, Caralt B, Messika J, Samper M, Sztrymf B, Hernández G, et al. An index combining respiratory rate and oxygenation to predict outcome of nasal high-flow therapy. *Am J Respir Crit Care Med.* (2019) 199:1368–76. doi: 10.1164/rccm.201803-0589OC
8. Liu S, Tan L, Moller K, Frerichs I, Yu T, Liu L, et al. Identification of regional overdistension, recruitment and cyclic alveolar collapse with electrical impedance tomography in an experimental ARDS model. *Crit Care.* (2016) 20:119. doi: 10.1186/s13054-016-1300-y
9. Franchineau G, Brechot N, Lebreton G, Hekimian G, Nieszkowska A, Trouillet JL, et al. Bedside contribution of electrical impedance tomography to setting positive end-expiratory pressure for extracorporeal membrane oxygenation-treated patients with severe acute respiratory distress syndrome. *Am J Respir Crit Care Med.* (2017) 196:447–57. doi: 10.1164/rccm.201605-1055OC
10. Perier F, Tuffet S, Maraffi T, Alcala G, Victor M, Haudebourg A-F, et al. Electrical impedance tomography to titrate positive end-expiratory pressure in COVID-19 acute respiratory distress syndrome. *Critical Care.* (2020) 24:678. doi: 10.1186/s13054-020-03414-3
11. Scaramuzzo G, Spadaro S, Corte FD, Waldmann AD, Bohm SH, Ragazzi, R, et al., Personalized positive end-expiratory pressure in acute respiratory distress syndrome: comparison between optimal distribution of regional ventilation and positive transpulmonary pressure. *Crit Care Med.* (2020) 48:1148–56. doi: 10.1097/CCM.0000000000004439

12. Krauss E, van der Beck D, Schmalz I, Wilhelm J, Tello S, Dartsch RC, et al. Evaluation of regional pulmonary ventilation in spontaneously breathing patients with idiopathic pulmonary fibrosis (IPF) employing electrical impedance tomography (EIT): a pilot study from the European IPF registry (eurIPFreg). *J Clin Med.* (2021) 10:192. doi: 10.3390/jcm10020192
13. Zhao Z, Peng SY, Chang MY, Hsu YL, Frerichs I, Chang HT, et al. Spontaneous breathing trials after prolonged mechanical ventilation monitored by electrical impedance tomography: an observational study. *Acta Anaesthesiol Scand.* (2017) 61:1166–75. doi: 10.1111/aas.12959
14. Hough JL, Pham TM, Schibler A. Physiologic effect of high-flow nasal cannula in infants with bronchiolitis. *Pediatr Crit Care Med.* (2014) 15:e214–219. doi: 10.1097/PCC.0000000000000112
15. Zhang R, He H, Yun L, Zhou X, Wang X, Chi Y, et al. Effect of postextubation high-flow nasal cannula therapy on lung recruitment and overdistension in high-risk patient. *Critical Care.* (2020) 24:82. doi: 10.1186/s13054-020-2809-7
16. Zhao Z, Möller K, Steinmann D, Frerichs I, Guttmann J. Evaluation of an electrical impedance tomography-based global inhomogeneity index for pulmonary ventilation distribution. *Intensive Care Med.* (2009) 35:1900–6. doi: 10.1007/s00134-009-1589-y
17. Frerichs I, Hahn G, Golisch W, Kurpitz M, Burchardi H, Hellige G. Monitoring perioperative changes in distribution of pulmonary ventilation by functional electrical impedance tomography. *Acta Anaesthesiol Scand.* (1998) 42:721–6. doi: 10.1111/j.1399-6576.1998.tb05308.x
18. Muders T, Luepschen H, Zinserling J, Greschus S, Fimmers R, Guenther U, et al. Tidal recruitment assessed by electrical impedance tomography and computed tomography in a porcine model of lung injury. *Crit Care Med.* (2012) 40:903–11. doi: 10.1097/CCM.0b013e318236f452
19. Roca O, Messika J, Caralt B. Garcia-de-Acilu M, Sztrymf B, Ricard JD, Masclans JR: Predicting success of high-flow nasal cannula in pneumonia patients with hypoxemic respiratory failure: The utility of the ROX index. *J Crit Care.* (2016) 35:200–5. doi: 10.1016/j.jcrc.2016.05.022
20. Rello J, Perez M, Roca O, Poulakou G, Souto J, Laborda C, et al. High-flow nasal therapy in adults with severe acute respiratory infection: a cohort study in patients with 2009 influenza A/H1N1v. *J Crit Care.* (2012) 27:434–9. doi: 10.1016/j.jcrc.2012.04.006
21. Kang BJ, Koh Y, Lim CM, Huh JW, Baek S, Han M, et al. Failure of high-flow nasal cannula therapy may delay intubation and increase mortality. *Intensive Care Med.* (2015) 41:623–32. doi: 10.1007/s00134-015-3693-5
22. Ricard JD, Roca O, Lemiale V, Corley A, Braunlich J, Jones P, et al. Use of nasal high flow oxygen during acute respiratory failure. *Intensive Care Med.* (2020) 46:2238–47. doi: 10.1007/s00134-020-06228-7
23. Grieco DL, Menga LS, Eleuteri D, Antonelli M. Patient self-inflicted lung injury: implications for acute hypoxemic respiratory failure and ARDS patients on non-invasive support. *Minerva Anestesiol.* (2019) 85:1014–23. doi: 10.23736/S0375-9393.19.13418-9
24. Yoshida T, Roldan R, Beraldo MA, Torsani V, Gomes S, De Santis RR, et al. Spontaneous effort during mechanical ventilation: maximal injury with less positive end-expiratory pressure. *Crit Care Med.* (2016) 44:e678–688. doi: 10.1097/CCM.0000000000001649
25. Sun Q, Liu L, Pan C, Zhao Z, Xu J, Liu A, et al. Effects of neurally adjusted ventilatory assist on air distribution and dead space in patients with acute exacerbation of chronic obstructive pulmonary disease. *Crit Care.* (2017) 21:126. doi: 10.1186/s13054-017-1714-1
26. He H, Chi Y, Long Y, Yuan S, Frerichs I, Moller K, et al. Influence of overdistension/recruitment induced by high positive end-expiratory pressure on ventilation-perfusion matching assessed by electrical impedance tomography with saline bolus. *Crit Care.* (2020) 24:586. doi: 10.1186/s13054-020-03301-x
27. Yuan Z, Han X, Wang L, Xue P, Sun Y, Frerichs I, et al. Oxygen therapy delivery and body position effects measured with electrical impedance tomography. *Respir Care.* (2020) 65:281–7. doi: 10.4187/respcare.07109
28. Perez-Teran P, Marin-Corral J, Dot I, Sans S, Munoz-Bermudez R, Bosch R, et al. Aeration changes induced by high flow nasal cannula are more homogeneous than those generated by non-invasive ventilation in healthy subjects. *J Crit Care.* (2019) 53:186–92. doi: 10.1016/j.jcrc.2019.06.009
29. Frerichs I, Becher T. Chest electrical impedance tomography measures in neonatology and paediatrics-a survey on clinical usefulness. *Physiol Meas.* (2019) 40:054001. doi: 10.1088/1361-6579/ab1946
30. Yang L, Dai M, Cao X, Möller K, Dargvainis M, Frerichs I, et al. Regional ventilation distribution in healthy lungs: can reference values be established for electrical impedance tomography parameters? *Ann Translational Med.* (2021) 9:789–789. doi: 10.21037/atm-20-7442

Conflict of Interest: ZZhao receives a consulting fee from Drager Medical.

The remaining authors declare that the research was conducted in the absence of any commercial or financial relationships that could be construed as a potential conflict of interest.

Publisher's Note: All claims expressed in this article are solely those of the authors and do not necessarily represent those of their affiliated organizations, or those of the publisher, the editors and the reviewers. Any product that may be evaluated in this article, or claim that may be made by its manufacturer, is not guaranteed or endorsed by the publisher.

frontiers in Medicine

ORIGINAL RESEARCH
published: 19 November 2021
doi: 10.3389/fmed.2021.773471

The Role of Electrical Impedance Tomography for Management of High-Risk Pulmonary Embolism in a Postoperative Patient

*Xinchen Wang, Hua Zhao and Na Cui**

Department of Critical Care Medicine, Peking Union Medical College Hospital, Chinese Academy of Medical Science and Peking Union Medical College, Beijing, China

Electrical impedance tomography (EIT) is a non-invasive, radiation-free and bedside imaging tool that is widely used for real-time monitoring of lung ventilation. Recently, it has been proposed for use in quantitative assessment of regional lung perfusion with hypertonic saline bolus injection and consequently for pulmonary embolism (PE) detection. Here, we present a case of high-risk PE in a postoperative patient, in which EIT monitoring provided us with useful information for diagnosis and decision-making, especially with the challenge of anticoagulation and risk of bleeding.

Keywords: electrical impedance tomography, pulmonary embolism (MeSH), postoperative, beside, anticoagulation, bleeding

OPEN ACCESS

Edited by:
Knut Moeller,
Furtwangen University, Germany

Reviewed by:
Jianfeng Wu,
The First Affiliated Hospital of Sun Yat-sen University, China
Birgit Stender,
Drägerwerk, Germany

****Correspondence:***
Na Cui
pumchcn@163.com

Specialty section:
This article was submitted to Intensive Care Medicine and Anesthesiology, a section of the journal Frontiers in Medicine

Received: *09 September 2021*
Accepted: *28 October 2021*
Published: *19 November 2021*

Citation:
Wang X, Zhao H and Cui N (2021) The Role of Electrical Impedance Tomography for Management of High-Risk Pulmonary Embolism in a Postoperative Patient. Front. Med. 8:773471. doi: 10.3389/fmed.2021.773471

INTRODUCTION

Pulmonary embolism (PE) is the third most frequent acute cardiovascular syndrome worldwide after myocardial infarction and stroke (1). High-risk PE, as indicated by the presence of hemodynamic instability, is a life-threatening situation that requires an immediate emergency diagnostic and therapeutic strategy at its occurrence (2). Furthermore, rapid and bedside methods to monitor pulmonary perfusion are actual demands for clinical decision-making during the management of high-risk PE. For example, postoperative patients with a complication of high-risk PE are more likely to experience hemorrhage during thrombolysis or large-dose anticoagulant therapy, necessitating the discontinuation of the anticoagulant therapy. However, for such patients, discontinuing intense anticoagulant therapy could lead to progression of the embolism and cause death. In this circumstance, rapid and bedside methods to monitor pulmonary perfusion will be especially helpful to gather more convincing and direct indications to make decisions.

Electrical impedance tomography (EIT) is a non-invasive, radiation-free imaging tool that is widely used for real-time monitoring of lung ventilation. EIT image reconstruction is based on the estimation of the resistivity changes that occur across the lungs with breathing (3). In several recent clinical studies, it has been proposed for use in quantitative assessment of regional lung perfusion with hypertonic saline bolus injection and consequently for PE detection (4, 5). Here, we present a case of EIT-guided management of high-risk PE in the intensive care unit (ICU) of Peking Union Medical College Hospital.

TABLE 1 | Data of PE-related monitoring at different stages of PE recovery.

	Day 1	Day 2	Day 5	Day 12
Milestone	Admission	After thrombolysis	Oxygenation improved	Relief from dyspnea and weaning
Heart rate, b.p.m.	114	76	104	96
MAP, mmHg	67	79	80	86
NE, ug/kg/min	1	0.2	0.413	0
CVP, mmHg	10	7	5	5
Pv-aCO2, mmHg	5.4	0.5	5.6	6.4
$ScvO_2$, %	69.4	84.2	65.4	72.6
Lac, mmol/L	2	0.7	0.8	0.5
WBC, $10^{9/L}$	7.70	7.98	11.52	13.77
P/F ratio, mmHg	156	161	291	347
D-Dimer, mg/L	28.5	318.5	4.92	11.37
Hb, g/L	129	122	93	88
Cr, mmol/L	152	161	133	272
cTnI, ug/L	0.051	0.065	0.027	<0.017
Respiratory conditions	PC 13 cmH2O, PEEP 6 cmH2O, FiO_2 45%, f 20 c.p.m.	PC 12cmH2O, PEEP 6 cmH2O, F FiO_2 45%, f 18 c.p.m.	PS 12cmH2O, PEEP 10 cmH2O, FiO_2 40%, RR 13 c.p.m.	Venturi, FiO_2 31%, RR 15 c.p.m.
MV	11.0 L/min	10.1 L/min	7.6 L/min	-
Percentage of pulmonary perfusion by EIT (right vs. left), %				
ROI 1	3 vs. 8	6 vs. 6	5 vs. 7	5 vs. 3
ROI 2	10 vs. 33	14 vs. 19	16 vs. 29	22 vs. 25
ROI 3	12 vs. 27	23 vs. 23	16 vs. 20	14 vs. 21
ROI 4	4 vs. 4	5 vs. 3	4 vs. 3	5 vs. 5
Shunt, %	35.34	9.96	17.76	14.63
Dead space, %	28.82	5.31	4.14	7.19
V/Q match, %	35.84	84.73	78.10	78.18
LU findings	L6: tissue-like signs	L6: tissue-like signs	L6 and R6: tissue-like signs	R4, L6, and R6: tissue-like signs
CT scan findings	Consolidation in the lower left lung	-	-	Consolidation in the lower bilateral lung.
TVR, m/s	3.4	2.9	2.0	Poor ultrasonic conditions.
CO, L/min	8.1	4.8	5.3	Poor ultrasonic conditions.
Events	Thrombolysis	Continuous anticoagulant therapy to achieve the APTT at 50–70 s.	Severe bleeding of the lower gastrointestinal tract. Suspension of anticoagulant therapy.	Suspension of anticoagulant therapy.

CASE DESCRIPTION

A 64-year-old man with a history of bladder cancer and prostate cancer, who had successfully undergone laparoscopic radical cystectomy and ileum conduit urinary diversion during this admission, was referred to the ICU due to sudden hypoxemia and extreme dyspnea on the sixth postoperative day. The patient had a respiratory rate (RR) of 40 times per minute and pulse oxyhemoglobin saturation (SpO_2) of 87% under 10 L/min oxygen supplied by an oxygen storage mask. In addition, the patient had a heart rate (HR) of 114 b.p.m., blood pressure (BP) of 149/73 mmHg, and body temperature of 37.6°C. After sedation, intubation was performed on the patient, and mechanical ventilation was then administered (VC mode, VT 400 ml, PEEP 5 cmH2O, FiO_2 40%). Continuous infusion of norepinephrine (NE) at a rate of around 1 ug/kg/min was given to the patient to maintain an MAP of 80 mmHg. Continuous infusion of Cisatracurium, a muscle relaxant, at 3 mg/h was later given to control the excessive inspiratory effort. Laboratory evaluation revealed an elevated D-D dimer concentration of 28.5 mg/L (Other lab results shown in **Table 1**). The Wells score was 7 (HR $\geq$ 100 b.p.m., surgery, active cancer, alternative diagnosis less likely than PE) and PE was strongly suspected. After informed consent was obtained, bedside EIT with hypertonic saline (10%)

Abbreviations: SpO2, pulse oxyhemoglobin saturation; b.p.m., beats per minute; c.p.m., counts per minute; VC, volume control; VT, tidal volume; PEEP, positive end-expiratory pressure; MAP, mean artery pressure; P/F, artery partial pressure of oxygen; FiO_2, fraction of inspired oxygen ratio; ROI, region of interest; LU, Lung ultrasound; ScvO2, Central venous oxygen saturation.

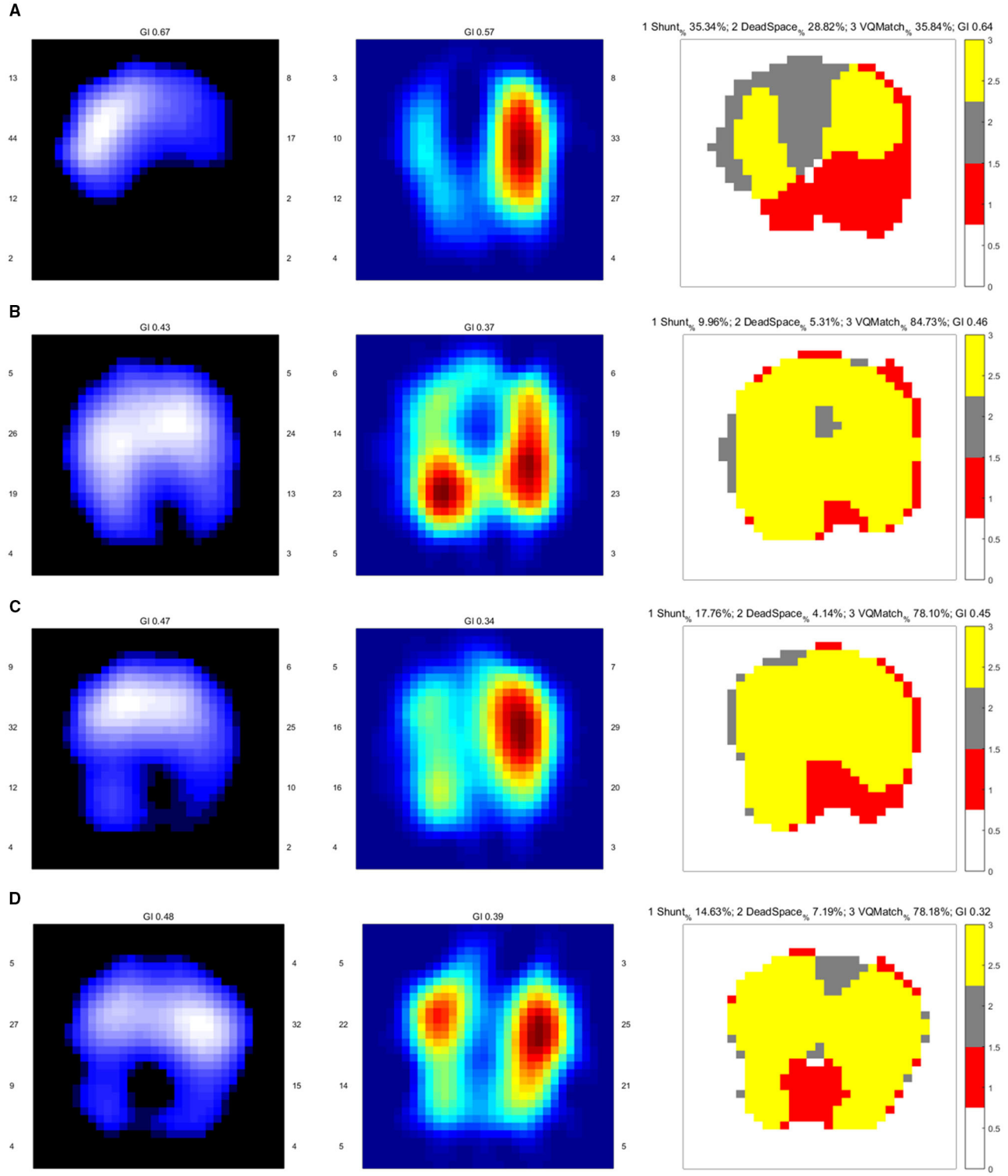

FIGURE 1 | EIT images of the functional ventilation distribution (dark blue areas indicated low ventilated regions and white areas indicated high ventilated regions), functional perfusion distribution (red areas indicated high-perfusion regions and blue areas indicated low-perfusion regions), and distribution of the regional ventilation/perfusion ratios (Ventilated regions were defined as pixels with impedance changes higher than 20% of the maximum tidal impedance variation in the functional ventilation image. Perfused regions were defined as pixels higher than 20% of the maximum bolus-related impedance change in the functional perfusion image. Gray areas indicated regions with high ventilation and low perfusion. Red areas indicated low ventilation and high perfusion regions. Yellow areas indicated good ventilation-perfusion matching). **(A)** On admission, there was a significant ventilation defect in the dorsal lung and perfusion defect in the right lung, leading us to

(Continued)

FIGURE 1 | perform CTPA for PE confirmation. The ventilation defect was later treated with lung recruitment and tracheal suction. **(B)** Ventilation improved after lung recruitment and tracheal suction. Regional perfusion in the right lung was restored after thrombolysis. **(C)** On Day 5, there was a ventilation defect in the left dorsal lung, with a significant shunt observed in the image of the ventilation/perfusion (V/Q) ratio distribution. **(D)** On Day 12, there were ventilation defects in the dorsal lung. The lung perfusion demonstrates symmetric in both lungs.

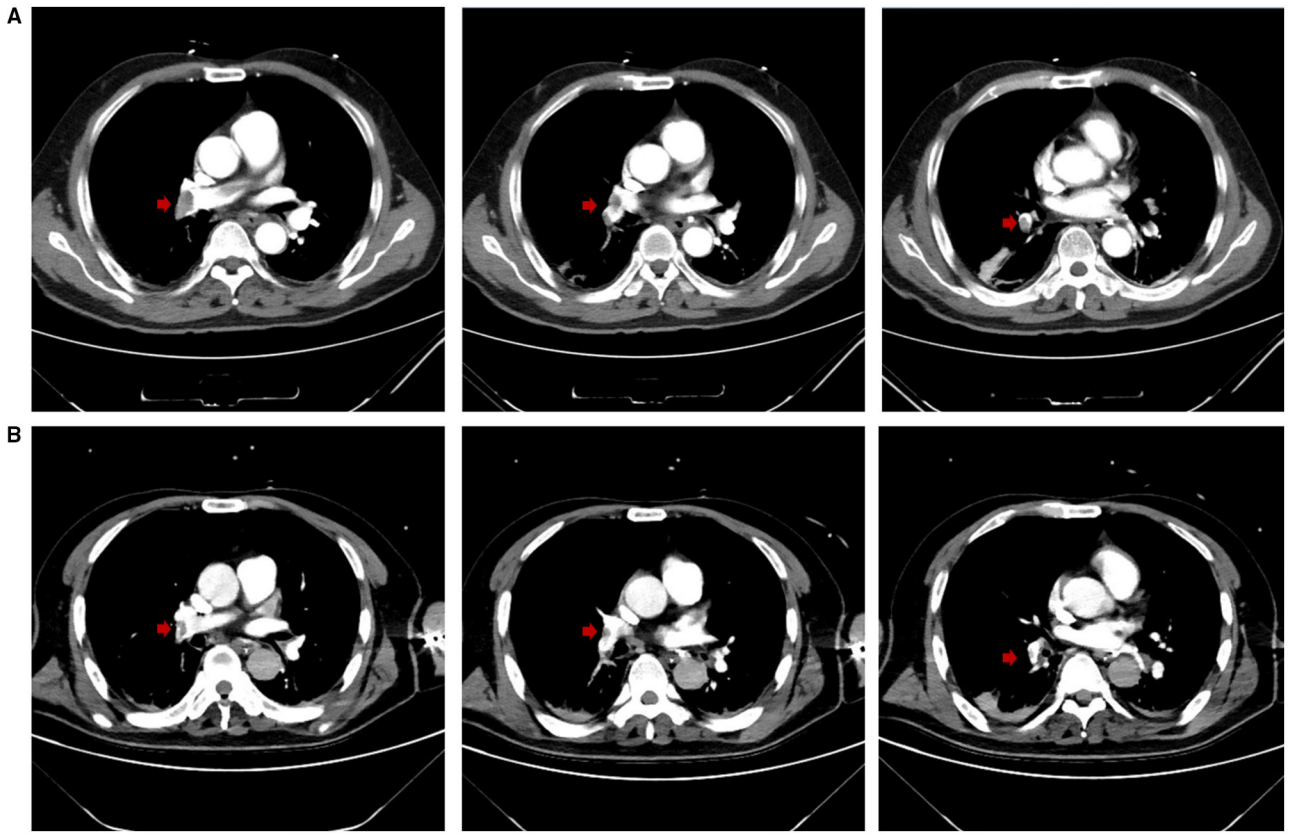

FIGURE 2 | (A) CTPA at admission demonstrated multiple embolisms in the right pulmonary trunk and right pulmonary artery branches (embolisms in the right pulmonary artery branches not shown). Red arrows highlight the locations of the emboli. **(B)** On Day 12, CTPA revealed reduced embolisms in the right pulmonary trunk and right pulmonary artery branches, and improved artery visualization could be observed. Red arrows highlight the locations of the emboli.

bolus infusion was performed to assess the regional pulmonary perfusion for PE detection. From the EIT pulmonary perfusion images, there was a significant perfusion defect in the right lung with dead space accounting for 28.82% (**Figure 1A**). Considering the life-threatening emergency of the suspected PE that requires urgent thrombolysis after its confirmation, we took the risk to transfer the patient for a CT pulmonary angiography (CTPA) examination. The CTPA showed multiple embolisms in the right pulmonary trunk, right pulmonary artery branches, and left artery branches (**Figure 2A**). During the screening of deep venous thrombosis, multiple calf muscle venous thrombosis was observed in the lower right extremities, which could be the source of PE.

Since the diagnosis of PE, the PESI score of the patient was 194 (64 years old, male sex, cancer, pulse rate $\geq$ 110 b.p.m., systolic BP $<$ 100 mmHg, RR $>$ 30 c.p.m., arterial oxyhemoglobin saturation $<$ 90%) with risk strata of Class V (very high mortality risk) (6). Bedside transthoracic echocardiography (TTE) was performed to evaluate the right ventricle function in particular. The systolic D-shaped left ventricle was observed from the parasternal short-axis view. The right ventricle (RV) was not clearly displayed in the apical four-chamber section, with an estimated ratio of less than 1:1 between the RV and the left ventricle (LV). The tricuspid valve regurgitation (TVR) was 3.09 m/s. The systolic function of RV measured by TAPSE was 2.3 cm. The left ventricular outflow tract (LVOT) velocity-time integral (VTI) was 24.5 at an HR of 105 b.p.m., and the estimated cardiac output (CO) was 8.07 L/min (**Figure 3**). Thrombolysis (alteplase 50 mg) was initiated immediately, three hours after which continuously-infused heparin was given to the patient to achieve the activated partial thromboplastin time (APTT) at 50–70 s.

After thrombolysis, another EIT with hypertonic saline bolus infusion was performed to observe lung perfusion. The EIT image showed that regional perfusion was restored in the right

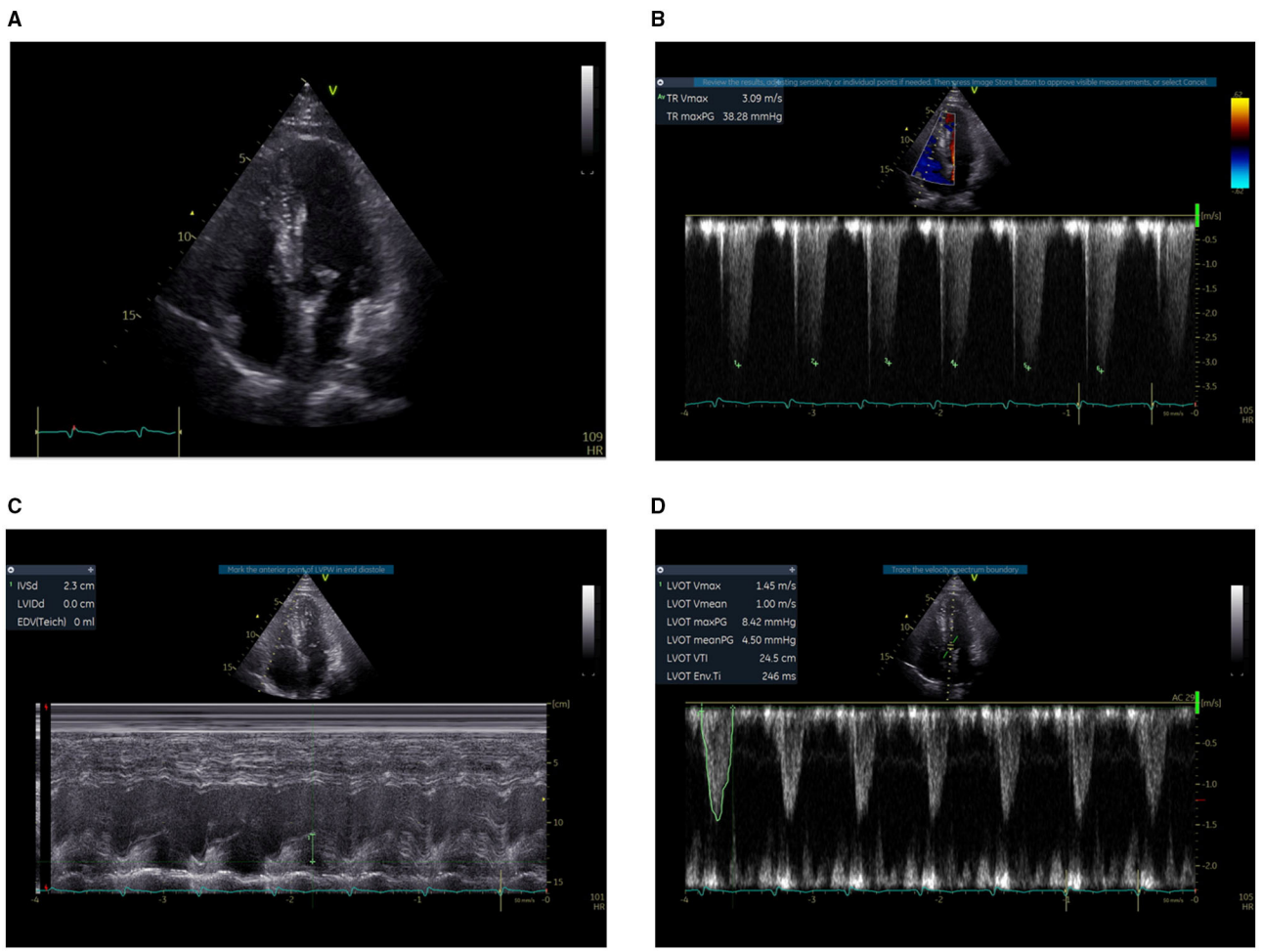

FIGURE 3 | Bedside TTE before thrombolysis. **(A)** The right ventricle was not clearly displayed, with an estimated ratio of less than 1:1 between the RV and the LV. **(B)** The TVR was 3.09 m/s. **(C)** The systolic function of the RV measured by TAPSE was 2.3 cm. **(D)** The LVOT VTI was 24.5 at an HR of 105 b.p.m. and the estimated CO was 8.07 L/min.

lung (**Figure 1B**). Meanwhile, bedside TTE revealed that the TVR was reduced to 2.9 m/s, and the RV did not further enlarge. All the evidence supported the efficacy of thrombolysis and anticoagulant therapy, thus the anticoagulant therapy was continued, with the patient's condition closely monitored. On the fifth day after thrombolysis (and since ICU admission), the patient experienced massive lower gastrointestinal bleeding, with his hemoglobin levels decreasing from 108 g/L to 88 g/L. The patient was in shock due to an estimated blood loss of 800 ml in one day, with an HR of 104 b.p.m. and MAP of around 80 mmHg, receiving a continuous infusion of NE at 0.413 ug/kg/min. According to EIT, the pulmonary perfusion had recovered and appeared bilaterally symmetric on the same day, while the hypoxemia of the patient improved from a P/F ratio of 161 to 291 mmHg. Therefore, the coagulant therapy was stopped. Meanwhile, the pulmonary ventilation image of EIT revealed a new ventilation defect in the left dorsal lung, with a significant shunt accounting for 17.76% in that area (**Figure 1C**). Combined with the lung ultrasound findings, tissue-like signs were detected in the L6 and R6 regions using a six-zone scanning protocol (**Figure 4**), while lung sliding and A-lines were observed in the other regions.

It was concluded that there could be consolidation in the dorsal region of bilateral lungs. Therefore, intermittent prone positioning and physical vibration were performed on the chest to help expel the sputum, and re-expand the collapsed lung. The bleeding did not stop until Day 10. On Day 12, the anticoagulant therapy was still suspended due to the high risk of bleeding. However, the patient was relieved from dyspnea, the oxygenation index improved further to a P/F ratio of 347 mmHg, and weaning had been successfully processed. The patient was taken for another CTPA examination, after which we performed EIT with hypertonic saline bolus infusion. CTPA revealed that the emboli in the right trunk, right pulmonary artery branches, and left artery branches had decreased in size, and the pulmonary artery was more visualized in the

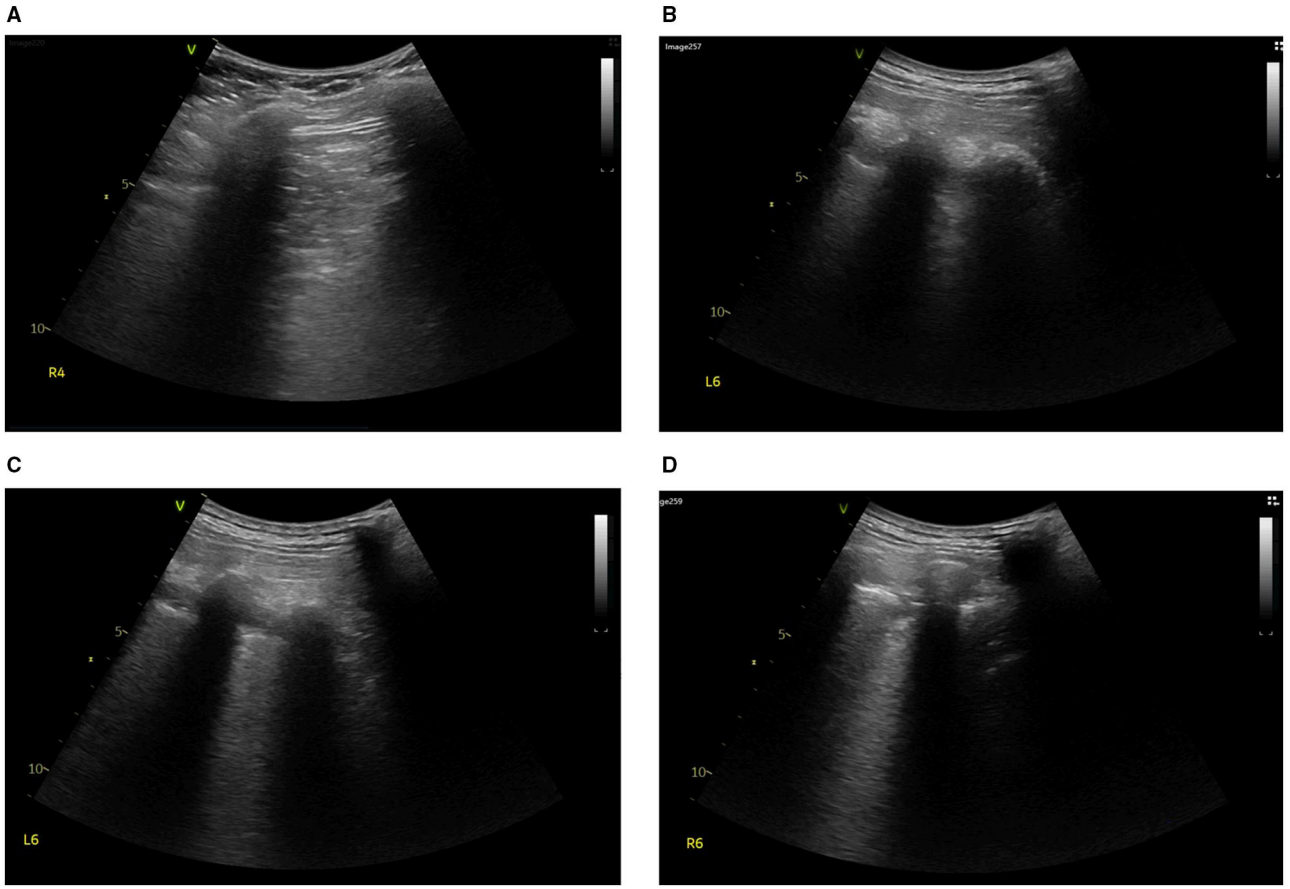

FIGURE 4 | On Day 5, lung ultrasound was performed to find the cause of ventilation defect in the left dorsal lung. Tissue-like signs were found in the region of **(A)** R4, **(B,C)** L6, and **(D)** R6.

angiography (**Figure 2B**). The pulmonary perfusion image of EIT revealed homogeneous perfusion in both the left and right lungs, indicating that the pulmonary perfusion of the lung did not worsen without anticoagulation (**Figure 1D**). Based on this information, we decided to continue closely monitoring the patient's condition without anticoagulation. The following day, the patient was extubated. The monitor revealed that the RR was 17 c.p.m., SpO2 was 99% under 2 L/min oxygen supplied by a nasal cannula, HR was 80-90 b.p.m., and BP was 148/76 mmHg with no vasopressor. The patient was relieved from hypoxemia and dyspnea, and recovered from hemorrhage. On Day 15, he was finally transferred to the general ward. The anticoagulation therapy was not restarted until Day 20, and the respiratory condition of the patient remained stable.

DISCUSSION

The 30 day mortality of high-risk PE (with PESI Class V or sPESI $\geq$ 1 point) is between 10.9 and 24.5% (2). In this case, EIT was used as a valuable bedside tool for clinical decision-making during the management of high-risk PE. As a result, the patient was successfully cured of the vital respiratory failure and circulatory shock caused by PE. Although CTPA has long been the traditional confirmation test of PE (3), for critical PE patients who are frequently in shock and have severe hypoxemia, the potential danger of transferring patients for CTPA has put clinicians and patients in a dilemma. A higher risk of contrast-induced nephropathy caused by CTPA is also a concern for patients with acute or chronic kidney disease complications. The EIT method for generating pulmonary perfusion images is a first-pass kinetic approach that involves administering a bolus of 10 ml hypertonic saline as a contrast agent through a central venous catheter during a breath-hold (7). It is inexpensive, portable, radiation-free, with minimal risk, and not restricted by the patients' posture. As a substitute for CTPA, its results have been proven to be highly reproducible (8), and its diagnostic efficacy of PE has recently been reported. A recent prospective observational study between PE and non-PE patients with acute respiratory failure has found that a higher dead space percentage, lower intrapulmonary shunt percentage,

and lower V/Q match can predict the presence of PE. The cutoff value of 30.37% for dead space percentage resulted in a sensitivity of 90.9% and a specificity of 98.6% for the PE diagnosis (4).

In this case, when PE was highly suspected, bedside EIT was performed to assess regional pulmonary perfusion instead of transferring the patient who had severe dyspnea and hemodynamic instability for CTPA. The pulmonary perfusion image of EIT revealed a significant perfusion defect of the right lung and urged us to perform CTPA. This is the first case report that PE had been early diagnosed by EIT, which further triggered a CTPA confirmation test. The perfusion defect detected by EIT was consistent with the CTPA findings, although the percentage of dead space detected in this case was lower than the previous study (4). One possible explanation is that poor ventilation of the dorsal lung caused by pulmonary atelectasis resulted in a lower calculated dead space percentage. Thus, the diagnosis of PE cannot be excluded even with a lower dead space percentage in such patients. The ventilation defect detected in the right lung at the occurrence of PE was suspected to be regional atelectasis, due to severe respiratory stress of the patient. After restraining excessive respiratory effort with the muscle relaxant, tracheal suction and lung recruitment, the ventilation defect was quickly reduced, as evidenced by the second EIT examination (**Figures 1A,B**).

In this case, the first question we faced was whether thrombolysis was having a sufficient effect, especially since clinical manifestations did not change prominently after they occurred. The pulmonary perfusion image of EIT revealed key information on the improvement of pulmonary perfusion. Combined with the improved TTE results, it answered our question and determined continuous anticoagulant therapy. When the patient experienced life-threatening lower gastrointestinal bleeding on Day 5, the anticoagulant therapy had to be stopped. However, the patient was still at high risk of PE with a Wells score of 7, and having another attack of PE could be deadly. The following anticoagulant therapy after thrombolysis in PE treatment aims at reducing the embolic burden and relieving the vascular obstruction, which could be indicated by the stable bilaterally symmetry pulmonary perfusion by EIT. In this case, the stability of pulmonary perfusion acquired by EIT was found to be consistent with the continued improvement of the patient's oxygenation index, dyspnea, and weaning, suggesting bedside monitoring of pulmonary perfusion could be of much value. Although the value of EIT for PE diagnosis has been widely reported, this is the first time EIT has been used as a valuable tool for clinical decision-making on the adjustment of anticoagulant therapy in a postoperative high-risk PE patient with a high risk of bleeding. Furthermore, it should be noted that the assessment of pulmonary perfusion by EIT cannot be replaced by CTPA in terms of the functional evaluation of lung perfusion. Smaller emboli were still present in situ according to the follow-up CTPA, but there was no indication of changing pulmonary perfusion.

On Day 5, a prominent ventilation defect with a pulmonary shunt was discovered during EIT monitoring. Combined with the lung ultrasound findings, regional consolidation was highly suspected, which was later verified by the follow-up CT scan (Figure not shown). Following that, the targeted treatment was initiated to re-expand the collapsed lung. Despite pulmonary perfusion, assessment of pulmonary ventilation by EIT also plays a key role in the diagnosis and treatment of different causes of dyspnea and hypoxemia. Therefore, we diagnosed lung consolidation and initiated targeted treatment for lung consolidation. Although lung consolidation did not appear to improve based on the later EIT image on Day 12, due to EIT, the therapy was expanded to include a broader range of respiratory treatments, instead of being limited to only PE treatment.

The role of EIT monitoring in the management of postoperative high-risk PE is a classic case of its practicability in critical settings. When patients are at high risk of transfer for CTPA, EIT with hypertonic saline bolus infusion could aid in the diagnosis of PE. Furthermore, EIT could be an important indication of pulmonary perfusion to guide or back up the adjustment of anticoagulant therapy when faced with a conflict between anticoagulation and the risk of bleeding. In addition, when combined with perfusion, EIT evaluation of pulmonary ventilation can aid in the diagnosis of other respiratory conditions, for example, lung consolidation. However, we cannot ignore the disadvantages of the technique, including low-resolution, complex image reconstruction procedure, limited field of view, and incompatibility with certain patients, such as those with a pacemaker (7). In this case, breath-holding was found to be particularly difficult for patients with dyspnea. Furthermore, EIT is unable to reflect the exact anatomical location of PE and detect small emboli. Therefore, it could be misleading to use it as the only indication to decide against anticoagulant therapy. In this case, the therapeutical decision was made based on a variety of clinical data, including but not limited to EIT. A full understanding of EIT in as many aspects as possible is required for its application in the clinical scenarios.

In conclusion, EIT could provide useful information for clinical decision-making in the context of both pulmonary perfusion and pulmonary ventilation during the diagnosis and treatment of high-risk PE, especially with the challenge of anticoagulation and risk of bleeding, which may benefit critically ill patients in the future.

DATA AVAILABILITY STATEMENT

The raw data supporting the conclusions of this article will be made available by the authors, without undue reservation.

ETHICS STATEMENT

Written informed consent was obtained from the individual(s) for the publication of any

potentially identifiable images or data included in this article.

AUTHOR CONTRIBUTIONS

XW and HZ collected study data and drafted the present manuscript. NC revised the manuscript. All authors read and approved the final version of the manuscript.

FUNDING

This work was supported by National Natural Science Foundation of China (No. 82072226), Beijing Municipal Science and Technology Commission (No. Z201100005520049), Non-profit Central Research Institute Fund of Chinese Academy of Medical Sciences (No. 2019XK320040), Tibet Natural Science Foundation (No. XZ2019ZR-ZY12(Z)), and Excellence Program of Key Clinical Specialty of Beijing in 2020 (No. ZK128001).

REFERENCES

1. Konstantinides SV, Meyer G, Becattini C, Bueno H, Geersing GJ, Harjola VP, et al. 2019 ESC Guidelines for the diagnosis and management of acute pulmonary embolism developed in collaboration with the European Respiratory Society (ERS): the task force for the diagnosis and management of acute pulmonary embolism of the European society of cardiology (ESC). *Eur Respir J.* (2019) 54:1901647. doi: 10.1183/13993003.01647-2019
2. Konstantinides SV, Meyer G, Becattini C, Bueno H, Geersing GJ, Harjola VP, et al. 2019 ESC Guidelines for the diagnosis and management of acute pulmonary embolism developed in collaboration with the European respiratory society (ERS). *Eur Heart J.* (2020) 41:543–603. doi: 10.1093/eurheartj/ehz405
3. Costa EL, Lima RG, Amato MB. Electrical impedance tomography. *Curr Opin Crit Care.* (2009) 15:18–24. doi: 10.1097/MCC.0b013e3283220e8c
4. He H, Chi Y, Long Y, Yuan S, Zhang R, Frerichs I, et al. Bedside evaluation of pulmonary embolism by saline contrast electrical impedance tomography method: a prospective observational study. *Am J Respir Crit Care Med.* (2020) 202:1464–8. doi: 10.1164/rccm.202005-1780LE
5. He H, Chi Y, Long Y, Yuan S, Zhang R, Yang Y, et al. Three broad classifications of acute respiratory failure etiologies based on regional ventilation and perfusion by electrical impedance tomography: a hypothesis-generating study. *Ann Intensive Care.* (2021) 11:134. doi: 10.1186/s13613-021-00921-6
6. Aujesky D, Obrosky DS, Stone RA, Auble TE, Perrier A, Cornuz J, et al. Derivation and validation of a prognostic model for pulmonary embolism. *Am J Respir Crit Care Med.* (2005) 172:1041–6. doi: 10.1164/rccm.200506-862OC
7. Bachmann MC, Morais C, Bugedo G, Bruhn A, Morales A, Borges JB, et al. Electrical impedance tomography in acute respiratory distress syndrome. *Crit Care.* (2018) 22:263. doi: 10.1186/s13054-018-2195-6
8. Smit HJ, Handoko ML, Vonk Noordegraaf A, Faes TJ, Postmus PE, de Vries PM, et al. Electrical impedance tomography to measure pulmonary perfusion: is the reproducibility high enough for clinical practice? *Physiol Meas.* (2003) 24:491–9. doi: 10.1088/0967-3334/24/2/359

Conflict of Interest: The authors declare that the research was conducted in the absence of any commercial or financial relationships that could be construed as a potential conflict of interest.

Publisher's Note: All claims expressed in this article are solely those of the authors and do not necessarily represent those of their affiliated organizations, or those of the publisher, the editors and the reviewers. Any product that may be evaluated in this article, or claim that may be made by its manufacturer, is not guaranteed or endorsed by the publisher.

frontiers in Medicine

ORIGINAL RESEARCH
published: 02 December 2021
doi: 10.3389/fmed.2021.748493

Electrical Impedance Tomography Predicts Weaning Success in Adult Patients With Delayed Upper Abdominal Surgery: A Single-Center Retrospective Study

Jiajia Li[1†], Fan Zeng[1†], Fuxun Yang[1†], Xiaoxiu Luo[1], Rongan Liu[1], Yinjie Ren[1], Yunping Lan[1], Yu Lei[1], Gaoping Zhao[2] and Xiaobo Huang[1*]*

[1] Department of Intensive Care Unit, Sichuan Academy of Medical Sciences and Sichuan Provincial People's Hospital, Chengdu, China, [2] Department of Gastrointestinal Surgery, Sichuan Academy of Medical Sciences and Sichuan Provincial People's Hospital, Chengdu, China

Objective: To evaluate the predictive value of electrical impedance tomography (EIT) in patients with delayed ventilator withdrawal after upper abdominal surgery.

Methods: We retrospectively analyzed data of patients who were ventilated >24 h after upper abdominal surgery between January 2018 and August 2019. The patients were divided into successful (group S) and failed (group F) weaning groups. EIT recordings were obtained at 0, 5, 15, and 30 min of spontaneous breathing trials (SBTs) with SBT at 0 min set as baseline. We assessed the change in delta end-expiratory lung impedance and tidal volume ratio (ΔEELI/VT) from baseline, the change in compliance change percentage variation (|Δ(CW-CL)|) from baseline, the standard deviation of regional ventilation delay index (RVDSD), and global inhomogeneity (GI) using generalized estimation equation analyses. Receiver operating characteristic curve analyses were performed to evaluate the predictive value of parameters indicating weaning success.

Results: Among the 32 included patients, ventilation weaning was successful in 23 patients but failed in nine. Generalized estimation equation analysis showed that compared with group F, the ΔEELI/VT was lower, and the GI, RVDSD, and (|Δ(CW-CL)|) were higher in group S. For predicting withdrawal failure, the areas under the curve of the ΔEELI/VT, (|Δ(CW-CL)|), and the RVDSD were 0.819, 0.918, and 0.918, and 0.816, 0.884, and 0.918 at 15 and 30 min during the SBTs, respectively.

Conclusion: The electrical impedance tomography may predict the success rate of ventilator weaning in patients with delayed ventilator withdrawal after upper abdominal surgery.

Keywords: success rate of weaning, upper abdominal surgery, electrical impedance tomography, mechanical ventilation, predict

OPEN ACCESS

Edited by:
Yun Long,
Peking Union Medical College Hospital (CAMS), China

Reviewed by:
Zhanqi Zhao,
Furtwangen University, Germany
Jianfeng Wu,
The First Affiliated Hospital of Sun Yat-sen University, China

***Correspondence:**
Gaoping Zhao
494827965@qq.com
Xiaobo Huang
drhuangxb@126.com

† These authors have contributed equally to this work

Specialty section:
This article was submitted to Intensive Care Medicine and Anesthesiology, a section of the journal Frontiers in Medicine

Received: *28 July 2021*
Accepted: *09 November 2021*
Published: *02 December 2021*

Citation:
Li J, Zeng F, Yang F, Luo X, Liu R, Ren Y, Lan Y, Lei Y, Zhao G and Huang X (2021) Electrical Impedance Tomography Predicts Weaning Success in Adult Patients With Delayed Upper Abdominal Surgery: A Single-Center Retrospective Study. Front. Med. 8:748493. doi: 10.3389/fmed.2021.748493

INTRODUCTION

Patients who are mechanically ventilated during upper abdominal surgery need to be weaned off of mechanical ventilation as soon as possible after they recover spontaneous breathing, which helps patients recover quickly. However, some patients experience varying degrees of post-operative lung function impairment because of reduced ventilatory muscle activity, diaphragmatic dysfunction, and decreased lung compliance (1). Older patients with preoperative lung disease or decreased lung function often require delayed extubation. The rapid shallow breathing index, occlusion pressure at 100 ms, and spontaneous breathing trials (SBTs) have been commonly used to predict weaning. However, the measured values of the rapid shallow breathing index and occlusion pressure at 100 ms can be inaccurate because of the patient's posture, airway stenosis, fever, and other factors. SBTs are commonly used in clinical practice, and its outcome is evaluated by objective parameters, such as the respiratory rate to tidal volume ratio (respiratory rate/VT) and arterial blood gases. Patients who pass the SBT can attempt ventilator weaning and endotracheal tube removal. However, some patients develop respiratory failure after weaning and need ventilator-assisted therapy. In patients requiring prolonged mechanical ventilation therapy, the rate of weaning failure is >10% (2). Failure to wean can increase the risk of mechanical ventilation complications and even increase the length of hospital stay and mortality. Therefore, it is necessary to identify a more specific way to evaluate the weaning process.

Electrical impedance tomography (EIT) is a new-generation, non-invasive functional imaging technology for real-time monitoring of pulmonary ventilation in patients. Based on different electrical impedances of tissues, gas, and liquid (which are increased by air and reduced by fluids and cells), real-time monitoring of pulmonary ventilation changes at the bedside is achieved by computer imaging technology (3, 4). Bickenbach et al. showed EIT enables monitoring of regional ventilation distribution during SBTs and is suitable to estimate whether an SBT probably will be beneficial for an individual patient (5). Recent clinical evidence has shown that the different etiologies of acute respiratory failure (ARF) have different regional lung ventilation and perfusion characteristics, as measured by the saline contrast EIT method (6). Zhang et al. demonstrated that EIT could identify the diverse effects of a high-flow nasal cannula on regional lung ventilation in post-extubation situations, which might be helpful to guide HFNC therapy in clinical practice (7). EIT is expected to become a new detection method for aiding mechanical ventilation withdrawal (5, 8). Accordingly, the purpose of this study was to evaluate the predictive value of the EIT in patients with delayed ventilator withdrawal after upper abdominal surgery.

MATERIALS AND METHODS

Patients

This retrospective study included intensive care unit patients who had undergone upper abdominal surgery between January 1, 2018 and August 31, 2019. They were stratified into successful weaning (group S) and weaning failure groups (group F). The inclusion criteria were as follows: (1) age > 18 years, (2) postoperative mechanical ventilation >24 h, (3) SBT performed before weaning, and (4) EIT monitoring performed during weaning. The exclusion criteria were as follows: (1) poor EIT images unsuitable for data analysis and (2) currently pregnant. The Ethics Committee of Sichuan Provincial People's Hospital approved the study. We have obtained the consent of all patients.

Weaning Process

An SBT was considered when the patient met the weaning criteria: (1) the primary disease causing respiratory failure was controlled; (2) partial pressure of oxygen (PaO_2)/fraction of inspired oxygen (FiO_2) ≥ 150 mmHg, with positive end-expiratory pressure ≤8 cm H_2O]; (3) stable hemodynamic state [heart rate (HR) ≤ 140 bpm, 90 mmHg < systolic blood pressure <160 mmHg, and no vasoactive drugs]; (4) strong ability of spontaneous breathing and coughing; (5) body temperature < 38°C; (6) no obvious respiratory acidosis [pH > 7.3, HCO_3^- <30 mmol/L, or partial pressure of carbon dioxide ($PaCO_2$) <45 mmH_2O]; (7) hemoglobin level ≥ 80 g/L; and (8) good mental status. Before beginning the SBT, the ventilator settings were adjusted to the pressure support ventilation mode, and the parameter settings were as follows: pressure support = 8 cmH_2O, FiO_2 = 40%, positive end-expiratory pressure ≤ 5 cmH_2O, and oxygen saturation (SpO_2) maintained at ≥ 92%; the ventilation time in the whole pressure support ventilation mode was longer than 30 min. For patients then underwent the SBT, ventilator therapy was discontinued while endotracheal intubation was retained. Oxygen was administered through the tracheal tube with oxygen-enriched humidified air for 30 min at a rate of 2–4 L/min; the vital signs and SpO_2 of the patients were monitored. Blood gas analysis was performed after 30 min. An SBT was classified as failed when any of the following conditions were met: (1) aggravation or recurrence of the primary disease (judged by a competent doctor); (2) respiratory rate ≥ 35 breaths/min, an increase of 50% from baseline, or ≤ 8 breaths/min; (3) hemodynamic instability (systolic blood pressure > 180 or < 90 mmHg, or pulse > 140 beats/min); (4) basal HR or blood pressure change rate > 20% or FiO_2 > 0.5, PaO_2 < 60 mmHg, or $PaCO_2$ increase > 10 mmHg; (5) pH < 7.32 or pH decrease > 0.07; and (6) anxiety, sweating, or irritability (judged by the doctor in charge). Patients who passed the SBT were extubated and administered oxygen using a nasal catheter or mask at a rate of 2–4 L/min. For patients who did not pass the SBT, the doctor chose the appropriate ventilation mode to continue mechanical ventilation according to the situation and recorded the weaning failure. Weaning failure was defined as follows: (1) failed SBT, (2) re-treatment with invasive or non-invasive ventilation within 48 h after extubation, and (3) death within 48 h after weaning. Acute Physiology and Chronic Health Evaluation II score, HR, mean arterial pressure (MAP), arterial blood gases index (pH, PaO_2, $PaCO_2$, and lactate levels), oxygenation index (PaO_2/FiO_2), and SpO_2 were recorded before weaning on the same day. We collected age, sex, type of sugery, Acute Physiology Score II values, SBT's result. At the same time, the HR, respiratory

rate, MAP, SpO_2, PaO_2, $PaCO_2$, at 0, 5, 15, and 30 min of SBTs were collected in both study groups.

EIT Data Acquisition and Analysis

When the patient met the weaning criteria, a silicon 16-electrode EIT belt of proper size was placed around the patients' chest between the 4th and 6th ribs and connected to the EIT device (PulmoVista 500; Dräger Medical GmbH, Lübeck, Germany). EIT scans are represented by 32 × 32 color-coded matrix images. A low pass filter with a cutoff frequency of 50 min^{-1} was applied to exclude cardiac-related variations. During all study phases, EIT data were generated by application of electrical current at 25 kHz, recorded by an EIT device. EIT measurements were started at the beginning of SBT and obtained for 5 min at 0, 5, 15, and 30 min during SBT. The last 2 min of each record were analyzed. We recorded the SBT data at 0 min as the baseline value. With the generated tidal images, four horizontal layers from the ventral to the dorsal side were defined as regions of interest (ROI) and numbered from 1 to 4. Global inhomogeneity (GI) was measured as previously described (9, 10). The end-expiratory lung impedance (EELI) was defined as the average end-expiratory global impedance values of 10 consecutive breaths in SBT. With SBT at 0 min set as baseline, the change in end-expiratory lung impedance (ΔEELI) was defined as the difference between the EELI value at other time points (SBT at 5, 15, and 30 min) and the EELI value at baseline time (11, 12). We recorded the tidal volume of five subsequent breathing cycles at the last 1 min before SBT and calculated the average value as tidal volume (VT). ΔEELI/VT was defined as ΔEELI divided by VT.

The standard deviation of the regional ventilation delay index (RVDSD) was used to express regional ventilation distribution. The global impedance-time curve ΔZ(t) was as the sum of the impedance changes of all pixels. The RVDSD was assessed by EIT as previously described (13, 14). We calculated compliance win (CW) and compliance loss (CL), expressed as a percentage, from the EIT recordings (15). Compliance change percentage variation (|Δ(CW-CL)|) was defined as the difference between CW and CL regarding SBT at 5, 15, and 30 min compared to SBT at 0 min.

Regional distribution of ventilation measurements was recorded on the PulmoVista 500 during monitoring sessions. Each recording was transferred to a USB storage device. Data were downloaded from the USB storage device to a Windows (Microsoft, Redmond, Washington) based personal computer. The EIT data were analyzed offline using the EIT Data Analysis Tool 6.1 and 6.1.20 (Dräger Medical GmbH, Lübeck, Germany) and MATLAB 8.3 (The Mathworks, Natick, MA, USA).

Statistical Analysis

Mean data were analyzed using SPSS software (version 22.0; IBM Corp., Armonk, NY, USA). Normally distributed data are presented as means ± standard deviations. Non-normally distributed data are presented as medians (interquartile intervals). Normally distributed and non-parametric continuous variables were compared using the Student's *t*-test and Mann–Whitney *U*-test, respectively. Basic clinical parameters were tested by the Wilcox non-parametric test. Repeated data were analyzed with a generalized estimation equation. The receiver operating characteristic curve was used to assess the accuracy of successful weaning. Cutoff values were obtained by calculating the Youden index, and the sensitivity and specificity were also determined. Considering the small sample size in this

TABLE 1 | Baseline characteristics of patient is at SBT 0 min.

	***S* (*n* = 23)**	***F* (*n* = 9)**	***p***
Age (year)	58.48 ± 12.76	64.44 ± 15.13	0.31
Mechanical ventilation hours (h)	60.00 ± 45.91	72.00 ± 36.72	0.19
APACHE II	12.70 ± 4.54	12.33 ± 3.46	0.80
ASA index			
I, *n* (%)	16(69.5)	6(66.7)	1.00
≥II, *n* (%)	7(30.4)	3(33.3)	1.00
Type of surgery			
High surgical aggression, *n* (%)	12 (52.2)	4 (0.44)	1.00
Pancreaticodoudenectomy, *n* (%)	3(13.0)	1(11.1)	
Esophagectomy, *n* (%)	4(17.4)	2(22.2)	
Total gastrectomy, *n* (%)	5(21.7)	1(11.1)	
Intermediate surgical aggression	11 (47.8)	5 (55.5)	1.00
Total colectomy, *n* (%)	5(21.7)	2(22.2)	
Rectal resection, *n* (%)	2(8.7)	0(0)	
Major liver resection, *n* (%)	4(17.4)	3(33.3)	
Chronic disease			
Hypertension, *n* (%)	6(26)	2(22.2)	
Diabetes, *n* (%)	5(21.7)	1(11.1)	
Chronic kidney disease, *n* (%)	2(8.7)	0	
Chronic liver disease, *n* (%)	3(13.0)	1(11.1)	
Chronic obstructive pulmonary disease, *n* (%)	4(17.4)	1(11.1)	
Smoking status			
Never, *n* (%)	3(13.0)	1(11.1)	
Former, *n* (%)	16(69.5)	6(66.7)	
Current, *n* (%)	4(17.4)	2 (22.2)	
RSBI	90.13 ± 14.18	109.11 ± 13.77	0.006
P0.1	3.10 ± 0.82	3.56 ± 1.00	0.224
HR (times/min)	87.17 ± 15.50	90.11 ± 18.41	0.753
RR (times/min)	18.17 ± 2.79	20.33 ± 1.94	0.107
MAP (mmHg)	82.13 ± 11.76	85.41 ± 16.04	0.378
SpO_2 (%)	99.52 ± 1.16	97.67 ± 2.12	0.002
pH	7.42 ± 0.07	7.43 ± 0.07	0.737
PaO_2 (mmHg)	112.58 ± 31.10	120.07 ± 51.47	0.917
$PaCO_2$ (mmHg)	39.40 ± 4.88	37.41 ± 6.72	0.450
PaO_2/FiO_2	281.45 ± 77.76	300.17 ± 128.68	0.917
Lac (mmol/L)	1.65 ± 0.68	1.51 ± 0.76	0.571

APACHE II, acute physiology and chronic health evaluation II; $PaCO_2$, arterial partial pressure of carbon dioxide; RSBI, rapid shallow breathing index; P0.1, occlusion pressure at 100 ms; HR, heart rate; RR, respiratory rate; MAP, Mean arterial pressure; SpO_2, saturation of pulse O_2; PaO_2, arterial partial pressure of oxygen; $PaCO_2$, arterial partial pressure of carbon dioxide; Lac, lactic acid; ASA, American Society of Anesthesiologists.

study, the positive and negative likelihood ratios were calculated using MedCalc software (version 19.0; MedCalc Software Ltd., Ostend, Belgium) to reduce the impact on sensitivity and specificity and evaluate the predictive value of each prediction index. Positive-predictive value, negative-predictive value, and diagnostic accuracy were also calculated. A $P < 0.05$ was considered statistically significant.

RESULTS

A total of 32 patients (22 men and 10 women) were included in this study. There were 23 patients in group S and 9 in group F. In group F, within 48 h after extubation, 5 patients received non-invasive ventilation only, 3 patients received invasive ventilation, and 1 patient was reintubated after failing to maintain with non-invasive ventilation. There were no significant differences in age, mechanical ventilation time, Acute Physiology and Chronic Health Evaluation II score, baseline HR, MAP, or values of arterial blood gases indices between the two groups ($P > 0.05$) for the SBT baseline (0 min) values (**Table 1**). However, there was a statistically significant difference in SpO_2 between the two groups before the SBTs ($P < 0.05$) (**Table 1**). At the end of the SBTs, there were no differences in HR, MAP, PaO_2/FiO_2, $PaCO_2$, or pH between the two groups (**Table 2**).

Generalized estimation equation analysis showed that ΔEELI/VT was lower in group F than in group S ($P = 0.01$) and was not associated with the measurement time ($P = 0.17$). The GI, RVDSD, and |Δ(CW-CL)| were higher in group F than in group S ($P = 0.00$, $P = 0.00$, $P = 0.00$) and were associated with the measurement time ($P = 0.00$; $P = 0.00$, $P = 0.01$). The value of ΔEELI/VT, GI, RVDSD, |Δ(CW-CL) | were show in **Table 3**.

The areas under the curve (AUCs) of the ΔEELI/VT of SBTs at 5, 15, and 30 min were 0.742,0.819,0.816, respectively. The cutoff value of the ΔEELI/VT of SBTs was −0.89 at SBT15 min, and the sensitivity and specificity for predicting weaning successful were 88.89 and 65.22%, respectively. The AUC of the |Δ(CW-CL)| of SBTs at 5 min was 0.981. The cutoff value of the |Δ(CW-CL)| of SBTs at 5 min was more than 7.7; the sensitivity and specificity for predicting weaning failure was 88.89 and 100%, respectively, the positive-predictive value was 100%, and the accuracy was 0.89. The AUC of the |Δ(CW-CL)| of SBTs at 15 min was 0.981; the cutoff value of the |Δ(CW-CL)| of SBTs at 15 min was more than 7.4; the sensitivity and specificity for predicting weaning failure was 100 and 95.65%, respectively; the positive-predictive value was 90%; and the accuracy was 0.96. The AUC of RVDSD of SBTs at 30 min was 0.918; the cutoff value of RVDSD of SBTs at 30 min was more than 15.7; the sensitivity and specificity for predicting weaning failure was 100 and 78.26%, respectively; the positive-predictive value was 64.3%; and the accuracy was 0.78 (**Figure 1**).

DISCUSSION

In this study, we found that compared to group S, ΔEELI/VT was lower, and the GI, RVDSD, and |Δ(CW-CL)| were higher in group F. In the early stage of SBT, the |Δ(CW-CL)|, as well as ΔEELI/VT, have a good predictive value of the failure rate of weaning, while the RVDSD has a good predictive value of the failure rate of weaning in the end stage of SBT. The present findings suggest that EIT, a new method to evaluate pulmonary gas distribution, might be a potential tool that could aid patients undergoing upper abdominal surgery with ventilatory weaning.

Because of the pain and repeated diaphragmatic stimulation experienced intraoperatively, pulmonary complications in patients are significantly higher after upper abdominal surgery than after cardiac surgery (16). In addition, due to the effects of anesthesia, mechanical ventilation, and changes in intrathoracic and abdominal pressure, the occurrence of early postoperative atelectasis is almost inevitable. Notably, early ventilator withdrawal can effectively prevent the occurrence of ventilator-associated pneumonia (17). Accordingly, for patients with mechanical ventilation after upper abdominal surgery, clinicians need to actively find an appropriate time to speed up the process of ventilator withdrawal to reduce the delayed extubation. Therefore, an ideal predictor of weaning is urgently needed in clinical settings.

EIT has been a major breakthrough in the field of biomedical engineering in recent decades. Because the electrical impedances of tissues, gas, and liquid are different, the computer collects the electrical impedance information and reconstructs it into an image. Accordingly, an image of the gas distribution in the process of lung ventilation is obtained. During mechanical breath, at the initial stage of inspiration, the increase in airway pressure causes the gas to enter the gravity-independent zone, while in the later stage of inspiration, the continuously inhaled gas is gradually distributed to the gravity-dependent zone. The context is more complicated during spontaneous breath. Therefore, alveolar ventilation has three characteristics: time distribution, spatial distribution, and global distribution. To date, EIT is the only method that can monitor the entire pathophysiological process of alveolar ventilation in real-time and dynamically at the bedside. Theoretically, it can reflect the whole lung and local conditions. In this study, the ΔEELI/VT, RVDSD, |Δ(CW-CL)|, and GI were used to evaluate weaning.

EIT can be used to monitor the compliance of local alveoli to increase or decrease and is not affected by positive pressure ventilation, which is more convenient for patients undergoing SBT. ΔEELI represents the variation in end-expiratory lung impedance during the SBT. The decrease in ΔEELI suggested that there may be part of the alveoli collapsed or the VT decreased. Because the EELI are infected by VT, we chose to use VT to reduce this heterogeneity. ΔEELI/VT reflected the change in end-expiratory lung impedance per unit volume at the different SBT time points, which may guide patients with ventilatory weaning. Our study found that compared to patients under successful weaning, patients experiencing weaning failure were characterized by greater ΔEELI/VT loss during STB, probably because alveolar collapse occurred more in group F, thereby resulting in decreased end-expiratory volume and reduced EELI. Longhini et al. (18) and Mauri et al. (19) also showed that ΔEELI was significantly higher in patients with successful weaning,

TABLE 2 | Patient's characteristics and arterial blood gases in patients at the end of SBT.

	***S* (*n* = 23)**	***F* (*n* = 9)**	***p***
HR (times/min)	88.91 ± 13.71	95.89 ± 18.14	0.25
RR (times/min)	19.82 ± 2.91	20.22 ± 3.93	0.76
MAP (mmHg)	83.4 ± 13.15	85.56 ± 12.89	0.63
SpO_2 (%)	99.13 ± 1.91	97.33 ± 3.57	0.18
pH	7.41 ± 0.05	7.42 ± 0.06	0.96
PaO_2 (mmHg)	110.76 ± 30.74	93.44 ± 38.39	0.19
$PaCO_2$ (mmHg)	42.07 ± 5.38	45.06 ± 14.13	0.55
PaO_2/FiO	285.3 ± 74.90	259.10 ± 92.00	0.41
Lac (mmol/L)	1.61 ± 0.58	1.80 ± 1.15	0.63

SBT, Spontaneous Breathing Trial; HR, Heart rate; RR, respiratory rate; MAP, mean arterial pressure; SpO_2, Pulse oxygen saturation; PaO_2, arterial partial pressure of oxygen; $PaCO_2$, arterial partial pressure of carbon dioxide; PaO_2/FiO_2, arterial partial pressure to inspired fraction of oxygen ratio; Lac, lactic acid.

TABLE 3 | EIT data in patients with extubation success and failure.

	SBT 0	SBT 5	SBT 15	SBT 30
ΔEELI/VT				
Extubation success (*n* = 23)	0	−0.81 ± 0.26	−0.81 ± 0.27	−0.81 ± 0.26
Extubation failure (*n* = 9)	0	−1.02 ± 0.19	−1.13 ± 0.20	−1.10 ± 0.19
P-value of extubation success vs. failure		0.03	0.00	0.01
RVD SD				
Extubation success (*n* = 23)	9.35 ± 1.62	11.66 ± 2.59	11.60 ± 1.64	13.12 ± 2.22
Extubation failure (*n* = 9)	10.72 ± 2.08	13.44 ± 1.94	14.88 ± 3.07	16.73 ± 1.06
P-value of extubation success vs. failure	0.29	0.07	0.00	0.00
Δ(CW-CL)				
Extubation success (*n* = 23)	0	2.72 ± 2.32	3.60 ± 3.82	2.38 ± 2.45
Extubation failure (*n* = 9)	0	16.78 ± 8.22	21.10 ± 9.21	11.38 ± 6.57
P-value of extubation success vs. failure		0.00	0.00	0.00
GI				
Extubation success (*n* = 23)	0.51 ± 0.14	0.67 ± 0.18	0.71 ± 0.18	0.76 ± 0.19
Extubation failure (*n* = 9)	0.65 ± 0.15	0.70 ± 0.14	1.13 ± 0.24	1.14 ± 0.24
P-value of extubation success vs. failure	0.02	0.60	0.00	0.00

ΔEELI/Vt, change from baseline of the end-expiratory lung impedance/the tidal volume in percentage; RVDSD, standard deviation of regional ventilation delay index; Δ(CW-CL), compliance change percentage variation; GI, global inhomogeneity.

consistent with our findings. RVDSD can show the time delay of the pulmonary ventilation area, which can be used as a parameter to reflect the time distribution of pulmonary ventilation. Muders et al. (13) observed a positive correlation between RVDSD and computed tomography imaging. The greater areas of the collapsed alveoli, the greater the value of RVDSD. In addition, Muders et al. found that due to increased alveolar collapse and overall lung heterogeneity, patients with failed weaning might not be able to maintain adequate alveolar ventilation. In our study, we found that the RVDSD values of SBTs in group F were higher than those in group S. Moreover, at the end of SBT, using the cutoff of 15.7, the AUC for predicting failure withdrawal was 0.91, the sensitivity was 100%, and the specificity was 78%, suggesting that the RVDSD maybe a good indicator at the end of SBT. GI—the proportion of the sum of the impedance value of the whole lung pixel and the average impedance value to the sum of the pixel impedance value in the whole lung area—is a parameter used to evaluate the ventilation state of the whole lung. In our study, the GI index of the two groups increased with increases SBT time, and the GI index of group F increased more significantly than that of group S. It is likely that during T-tube ventilation, part of the alveoli collapsed due to the lack of positive pressure ventilation. In group F, the adjustment of spontaneous respiration could not maintain the normal opening of alveoli, especially near the diaphragm, thereby leading to an increase in uneven gas distribution in the lungs and a decrease in alveolar ventilation, which resulted in weaning failure. Pulmonary compliance is important in the regulation of pulmonary ventilation. Previous studies found that poor pulmonary compliance during SBT was associated with extubation failure, with poor accuracy for predicting weaning success, especially when weaning was based on the value of decreased compliance alone (20, 21). Our study found that the |Δ(CW-CL)| was significantly higher in patients with failed

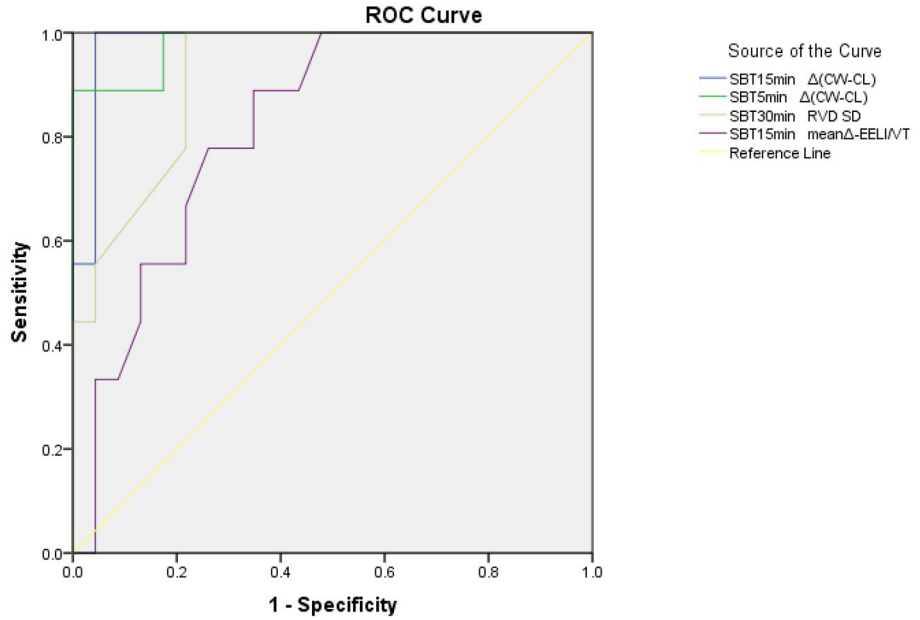

FIGURE 1 | A ROC of prognostic variables for patients. ΔEELI/Vt, change from baseline of the end-expiratory lung impedance/the tidal volume in percentage; RVDSD, standard deviation of regional ventilation delay index; Δ(CW-CL), compliance change percentage variation; GI, global inhomogeneity.

weaning than in those with successful weaning. Especially in the early time of SBT, the value of |Δ(CW-CL)| with failure group was more obviously. It may be related to excessive or weak spontaneous breathing. Excessive spontaneous breathing can easily lead to ventilator fatigue and self-induced lung damage, while weak spontaneous breathing may lead to carbon dioxide retention; both excessive and weak spontaneous breathing lead to failed ventilator weaning. In our study, we considered that |Δ(CW-CL)| may be a good prediction parameter in the early stages of SBT.

Our study has some limitations. First, we did not monitor the increase in intra-abdominal pressure, which may have affected pulmonary compliance, diaphragmatic movement, and transpulmonary pressure, thus affecting the patient's spontaneous breathing. Notably, the phenomenon of increased abdominal pressure was not recorded in any patient after physical examination. Second, this study was a retrospective study, and the weaning method used was an SBT; therefore, it was impossible to compare the related guiding indicators of EIT and the predictive values of SBTs for weaning. These limitations need to be addressed in future clinical studies.

CONCLUSIONS

This study found that GI, the RVDSD, and the |Δ(CW-CL)| of SBTs were higher, while ΔEELI/VT was lower, in group F than in group S. In the early stage of SBT, the |Δ(CW-CL)|, as well as ΔEELI/VT, may have good predictive values for weaning failure rate, while the RVDSD may have a good predictive value for weaning failure rate in the end stage of SBT. These findings suggest that EIT may became a predictor of ventilator weaning in patients undergoing upper abdominal surgery.

DATA AVAILABILITY STATEMENT

The original contributions presented in the study are included in the article/supplementary material, further inquiries can be directed to the corresponding authors.

ETHICS STATEMENT

The studies involving human participants were reviewed and approved by the Ethics Committee of Sichuan Provincial People's Hospital affiliated to Sichuan Provincial People's Hospital. Written informed consent for participation was not required for this study in accordance with the national legislation and the institutional requirements.

AUTHOR CONTRIBUTIONS

JL and FZ wrote the paper. RL, YLa, and FY were responsible for the program implementation. FZ and XL were responsible for data analysis. YR, YLe, and XH were responsible for data collection. GZ were responsible for evolution of overarching research goals and aims, management and coordination responsibility for the research activity planning and execution. All authors contributed to the study design, and read and approved the submitted version of the manuscript.

FUNDING

The authors declare that this study received funding from the Science and Technology Support Program of Sichuan Province, China (Grant Numbers 2017SZ0138 and 20ZDYF1870) and Funding of Provincial People's Hospital Program (Grant Number 2020ZX02). The funders were not involved in the study design, collection, analysis, interpretation of data, the writing of this article or the decision to submit it for publication.

REFERENCES

1. Dureuil B, Cantineau JP, Desmonts JM. Effects of upper or lower abdominal surgery on diaphragmatic function. *Br J Anaesth.* (1987) 59:1230–5. doi: 10.1093/bja/59.10.1230
2. Nozawa E, Azeka E, Ignez ZM, Feltrim Z, Auler Junior JO. Factors associated with failure of weaning from long-term mechanical ventilation after cardiac surgery. *Int Heart J.* (2005) 46:819–31. doi: 10.1536/ihj.46.819
3. Victorino JA, Borges JB, Okamoto VN, Matos GFJ, Tucci MR, Caramez MPR, et al. Imbalances in regional lung ventilation: a validation study on electrical impedance tomography. *Am J Respir Crit Care Med.* (2004) 169:791–800. doi: 10.1164/rccm.200301-133OC
4. Yang L, Dai M, Xu C, Zhang G, Li W, Fu F, et al. The frequency spectral properties of electrode-skin contact impedance on human head and its frequency-dependent effects on frequency-difference eit in stroke detection from 10Hz to 1MHz. *PLoS ONE.* (2017) 12:e0170563. doi: 10.1371/journal.pone.0170563
5. Bickenbach J, Czaplik M, Polier M, Marx G, Marx N, Dreher M. Electrical impedance tomography for predicting failure of spontaneous breathing trials in patients with prolonged weaning. *Critical Care.* (2017) 21:177. doi: 10.1186/s13054-017-1758-2
6. He H, Chi Y, Long Y, Yuan S, Zhang R, Yang Y, et al. Three broad classifications of acute respiratory failure etiologies based on regional ventilation and perfusion by electrical impedance tomography: a hypothesis-generating study. *Ann Intensive Care.* (2021) 11:134. doi: 10.1186/s13613-021-00921-6
7. Zhang R, He H, Yun L, Zhou X, Wang X, Chi Y, et al. Effect of postextubation high-flow nasal cannula therapy on lung recruitment and overdistension in high-risk patient. *Crit Care.* (2020) 24:82. doi: 10.1186/s13054-020-2809-7
8. Liu F, Guo F. Research progress of weaning from mechanical ventilation guided by electrical impedance tomography. *Zhonghua Wei Zhong Bing Ji Jiu Yi Xue.* (2019) 31:241–3. doi: 10.3760/cma.j.issn.2095-4352.2019.02.025
9. Zhao Z, Moller K, Steinmann D, Frerichs I, Guttmann J. Evaluation of an electrical impedance tomography-based Global Inhomogeneity Index for pulmonary ventilation distribution. *Intensive Care Med.* (2009) 35:1900–6. doi: 10.1007/s00134-009-1589-y
10. Trenk F, Mendes L, Carvalho P, Paiva RP, Henriques J, Maglaveras N, et al. Evaluation of lung ventilation distribution in chronic obstructive pulmonary disease patients using the global inhomogeneity index. In: *Annual International Conference of the IEEE Engineering in Medicine and Biology Society*. Piscatawy, NJ (2016). p. 5286–9. doi: 10.1109/EMBC.2016.7591920
11. Mauri T, Eronia N, Abbruzzese C, Marcolin R, Coppadoro A, Spadaro S, et al. Effects of sigh on regional lung strain and ventilation heterogeneity in acute respiratory failure patients undergoing assisted mechanical ventilation. *Crit Care Med.* (2015) 43:1823–31. doi: 10.1097/CCM.0000000000001083
12. Rara A, Roubik K, Tyll T. Effects of pleural effusion drainage in the mechanically ventilated patient as monitored by electrical impedance tomography and end-expiratory lung volume: A pilot study. *J Crit Care.* (2020) 59:76–80. doi: 10.1016/j.jcrc.2020.06.001
13. Muders T, Luepschen H, Zinserling J, Greschus S, Fimmers R, Guenther U, et al. Tidal recruitment assessed by electrical impedance tomography and computed tomography in a porcine model of lung injury. *Crit Care Med.* (2012) 40:903–11. doi: 10.1097/CCM.0b013e318236f452
14. Muders T, Hentze B, Simon P, Girrbach F, Doebler MRG, Leonhardt S, et al. A modified method to assess tidal recruitment by electrical impedance tomography. *J Clin Med.* (2019) 8:1161. doi: 10.3390/jcm8081161
15. Spatenkova V, Teschner E, Jedlicka J. Evaluation of regional ventilation by electric impedance tomography during percutaneous dilatational tracheostomy in neurocritical care: a pilot study. *BMC Neurol.* (2020) 20:374. doi: 10.1186/s12883-020-01948-1
16. Mitchell C, Garrahy P, Peake P. Postoperative respiratory morbidity: identification and risk factors. *Austr N Zeal J Surg.* (1982) 52:203–9. doi: 10.1111/j.1445-2197.1982.tb06103.x
17. Robba C, Rebora P, Banzato E, Wiegers EJA, Stocchetti N, Menon DK, et al. Incidence, risk factors, and effects on outcome of ventilator-associated pneumonia in patients with traumatic brain injury: analysis of a large, multicenter, prospective, observational longitudinal study. *Chest.* (2020) 158:2292–303. doi: 10.1016/j.chest.2020.06.064
18. Longhini F, Maugeri J, Andreoni C, Ronco C, Bruni A, Garofalo E, et al. Electrical impedance tomography during spontaneous breathing trials and after extubation in critically ill patients at high risk for extubation failure: a multicenter observational study. *Ann Intensive Care.* (2019) 9:88. doi: 10.1186/s13613-019-0565-0
19. Mauri T, Bellani G, Confalonieri A, Tagliabue P, Turella M, Coppadoro A, et al. Topographic distribution of tidal ventilation in acute respiratory distress syndrome: effects of positive end-expiratory pressure and pressure support. *Crit Care Med.* (2013) 41:1664–73. doi: 10.1097/CCM.0b013e318287f6e7
20. Amato M. Beneficial effects of the "open lung approach" with low distending pressures in acute respiratory distress syndrome. A prospective randomized study on mechanical ventilation. *Am J Respir Crit Care Med.* (1995) 152:1835–46.
21. Yugo O, Takehiko A, Sayuri B, Suzuki H, Kanda K, Yoda T, et al. Lung-thorax compliance measured during a spontaneous breathing trial is a good index of extubation failure in the surgical intensive care unit: a retrospective cohort study. *J Intens Care.* (2018) 6:44. doi: 10.1186/s40560-018-0313-9

Conflict of Interest: The authors declare that the research was conducted in the absence of any commercial or financial relationships that could be construed as a potential conflict of interest.

Publisher's Note: All claims expressed in this article are solely those of the authors and do not necessarily represent those of their affiliated organizations, or those of the publisher, the editors and the reviewers. Any product that may be evaluated in this article, or claim that may be made by its manufacturer, is not guaranteed or endorsed by the publisher.

frontiers in Medicine

REVIEW
published: 10 January 2022
doi: 10.3389/fmed.2021.817758

Advances in Diagnostic Imaging of Hepatopulmonary Syndrome

*Bi-Wei Luo and Zhi-Yong Du**

Department of Hepatobiliary and Pancreas Surgery, Shenzhen People's Hospital (The Second Clinical Medical College, Jinan University; The First Affiliated Hospital, Southern University of Science and Technology), Shenzhen, China

Hepatopulmonary syndrome (HPS) is a serious pulmonary complication of progressive liver disease that leads to a poor clinical prognosis. Patients with HPS may develop acute respiratory failure, which requires intensive care and therapy. At present, the only effective treatment is liver transplantation; therefore, early diagnosis and timely treatment are of considerable significance. The three main features of HPS are liver disease, oxygenation disorder, and intrapulmonary vascular dilatation (IPVD). Diagnosing HPS is challenging due to the difficulty in detecting the presence or absence of IPVD. As such, imaging examination is very important for detecting IPVD. This paper reviews the imaging methods for diagnosing HPS such as ultrasound, dynamic pulmonary perfusion imaging, pulmonary angiography, and computed tomography.

Keywords: hepatopulmonary syndrome, diagnostic imaging, liver disease, IPVD, pulmonary vasodilation

OPEN ACCESS

Edited by:
Zhanqi Zhao,
Furtwangen University, Germany

Reviewed by:
Zhiyu Xiao,
Sun Yat-sen University, China
Cale Kassel,
University of Nebraska Medical Center, United States

***Correspondence:**
Zhi-Yong Du
duzhiyong88@163.com

Specialty section:
This article was submitted to Intensive Care Medicine and Anesthesiology, a section of the journal Frontiers in Medicine

Received: *18 November 2021*
Accepted: *16 December 2021*
Published: *10 January 2022*

Citation:
Luo B-W and Du Z-Y (2022) Advances in Diagnostic Imaging of Hepatopulmonary Syndrome. Front. Med. 8:817758. doi: 10.3389/fmed.2021.817758

INTRODUCTION

When liver disease progresses to a certain stage, it is followed by the onset of pulmonary vasodilation, pulmonary gas exchange disorder, decrease in the arterial oxygen partial pressure, and clinical manifestations, which is called hepatopulmonary syndrome. In 1956, Rydell and Hoffbauer first reported a patient with liver cirrhosis complicated with a pulmonary arteriovenous fistula and described the pathophysiology of hypoxemia (1). In 1977, Kennedy and Knudson first used the term "hepatopulmonary syndrome (HPS)" to describe pulmonary vascular disease secondary to liver cirrhosis and it has been used thereafter (2). Subsequently, Sherlock further elaborated on hepatopulmonary syndrome (3). There is a clear connection between hypoxemia and liver disease. In presence of liver disease, it appears that pulmonary vasodilatation (PV) leads to a mismatch between ventilation/perfusion and diffusing capacity. The diagnostic criteria for HPS: (1) presence of liver disease, (2) evidence of intrapulmonary vascular dilatation (IPVD), which is also the basic pathological change, and (3) a pulmonary bubble arterial oxygen differential pressure [P [A-a] O_2 gradient] that is $\geq$15 mmHg (or >20 mmHg if age $\geq$65 years). The severity of HPS can be classified according to the PaO_2 into either mild (PaO_2 $\geq$80 mmHg), moderate (PaO_2 60–79 mmHg), severe (PaO_2 50–59 mmHg), or very severe (PaO_2 <50 mmHg) (4). HPS mostly occurs in patients with liver cirrhosis, with an incidence rate of 9.45–42.5% (5–10). HPS is a serious pulmonary complication of end-stage liver disease. The mortality of patients with HPS is significantly high and the prognosis is poor (10). Early detection and timely treatment may help improve the prognosis. HPS should be considered if there is abnormal pulmonary arterial oxygenation in the presence of liver disease; however, abnormal blood oxygen saturation alone is not enough to diagnose HPS (9). The focus of clinical diagnosis is to identify evidence of PV in patients with chronic liver disease

complicated with hypoxemia. Therefore, clinical assessment must be combined with the results of imaging examination. This paper presents a comprehensive review of the latest developments in the diagnostic imaging of HPS.

PROGRESS IN ULTRASOUND USE FOR THE DIAGNOSIS OF HPS

With the onset of HPS, patients have a higher cardiac output and hyperdynamic circulation, resulting in corresponding changes in the cardiac structure. HPS can be indirectly diagnosed by measuring the cardiac structure using cardiac color Doppler ultrasound. Zamirian conducted a cardiac B-ultrasound examination on adult patients with confirmed HPS and found that the left atrial volume (LAV) was increased significantly. In patients with liver cirrhosis, HPS is considered if the measured LAV is >50 ml, and sensitivity and specificity are estimated to be 86.3 and 81.2%, respectively (11). This is mainly due to the right to left shunt in patients with HPS, resulting in increased cardiac output and increased left heart volume (11). A previous study proved that increased LAV can reflect the presence of HPS in patients with liver cirrhosis, and increased systemic blood velocity through the mitral valve can also indirectly indicate the presence of HPS (12). Moreover, Soulaidopoulos found that absolute left ventricular (LV) global longitudinal strain (GLS) values are significantly lower in patients with HPS compared to cirrhotic patients without HPS (13). Furthermore, results from a previous study suggest that systolic pulmonary artery pressure, right ventricle wall width, and early filling (E) and late filling (A) ratio (E/A ratio) can predict IPVD (14). The right ventricular diastolic dysfunction rate also increases significantly in patients with liver cirrhosis, especially in patients with HPS (15). As HPS can cause changes in the cardiac structure, cardiac ultrasound measurement can help in making an indirect diagnosis. This method is simple and convenient and especially suitable for preliminary screening of HPS in primary medical units (16).

PROGRESS IN CONTRAST ENHANCED ECHOCARDIOGRAPHY (CEE) FOR THE DIAGNOSIS OF HPS

The hand vibration method is used to produce microbubbles with a diameter ≤90 μm in normal saline, followed by injection into an upper limb vein of the patient. If the patient does not have a right to left shunt, the microbubbles will be captured and absorbed by the pulmonary capillary bed, and will not be able to reach the left cardiac system. Conversely, if the subject has pulmonary capillary dilation or a right to left shunt, the microbubbles will reach the left cardiac system, and can be detected in the left heart by ultrasonic examination. This method is called contrast-enhanced echocardiography. At present, the commonly used methods are contrast-enhanced transthoracic echocardiography (CTTE) and contrast-enhanced transesophageal echocardiography (CTEE). CTTE is a simple, non-invasive technique, low cost, and safe. However, CTEE is an invasive procedure that is relatively complex and entails a high cost. However, CTEE can provide excellent image quality, has a higher sensitivity that can improve the detection rate, and is significantly better for the diagnosis of PV compared to CTTE (17–19).

Some researchers have attempted to increase the sensitivity of CEE by changing the operation mode. For example, CEE examination in a standing position is observed to be better than that in a supine position, which may be due to the expansion of the pulmonary basal blood vessels and increased blood flow because of gravity (20, 21). Moreover, 3D CEE can obtain more 2D images and provide more data for analysis. CEE has a higher sensitivity and can better diagnose HPS compared to CTEE (22). A previous study estimated the erythrocyte pulmonary transit time (PTT) by detecting the time from the right atrium to the left atrium by CEE. It was found that PTT may be a useful parameter for evaluating arterial oxygenation in patients with chronic liver disease with early HPS (23). Another study also revealed that contrast enhanced transcranial Doppler was more sensitive for the detection of IPVD with a low false positive rate (24).

CEE is the most commonly used diagnostic imaging method for PV and the right to left shunt. It is simple, convenient, minimally invasive, and highly sensitive. At present, it is the gold standard for diagnosis. CEE also has some limitations. As an example, since many patients with liver cirrhosis may have normal blood gas content, the positive detection rate for such patients is only 40% by CEE. Further, other diseases of the lung can also lead to abnormal gas exchange. Therefore, using CEE, positive findings in the lungs alone are not enough for the diagnosis of HPS.

PROGRESS IN TECHNETIUM 99M-LABELED MACROAGGREGATED ALBUMIN (TC-MMA) DYNAMIC LUNG PERFUSION SCAN FOR THE DIAGNOSIS OF HPS

Dynamic pulmonary perfusion imaging is one of the common methods for diagnosing pulmonary vascular abnormalities in HPS. Technetium labeled human serum albumin polymer particle is a large albumin particle with a diameter >20 μm. A certain amount of Tc-MMA is injected into the peripheral vein of the patient at one time. The whole process of the radionuclide passing through cardiopulmonary vessels is recorded in the anterior and posterior positions by the γ camera during cardiovascular dynamic imaging. After 5 min, the posterior and anterior positions are taken for whole-body imaging, and the computer is used for synchronous data collection and imaging. The whole-body and bilateral lung radioactivity counts are calculated by the region of interest method, and the right to left shunt ratio of Tc-MMA is also calculated. Tc-MMA persists in the capillary beds with a diameter of 8–15 μm, and when the pulmonary capillaries show abnormal dilation and arteriovenous communication, Tc-MMA can pass through the abnormally dilated pulmonary vessels. This can help in obtaining extrapulmonary organ imaging and determining the intrapulmonary partial flow, which can help to diagnose patients

with HPS (25, 26). Zhao et al. evaluated the sensitivity, specificity, and accuracy of the brain and systemic uptake of 99mTc-MAA in IPVD, and found that the whole-body uptake was better than simple brain uptake (27). The overall sensitivity of 99mTc-MAA in the diagnosis of HPS is 18.9% in all HPS cases, which is relatively low, but it is 66.7% in severe to very severe cases. Consequently, it can be used in patients with pulmonary disease and severe to very severe HPS (28).

Tc-MAA perfusion lung scan is more sensitive than CEE in detecting an intrapulmonary shunt in children with HPS (29). Some studies have suggested that there is no significant difference between the two in detecting an intrapulmonary shunt in children with HPS (6). In general, the detection sensitivity of 99mTc-MAA is lower than that of CEE, although its specificity is higher than that of CEE for the diagnosis of HPS. However, the greatest limitation of this imaging examination is that it cannot distinguish between an intracardiac and intrapulmonary shunt, nor can it evaluate cardiac function and pulmonary artery pressure. In addition, it can produce false positive results because non-bound technetium can pass through the vessels with a normal width.

PROGRESS IN PULMONARY ANGIOGRAPHY FOR THE DIAGNOSIS OF HPS

Pulmonary angiography refers to selective pulmonary angiography carried out by puncture of peripheral blood vessels (usually femoral veins) and insertion of catheters. According to the different angiographic manifestations and pathophysiological characteristics, HPS can be divided into type I and type II (30). In type I, normal or diffuse, small, spider-like branching dilatations can be seen in the early stage. With the progression of dilatation, blotchy or spongy diffuse dilatation can be observed. Type II is relatively rare, showing anatomic arteriovenous malformations similar to spider nevus (31). Pulmonary angiography can directly reveal the dilated blood vessels and can also be used for embolization and other treatments (32). In addition, the determination of PTT by pulmonary angiography is very useful for the diagnosis of HPS, with higher sensitivity compared to the Tc-MAA lung perfusion scan, and may even be used to quantify the degree of intrapulmonary shunting (33).

Pulmonary angiography has not been widely used in clinical settings as it is invasive and expensive. It is mainly used in patients with persistent hypoxemia who have a poor response to inhaled pure oxygen and need intrapulmonary vascular embolization. In some HPS patients, PV is microscopic, and pulmonary angiography may not reveal any abnormality.

ADVANCES IN THE COMPUTED TOMOGRAPHY (CT) DIAGNOSIS OF HPS

The principal manifestations of chest CT in HPS include thickening and distortion of the lung basal texture, medium-sized nodular or reticular nodular shadows at the bottom of the lung, arteriovenous malformations, cardiac enlargement, and pulmonary artery widening (34). In addition to the number and location of pulmonary arteriovenous malformations, CT can also display the lung parenchyma pattern such as a mosaic pattern, which is characterized by alternating low attenuation areas (pulmonary vessels with reduced diameter) and high attenuation areas (pulmonary vessels with normal diameter). This mosaic pattern of the lung parenchyma is speculated to be associated with HPS and may be a potentially useful marker for the diagnosis of HPS, but still needs to be confirmed by large research studies (34).

High-resolution CT (HRCT) can show the expansion of the subpleural vessels that extend to the pleura, which is helpful for the diagnosis of HPS (35). Chest HRCT can also help in the diagnosis of HPS by calculating the ratio of the pulmonary artery to the bronchial diameter in the basal segment of the right lower lobe (36). Some studies have shown that although the arterial bronchial ratio of the basal segment in patients with liver disease is greater than that in the normal control group, this vasodilation is not serious in patients with HPS (37), and the incidence is low (7). CT cannot adequately distinguish if liver disease is complicated by HPS. For example, in a patient with HPS complicated with emphysema, an intrapulmonary shunt examination by 99mTc-MAA showed that the systemic shunt rate was 43% and there was no vasodilation on chest CT (38). Therefore, more research data are needed to support CT imaging for HPS.

In one study, lung images were obtained by single-photon emission computed tomography and CT. After merging, the images revealed that there were subpleural reticular nodular shadows and/or dilated blood vessels at the bottom of the lung in patients with HPS. This seems to be a characteristic CT manifestation of intrapulmonary arteriovenous communications in the lungs of HPS patients (39).

DISCUSSION

With the development of HPS in patients with liver disease, there are different degrees of abnormal dilatation of the pulmonary vessels. The rapid and accurate diagnosis of HPS through an imaging examination is particularly important. Routine cardiac B-ultrasound can indirectly diagnose HPS by measuring the changes in the ventricular structure. At present, contrast echocardiography and Tc-MAA dynamic lung perfusion imaging can indirectly indicate the existence of an intrapulmonary right to left shunt. It is the most used examination method in the clinic, with a high sensitivity but low specificity. Pulmonary angiography can directly show the changes in the pulmonary vessels with high sensitivity and specificity, but it is more traumatic, expensive, and limited in application. CT can directly show the morphological changes in the pulmonary vessels, and facilitate the diagnosis of HPS based on specific signs. Although there are still some controversies, it can help in the diagnosis of HPS. With the recent developments in multi-energy computed tomography (MECT) diagnostic technology, it has been used in the clinical diagnosis of various diseases

of the whole body, especially vascular imaging. Researchers have applied MECT in the diagnosis of pulmonary vascular disease because it provides additional information for assessing the pulmonary vascular system (40). MECT provides new avenues for research and may become a new diagnostic method for HPS.

Overall, the progress of research on the diagnostic imaging of HPS has been relatively slow. In the future, there is a need to increase the clinical and basic research on HPS to further deepen the understanding of its pathogenesis and investigate new examination techniques to improve diagnostic efficiency.

AUTHOR CONTRIBUTIONS

B-WL: writing—original draft. Z-YD: writing—review and editing and funding acquisition. All authors contributed to the article and approved the submitted version.

FUNDING

This work was supported by Shenzhen Key Medical Discipline Construction Fund (No. SZXK015) and Science and Technology Innovation Foundation of Shenzhen (JCYJ20190807144807510).

REFERENCES

1. Hoffbauer FW, Rydell R. Multiple pulmonary arteriovenous fistulas in juvenile cirrhosis. *Am J Med.* (1956) 21:450–60. doi: 10.1016/0002-9343(56)90043-2
2. Kennedy TC, Knudson RJ. Exercise-aggravated hypoxemia and orthodeoxia in cirrhosis. *Chest.* (1977) 72:305–9. doi: 10.1378/chest.72.3.305
3. Sherlock S, Dooley J. *Sherlock's Diseases of the Liver and Biliary System*. 8th ed. Oxford: Blackwell Scientific (1989). doi: 10.1097/00004836-199008000-00036
4. Raevens S, Geerts A, Devisscher L, Van Vlierberghe H, Van Steenkiste C, Colle I. Recent advances in the approach to hepatopulmonary syndrome and portopulmonary hypertension. *Acta Gastro Enterol Belgica.* (2021) 84:95–9. doi: 10.51821/84.1.200
5. Cárdenas Ramírez B, Padilla-Machaca PM, Mantilla Cruzatti O, Rivera Romaní J, Rondón Leyva C, Chaman Ortiz JC. [Hepatopulmonar syndrome and liver transplantation: experience in the transplantation department of the Guillermo Almenara Irigoyen National Hospital - EsSalud]. *Rev Gastroenterol Peru*. (2018) 38:242–7.
6. Ceza MR, Garcia E, Anselmi CE, Epifanio M, Melere MU, Ferreira CT, et al. Prevalence and characteristics of hepatopulmonary syndrome in children with cirrhosis in southern Brazil. *Eur J Gastroenterol Hepatol.* (2019) 31:10–5. doi: 10.1097/MEG.0000000000001207
7. Folador L, Torres FS, Zampieri JF, Machado BC, Knorst MM, Gazzana MB. Hepatopulmonary syndrome has low prevalence of pulmonary vascular abnormalities on chest computed tomography. *PLoS ONE.* (2019) 14:e0223805. doi: 10.1371/journal.pone.0223805
8. Khiangte B, Kothakota SR, Sasidharan M, Kareem H, Joshi S, Kumar VV, et al. Prevalence and determinants of hepatopulmonary syndrome in decompensated chronic liver disease. *Indian J Gastroenterol.* (2020) 39:362–9. doi: 10.1007/s12664-020-01052-9
9. Rose SCP, Cunha DV, Medeiros SBC, Trevizoli JE, Carneiro MV, Freitas WM, et al. Correlation between hepatopulmonary syndrome and oxygen saturation pulse oximetry in cirrhotic patients. *Rev Assoc Med Brasil.* (1992) (2020) 66:1577–82. doi: 10.1590/1806-9282.66.11.1577
10. Han SK, Kim MY, Kang SH, Suk KT, Baik SK. Hepatopulmonary syndrome is related to the development of acute-on-chronic liver failure and poor prognosis in cirrhotic patients. *Hepatol Int.* (2021) 15:1207–14. doi: 10.1007/s12072-021-10226-2
11. Zamirian M, Aslani A, Sharifkazemi MB. Prediction of intrapulmonary right to left shunt with left atrial size in patients with liver cirrhosis. *Eur J Echocardiogr.* (2008) 9:1–4. doi: 10.1016/j.euje.2006.10.003
12. Pouriki S, Alexopoulou A, Chrysochoou C, Raftopoulos L, Papatheodoridis G, Stefanadis C, et al. Left ventricle enlargement and increased systolic velocity in the mitral valve are indirect markers of the hepatopulmonary syndrome. *Liver Int.* (2011) 31:1388–94. doi: 10.1111/j.1478-3231.2011.02591.x
13. Soulaidopoulos S, Vlachou M, Cholongitas E, Giannakoulas G, Panagiotidis T, Drakopoulou M, et al. Assessment of biventricular function in patients with hepatopulmonary syndrome. *Int J Cardiovasc Imaging.* (2021) 37:2891–900. doi: 10.1007/s10554-021-02260-w
14. Voiosu A, Voiosu T, Stănescu CM, Chirilă L, Băicuş C, Voiosu R. Novel predictors of intrapulmonary vascular dilatations in cirrhosis: extending the role of pulse oximetry and echocardiography. *Acta Gastro Enterol Belg.* (2013) 76:241–5.
15. Karabulut A, Iltumur K, Yalcin K, Toprak N. Hepatopulmonary syndrome and right ventricular diastolic functions: an echocardiographic examination. *Echocardiography.* (2006) 23:271–8. doi: 10.1111/j.1540-8175.2006.00210.x
16. Alves Pinto R, Rodrigues J, Almeida PB. Echocardiographic diagnosis of hepatopulmonary syndrome: a valuable tool to remember. *Intern Emerg Med.* (2021) 16:2299–300. doi: 10.1007/s11739-021-02731-x
17. Aller R, Moya JL, Moreira V, Boixeda D, Cano A, Picher J, et al. Diagnosis of hepatopulmonary syndrome with contrast transesophageal echocardiography: advantages over contrast transthoracic echocardiography. *Digest Dis Sci.* (1999) 44:1243–8. doi: 10.1023/A:1026657114256
18. Fischer CH, Campos O, Fernandes WB, Kondo M, Souza FL, De Andrade JL, et al. Role of contrast-enhanced transesophageal echocardiography for detection of and scoring intrapulmonary vascular dilatation. *Echocardiography.* (2010) 27:1233–7. doi: 10.1111/j.1540-8175.2010.01228.x
19. Gouvea A, Fischer CH, Arakaki JSO, Mancuso FJ, Brant P, Moisés VA, et al. Value of contrast transesophageal echocardiography in the detection of intrapulmonary vascular dilatations in hepatosplenic schistosomiasis. *Arq Brasil Cardiol.* (2019) 113:915–22. doi: 10.5935/abc.20190200
20. Lenci I, Alvior A, Manzia TM, Toti L, Neuberger J, Steeds R. Saline contrast echocardiography in patients with hepatopulmonary syndrome awaiting liver transplantation. *J Am Soc Echocardiogr.* (2009) 22:89–94. doi: 10.1016/j.echo.2008.09.020
21. Sekioka A, Nii M, Fukumoto K, Miyake H, Urushihara N. Hepatopulmonary syndrome revealed via echocardiography in the upright position. *Pediatr Int.* (2020) 62:646–7. doi: 10.1111/ped.14145
22. Gaber R, Ziada DH, Kotb NA, Abo El-Magd GH, Hamisa M. Detection of hepatopulmonary syndrome in patients with liver cirrhosis using 3D contrast echocardiography. *Arab J Gastroenterol.* (2012) 13:14–9. doi: 10.1016/j.ajg.2012.03.004
23. Katsuta Y, Honma H, Zhang XJ, Ohsuga M, Komeichi H, Shimizu S, et al. Pulmonary blood transit time and impaired arterial oxygenation in patients with chronic liver disease. *J Gastroenterol.* (2005) 40:57–63. doi: 10.1007/s00535-004-1495-6
24. Ramírez Moreno JM, Millán Núñez MV, Rodríguez Carrasco M, Ceberino D, Romaskevych-Kryvulya O, Constantino Silva AB, et al. [Detection of an intrapulmonary shunt in patients with liver cirrhosis through contrast-enhanced transcranial Doppler. A study of prevalence, pattern characterization, and diagnostic validity]. *Gastroenterol Hepatol.* (2015) 38:475–83. doi: 10.1016/j.gastrohep.2015.02.006
25. Fragaki M, Sifaki-Pistolla D, Samonakis DN, Koulentaki M, Koukouraki S, Stathaki M, et al. Screening for hepatopulmonary syndrome in cirrhotic patients using Technetium 99m-macroaggregated Albumin Perfusion Lung Scan (Tc-MAA): diagnostic approach and clinical correlations. *J Clin Gastroenterol.* (2018) 52:828–34. doi: 10.1097/MCG.0000000000000926
26. Surasi DS, Manapragada P, Bhambhvani P. Lung perfusion imaging in hepatopulmonary syndrome using (99m)Tc macroaggregated albumin. *J Nuclear Cardiol.* (2015) 22:586–8. doi: 10.1007/s12350-014-9990-5
27. Zhao H, Tsauo J, Zhang XW, Ma HY, Weng NN, Tang GS, et al. Technetium-99m-labeled macroaggregated albumin lung perfusion scan for diagnosis of hepatopulmonary syndrome: a prospective study comparing brain uptake and whole-body uptake. *World J Gastroenterol.* (2020) 26:1088–97. doi: 10.3748/wjg.v26.i10.1088

28. Grilo I, Pascasio JM, Tirado JL, López-Pardo FJ, Ortega-Ruiz F, Sousa JM, et al. The utility of the macro-aggregated albumin lung perfusion scan in the diagnosis and prognosis of hepatopulmonary syndrome in cirrhotic patients candidates for liver transplantation. *Rev Esp Enferm Dig.* (2017) 109:335–43. doi: 10.17235/reed.2017.4219/2016
29. El-Shabrawi MH, Omran S, Wageeh S, Isa M, Okasha S, Mohsen NA, et al. (99m)Technetium-macroaggregated albumin perfusion lung scan versus contrast enhanced echocardiography in the diagnosis of the hepatopulmonary syndrome in children with chronic liver disease. *Eur J Gastroenterol Hepatol.* (2010) 22:1006–12. doi: 10.1097/MEG.0b013e328336562e
30. Krowka MJ, Dickson ER, Cortese DA. Hepatopulmonary syndrome. Clinical observations and lack of therapeutic response to somatostatin analogue. *Chest.* (1993) 104:515–21. doi: 10.1378/chest.104.2.515
31. Krowka MJ, Cortese DA. Hepatopulmonary syndrome. Current concepts in diagnostic and therapeutic considerations. *Chest.* (1994) 105:1528–37. doi: 10.1378/chest.105.5.1528
32. Ryu JK, Oh JH. Hepatopulmonary syndrome: angiography and therapeutic embolization. *Clin Imaging.* (2003) 27:97–100. doi: 10.1016/S0899-7071(02)00511-9
33. Zhao H, Tsauo J, Zhang X, Ma H, Weng N, Wang L, et al. Pulmonary transit time derived from pulmonary angiography for the diagnosis of hepatopulmonary syndrome. *Liver Int.* (2018) 38:1974–81. doi: 10.1111/liv.13741
34. Gorospe Sarasúa L, Olavarría-Delgado A, Farfán-Leal FE, Pérez-Templado Ladrón de Guevara J. Hepatopulmonary syndrome with large pulmonary arteriovenous malformations: CT findings with emphasis on its association with a mosaic pattern of the lung parenchyma. *Rev Esp Enferm Dig.* (2017) 109:369.
35. Kumar S, Arora A, Bhatia V. Hepatopulmonary syndrome: a clinico-radiological diagnosis. *Indian J Gastroenterol.* (2013) 32:209–10. doi: 10.1007/s12664-013-0309-2
36. Köksal D, Kaçar S, Köksal AS, Tüfekçioglu O, Küçükay F, Okten S, et al. Evaluation of intrapulmonary vascular dilatations with high-resolution computed thorax tomography in patients with hepatopulmonary syndrome. *J Clin Gastroenterol.* (2006) 40:77–83. doi: 10.1097/01.mcg.0000190775.57903.86
37. Chen YA, Prabhudesai V, Castel H, Gupta S. CT scan does not differentiate patients with hepatopulmonary syndrome from other patients with liver disease. *PLoS ONE.* (2016) 11:e0158637. doi: 10.1371/journal.pone.0158637
38. Taniguchi H, Kanbara K, Imanishi S, Abo H, Izumi S. [Case of hepatopulmonary syndrome with no vascular dilation in chest CT]. *Nihon Kokyuki Gakkai Zasshi*. (2008) 46:466–9.
39. Suga K, Kawakami Y, Iwanaga H, Tokuda O, Matsunaga N. Findings of hepatopulmonary syndrome on breath-hold perfusion SPECT-CT fusion images. *Ann Nuclear Med.* (2009) 23:413–9. doi: 10.1007/s12149-009-0250-8
40. Rajiah P, Tanabe Y, Partovi S, Moore A. State of the art: utility of multi-energy CT in the evaluation of pulmonary vasculature. *Int J Cardiovasc Imaging.* (2019) 35:1509–24. doi: 10.1007/s10554-019-01615-8

Conflict of Interest: The authors declare that the research was conducted in the absence of any commercial or financial relationships that could be construed as a potential conflict of interest.

frontiers in Medicine

ORIGINAL RESEARCH
published: 31 January 2022
doi: 10.3389/fmed.2022.817590

Removing Clinical Motion Artifacts During Ventilation Monitoring With Electrical Impedance Tomography: Introduction of Methodology and Validation With Simulation and Patient Data

Lin Yang[1†], Shuoyao Qu[2†], Yanwei Zhang[3], Ge Zhang[3,4], Hang Wang[1], Bin Yang[5], Canhua Xu[5], Meng Dai[5] and Xinsheng Cao[1*]*

[1] Department of Aerospace Medicine, Fourth Military Medical University, Xi'an, China, [2] Department of Pulmonary and Critical Care Medicine, Xijing Hospital, Fourth Military Medical University, Xi'an, China, [3] Department of Medical Imaging, Bethune International Peace Hospital, Shijiazhuang, China, [4] Department of Medical Imaging, Henan Provincial People's Hospital and the People's Hospital of Zhengzhou University, Zhengzhou, China, [5] Department of Biomedical Engineering, Fourth Military Medical University, Xi'an, China

OPEN ACCESS

Edited by:
Huaiwu He,
Peking Union Medical College Hospital (CAMS), China

Reviewed by:
Ling Sang,
Guangzhou Institute of Respiratory Health, China
Dong Liu,
University of Science and Technology of China, China

***Correspondence:**
Meng Dai
daimeng@fmmu.edu.cn
Xinsheng Cao
caoxinsh@fmmu.edu.cn

[†]These authors have contributed equally to this work

Specialty section:
This article was submitted to Intensive Care Medicine and Anesthesiology, a section of the journal Frontiers in Medicine

Received: 18 November 2021
Accepted: 10 January 2022
Published: 31 January 2022

Citation:
Yang L, Qu S, Zhang Y, Zhang G, Wang H, Yang B, Xu C, Dai M and Cao X (2022) Removing Clinical Motion Artifacts During Ventilation Monitoring With Electrical Impedance Tomography: Introduction of Methodology and Validation With Simulation and Patient Data. Front. Med. 9:817590. doi: 10.3389/fmed.2022.817590

Objective: Electrical impedance tomography (EIT) is a bedside tool for lung ventilation and perfusion assessment. However, the ability for long-term monitoring diminished due to interferences from clinical interventions and motion artifacts. The purpose of this study is to investigate the feasibility of the discrete wavelet transform (DWT) to detect and remove the common types of motion artifacts in thoracic EIT.

Methods: Baseline drifting, step-like and spike-like interferences were simulated to mimic three common types of motion artifacts. The discrete wavelet decomposition was employed to characterize those motion artifacts in different frequency levels with different wavelet coefficients, and those motion artifacts were then attenuated by suppressing the relevant wavelet coefficients. Further validation was conducted in two patients when motion artifacts were introduced through pulsating mattress and deliberate body movements. The db8 wavelet was used to decompose the contaminated signals into several sublevels.

Results: In the simulation study, it was shown that, after being processed by DWT, the signal consistency improved by 92.98% for baseline drifting, 97.83% for the step-like artifact, and 62.83% for the spike-like artifact; the signal similarity improved by 77.49% for baseline drifting, 73.47% for the step-like artifact, and 2.35% for the spike-like artifact. Results from patient data demonstrated the EIT image errors decreased by 89.24% (baseline drifting), 88.45% (step-like artifact), and 97.80% (spike-like artifact), respectively; the data correlations between EIT images without artifacts and the processed were all > 0.95.

Conclusion: This study found that DWT is a universal and effective tool to detect and remove these motion artifacts.

Keywords: thoracic electrical impedance tomography, discrete wavelet transform, motion artifacts, chronic obstructive pulmonary disease, acute respiratory distress syndrome

INTRODUCTION

Electrical impedance tomography (EIT) images the internal impedance distribution from current stimulations and voltage measurements on the body surface (1). As it is a non-invasive and radiation-free imaging modality that can be used in real-time at the bedside, the medical community is very interested in this technique and attempts to apply it into clinical practice, such as monitoring lung ventilation of ICU patients (2), observing the progress of brain injury (3), early detection of breast cancer (4), etc. Among these medical applications, thoracic EIT for ICU patients is one of the most active and promising areas (5), and it focuses explicitly on several directions, including titration of tidal volume or positive end-expiratory pressure, comparison of various ventilation modes, evaluation of lung recruitability and effect of recruitment maneuver, evaluation of suctioning or rehabilitation, monitoring the ventilation distribution for patients with spontaneous breathing, perioperative monitoring and evaluation of regional lung function, etc. (6). In pulmonary and critical care medicine, thoracic EIT is increasingly accepted in hospitals because it can provide different measures of lung function on a regional level and visualize their distribution within the chest, which other established techniques cannot substitute (7).

However, EIT is currently close to but not yet a routine clinical examination method. One of the critical factors limiting its daily use is that EIT might be inherently vulnerable to the source of interference signals, especially to motion artifacts in clinical settings (8). Motion artifacts caused by patients' deliberate movement, medical treatment or nursing are inevitable and may often hinder acquiring, evaluating, and interpreting EIT data (9).

Specifically, for thoracic EIT, motion artifacts mainly include three types: baseline drifting, step-like signal, and spike-like signal. The baseline drifting is a slow-varying disturbance, typically generated by repetitive interferences. The pulsating air suspension mattress that repetitively inflates and deflates is a common source of such artifact (9) (**Figure 1**, left). The step-like signal is a frequent disturbance where the baseline of the impedance signal changes suddenly due to the influence of body movement (e.g., postural change) and does not return to the previous level after the body movement (**Figure 1**, middle). The spike-like signal is also a frequent disturbance in which the baseline of the impedance signal does return to the previous level after the movement (**Figure 1**, right). However, to our knowledge, there is currently no study focusing on eliminating motion artifacts in chest EIT for clinical use.

Therefore, we aim to establish a universal signal processing framework for removing these three common types of clinical motion artifacts for chest EIT. The present study introduced the engineering field's discrete wavelet transform (DWT) into our framework and validated it with simulation and patient data.

METHODS

In this section, we introduced the EIT imaging formula and then modeled EIT measured data, which were corrupted by motion artifacts, with DWT; the motion artifacts were subsequently removed by processing the coefficients of DWT. Our framework of motion artifact removal was finally validated with simulation and patient data.

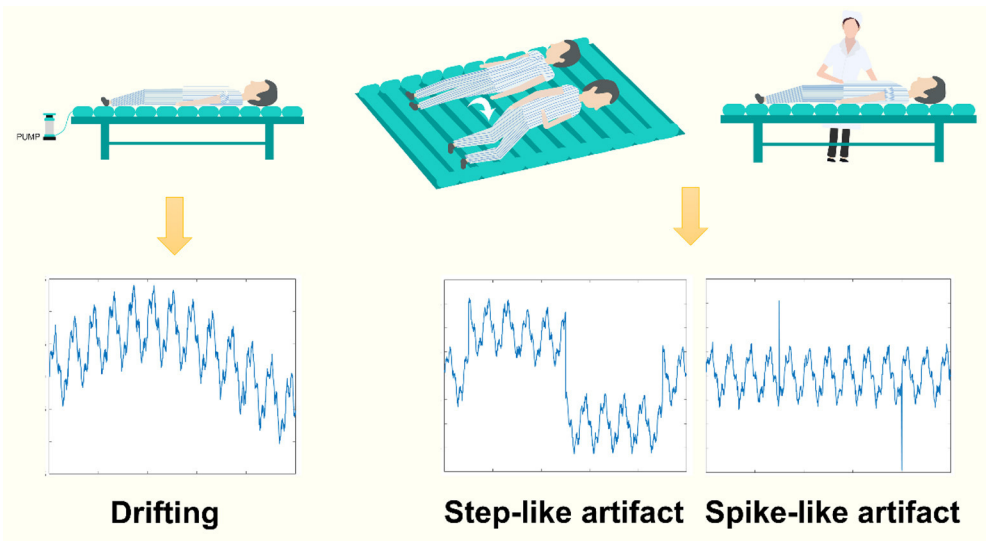

FIGURE 1 | The common types of motion artifacts in clinical EIT. Left: baseline drifting, a slow-varying signal added to the EIT data, often generated by a source of repetitive signals, e.g., an air suspension mattress. Middle and right: the step-like and spike-like artifacts, two types of abrupt varying artifacts, often caused by patients' deliberate body movements or nursing.

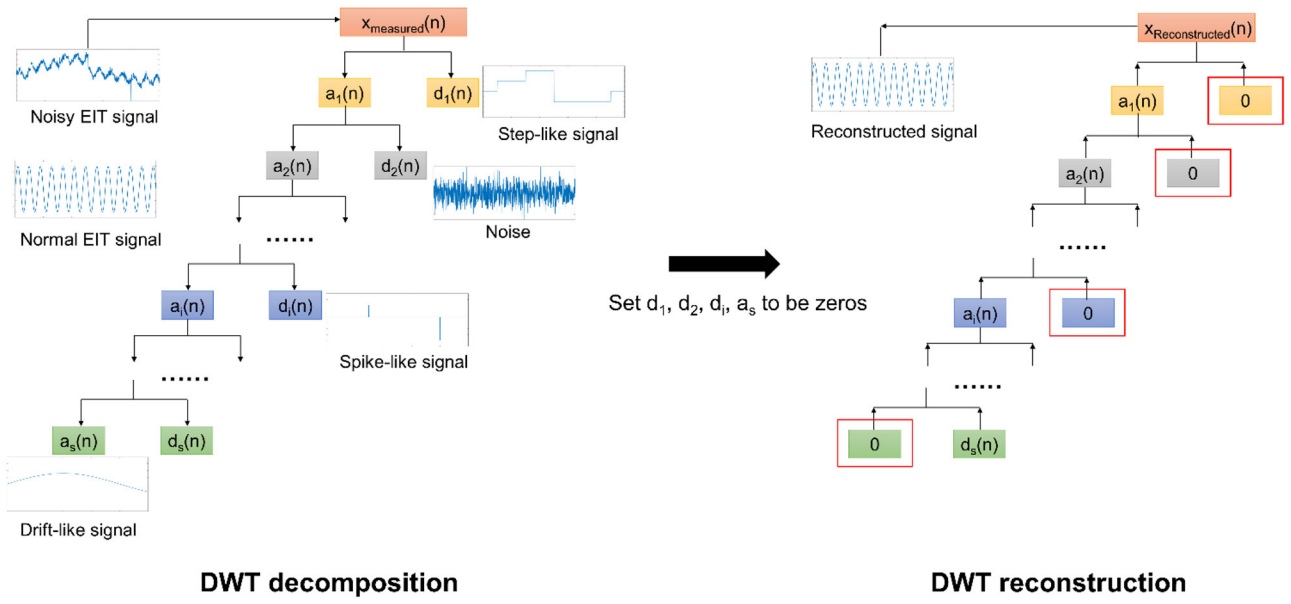

FIGURE 2 | The DWT scheme for EIT motion artifact removal. In the DWT decomposition, the noisy EIT signal is decomposed into a slow-varying signal $a_1(n)$and a fast-varying signal $d_1(n)$ at the first level. This processing is repeated with respect to $a_i(n)$ until those three types of motion artifacts can be portrayed by $a_i(n)$ and $d_i(n)$. In the DWT rebuild, we first set these $a_i(n)$ and $d_i(n)$ corresponding to motion artifacts to be zeros and then rebuild the EIT signal using the remaining $a_i(n)$ and $d_i(n)$. The reconstructed EIT signal would eliminate the motion artifacts.

EIT Imaging Formula

In EIT, 16 electrodes are usually employed to excite the currents and measure the voltages. We used the "adjacent excitation" mode in this study so that for each frame $\mathbf{x}$, $16 \times 13 = 208$ data could be measured. Namely, there are 208 channels of EIT data against time. Next, we can present dynamic and linear EIT image reconstruction by the following formula:

$$\mathbf{y} = \mathbf{B}(\mathbf{x}_c - \mathbf{x}_{ref})$$

where $\mathbf{x}_c$ denotes the voltage measurements in the current frame while $\mathbf{x}_{ref}$ represents the measurements of the reference frame. $\mathbf{y}$ reflects the impedance variation distribution between the current frame and the reference frame. $\mathbf{B}$ is the inversion of sensitivity matrix (10).

Modeling Motion Artifacts With DWT

Given that $x_{measured}(n)$ is one channel of EIT data affected by motion artifacts, we can represent it as (11–13):

$$x_{measured}(n) = x_{breathing}(n) + x_{motion}(n)$$

where $x_{breathing}(n)$ is boundary voltage variation from breathings and $x_{motion}(n)$ is the motion-artifact component.

The DWT processing is shown in **Figure 2**. It is composed of two parts: decomposition and rebuild (12, 14, 15). In decomposition processing, using the so-called wavelet functions and the scaling functions, DWT decomposes the noisy EIT signal (corrupted by motion artifacts) into a relatively slow-varying signal $a_1(n)$ (approximation coefficients) and a fast-varying signal (detail coefficients) at the first step. Theoretically, the obtained signals often represent a type of motion artifact. e.g., $d_1(n)$ may reflect the step-like artifacts. Next, we continued to decompose $a_1(n)$ to obtain the second-level slow-varying signal $a_2(n)$and the fast-varying signal $d_2(n)$. We repeat decomposing the slow-varying signal $a_i(n)$ at each level until all three types of motion artifacts are correctly portrayed by $a_i(n)$ or $d_i(n)$. In addition, as the baseline drifting can be considered a slow-varying signal, it would be depicted by $a_s(n)$.

Conversely, in the rebuild processing, we constructed the EIT signals with a bunch of $a_i(n)$ and $d_i(n)$, also using the wavelet function and the scaling function. Nevertheless, we need to set $a_i(n)$ and $d_i(n)$ in relation to the corresponding motion artifacts to be zeros before rebuild. As such, those three types of motion artifacts in EIT signals can be appropriately removed.

In this study, we empirically selected the db8 function as mother wavelet by comprison, and the mathematical scheme is described in detail in the **Supplementary Material**.

Simulation Validation

To evaluate the performance of the proposed framework for motion artifact removal, we first carried out experiments using simulated data with Matlab 2016b (MathWorks, Inc., Natick, USA).

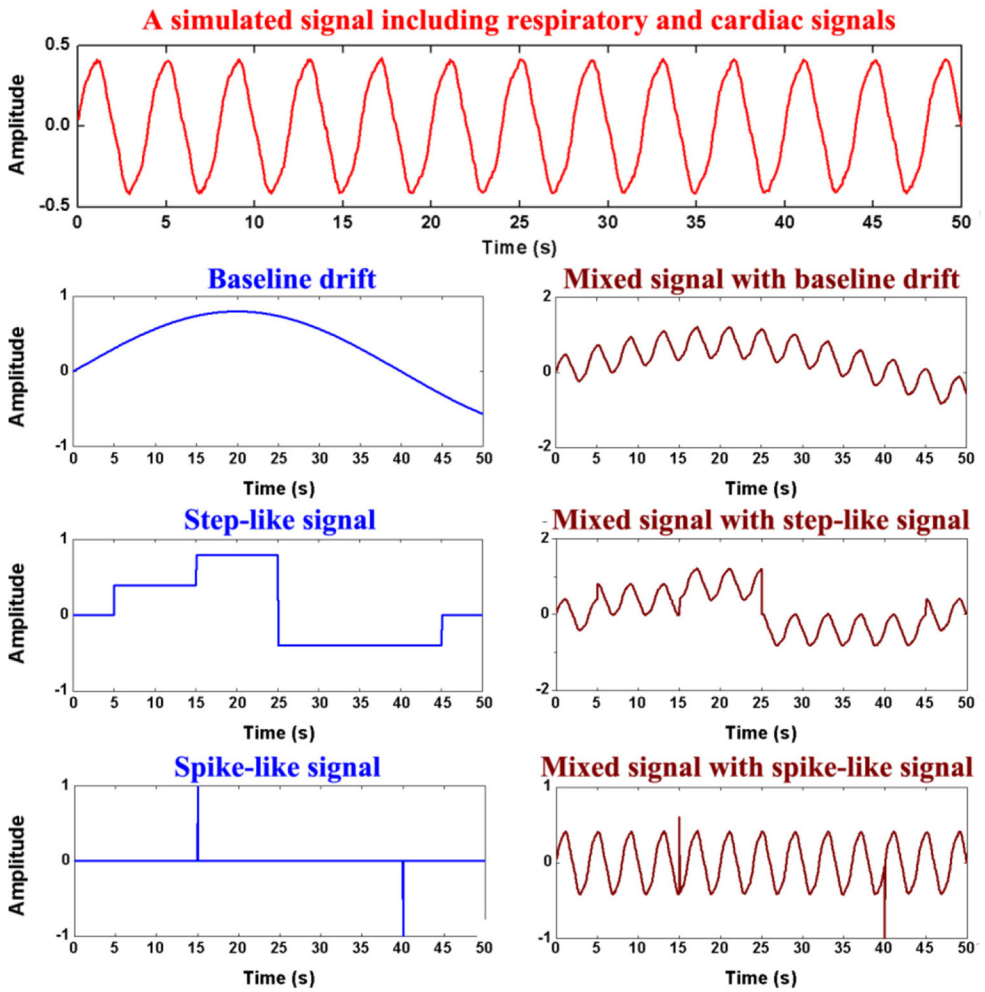

FIGURE 3 | Generation of the simulation data. The first row shows simulated respiratory and cardiac signals, the second row the simulated baseline drifting artifact, the third row the simulated step-like artifact, the last row the simulated spike-like artifact.

We generate a 1-D sine wave signal containing typical oscillations to simulate EIT breathing oscillations with additional Gaussian noise:

$$x_{simulate}(t) = \frac{1}{2}\sum_{i=1}^{2}\mu_i \sin(\omega_i t) + \lambda\sigma(t)$$

where $\omega = 2\pi f$, μ represents the oscillation amplitude of the sine wave, $\sigma(t)$ denotes Gaussian white noise, λ represents the amplitude of the Gaussian white noise, and the amplitude range for $x_{simulate}(t)$ is from -1 to 1. Here we include two sine waves in the mixed signal: (1) respiratory signal, $f = 0.25$ Hz, $\mu = 0.9$; (2) cardiac signal, $f = 1$ Hz, $\mu = 0.2$. The sampling frequency of the simulated signal was set to 20 Hz and the length was 5,000 samples.

Finally, three time-series data were mixed into $x_{simulate}$, which mimics the three forms of motion artifacts: baseline drifting, step-like signals and spike-like signals (As shown in **Figure 3**).

After the DWT rebuild, evaluations were carried out to estimate the agreement between the processed signal $y(t)$ and the original simulated signal without motion artifacts $x(t)$. The parameters percent root difference (PRD) and coefficient of determination (R^2) were defined as follows (16). PRD evaluates the consistency between $x(t)$ and $y(t)$; The greater PRD is, the smaller the consistency is. R^2 evaluates the similarity between $x(t)$ and $y(t)$; the largerR^2 means the greater similarity.

$$PRD = 100\% \times \sqrt{\sum_{i=1}^{N}(x(t_i) - y(t_i))^2 \left(\sum_{i=1}^{N} x^2(t_i)\right)^{-1}}$$

$$R^2 = \frac{\sum_{i=1}^{N}\left(y(t_i) - \overline{x(t)}\right)^2}{\sum_{i=1}^{N}\left(x(t_i) - \overline{x(t)}\right)^2}$$

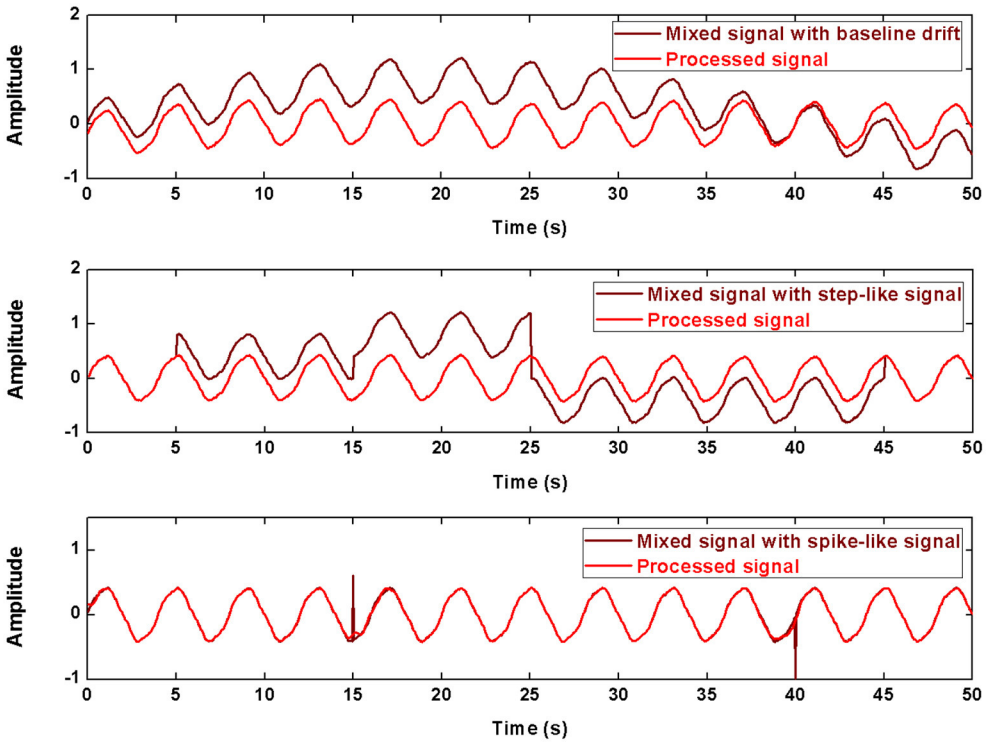

FIGURE 4 | The processed signals in simulation using DWT. The first row shows the result about baseline drifting removal, the second row about step-like artifact removal, the last row about spike-like artifact removal.

TABLE 1 | The evaluation parameters before and after being processed in the simulation.

	PRD	R^2
Drifting	1.8653	4.3202
Drifting-processed	0.1310	0.9726
Step-like artifact	1.6701	3.7737
Step-processed	0.0362	1.0011
Spike-like artifact	0.1578	1.0151
Spike-processed	0.0586	0.9913

Patient Data Validation

The clinical data were acquired in the pulmonary and critical care department of Xijing Hospital, Fourth Military Medical University, Xi'an, China. This study was approved by the human research ethics committee of the Fourth Military Medical University (KY20203282-1), and written informed consent was obtained from patients' nearest relatives. In this scenario, two male patients were included. An EIT electrode belt was attached around the thorax in the fourth intercostal space. The EIT system (PulmoVista 500, Draeger Medical, Luebeck, Germany) was used for recording at a sampling rate of 20 Hz. Image reconstruction was performed using the Graz consensus reconstruction algorithm for EIT (GREIT) algorithm (17).

Patient 1 had moderate acute respiratory distress syndrome. He was mechanically ventilated under volume-control mode. In the EIT data from Patient 1, baseline drifting by a pulsating mattress and the typical step-like artifacts were observed.

Patient 2, with moderate chronic obstructive pulmonary disease, undertook pulmonary rehabilitation. In the EIT data from Patient 2, we found the typical spike-like artifacts caused by his deliberate movements.

After the DWT rebuild, the EIT images before and after being processed were quantitively evaluated for similarity as follows,

$$\text{Image}_{error} = \frac{\sum |A_i - B_i|}{\sum |R_i|}$$

where A and B represent two different EIT images and R denotes the EIT image reconstructed using EIT data with no artifacts. The smaller Image_{error} is, the more similar the two images are.

$$\text{Image}_{\text{corr}} = \frac{\sum_m \sum_n \left(A_{mn} - \bar{A}\right)\left(B_{mn} - \bar{B}\right)}{\sqrt{\left(\sum_m \sum_n \left(A_{mn} - \bar{A}\right)^2\right)\left(\sum_m \sum_n \left(B_{mn} - \bar{B}\right)^2\right)}}$$

where A and B represent two different EIT images; A_{mn} and B_{mn} denote the pixel values of mth row and nth column in the image A and B, respectively; $\bar{A}$ and $\bar{B}$ are the mean values of an image A

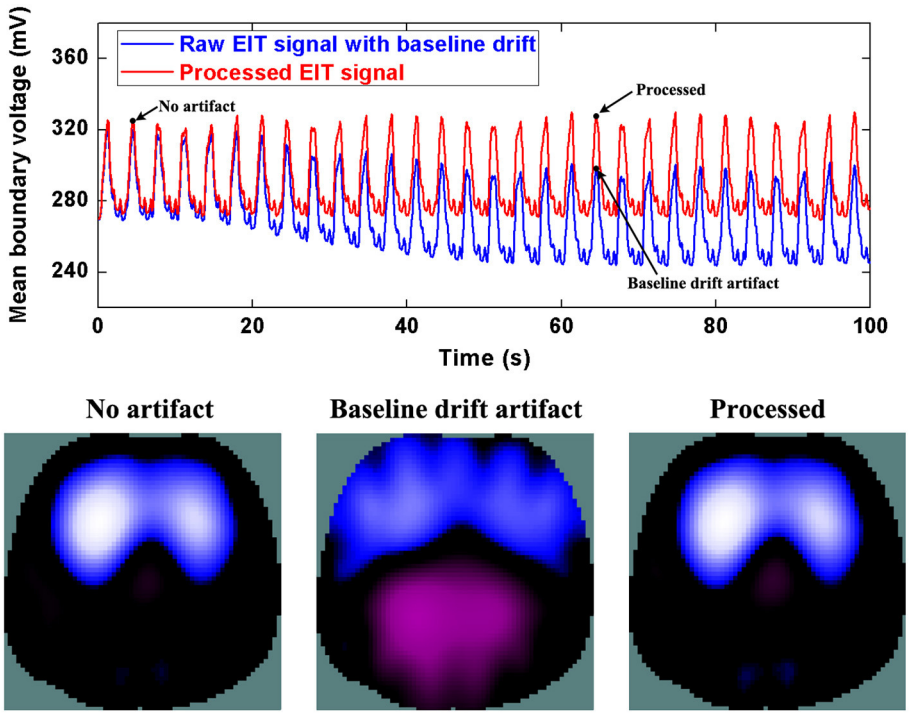

FIGURE 5 | The DWT processing results for baseline drifting removal in patient data. The first row shows the DWT processing result in EIT measured data. The blue line represents the drifting artifact in typical patient data, the red line the corrected data without drifting. The second row includes EIT images without the artifact, with the artifact, and after being processed.

and B, respectively. The $\text{Image}_{\text{corr}}$ ranges from −1 to 1.1 means the complete positive correlation.

RESULTS

Simulation Validation

The processing results for the simulated data are shown in **Figure 4** and **Table 1**. In baseline detrending, approximation coefficients of Level 6 were excluded in the signal rebuild. In step-like signal correction, only detail coefficients of Level 1 were used to identify the exact location of abrupt changes. Finally, the detail coefficients of Level 1 to the Level 4 were included to perform spike removal. As shown in **Figure 4**, all three types of simulated artifacts were effectively restrained after being processed. The proposed framework yielded an improvement in signal quality in all three cases. Specifically, it can be demonstrated that the data consistency evaluated by PRD for the drifting removal improved by 92.98%, for the step-like artifact by 97.83%, and for the spike-like artifact by 62.86%; the data similarity assessed by R^2 for the drifting removal improved by 77.49%, for the step-like artifact by 73.47%, and for the spike-like artifact by 2.35%.

Patient Data Validation

Figure 5 shows the processed results of baseline drifting removal. We can observe the significant artifacts caused by baseline drifting from the boundary voltages and EIT images. After being processed, the artifacts in the boundary voltages and EIT images are notably reduced. In addition, due to the influence of baseline drifting (the purple region in EIT images), we cannot identify whether the ARDS patient's regional lung ventilation distribution only includes the ventral side, i.e., whether the patient's lungs are only ventilated on the ventral side. Nevertheless, we can confirm this after EIT data was processed.

Similarly, **Figure 6** and **7** show step- and spike-like artifact removal processing, with improvement in the averaged waveform of all channels of EIT data and reconstructed EIT images, respectively. As expected, both measurements and images were considerably improved by restoring intrinsic ventilation distribution.

The evaluation parameters for EIT images before and after being processed are listed in **Table 2**. The image errors decreased by 89.24% (baseline drifting), 88.45% (Step-like artifacts), and 97.80% (Spike-like artifacts). After being processed, the correlations between EIT images without artifacts and the processed ones were all > 0.95.

DISCUSSION

Thoracic EIT provides unique information on regional lung ventilation and aeration changes of patients for clinicians at the bedside. However, frequent movement interferences in clinical environments would inevitably compromise EIT data

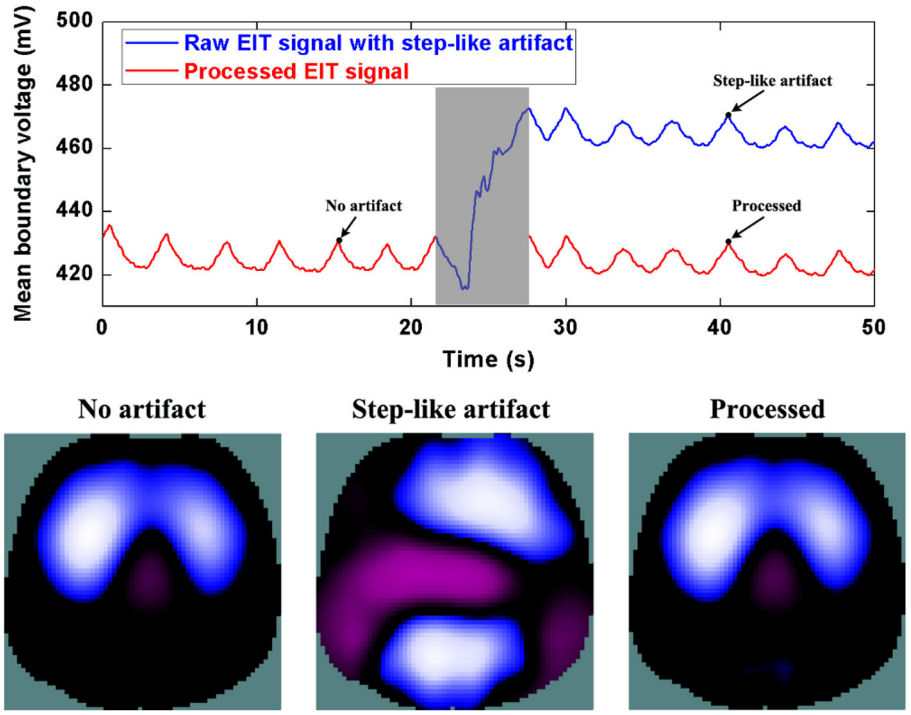

FIGURE 6 | The DWT processing results for step-like artifact removal in patient data. The first row shows the DWT processing result in EIT measured data. The blue line represents the step-like artifact in typical patient data, the red line the corrected data without the step-like artifact. The second row includes EIT images without the artifact, with the artifact, and after being processed.

and consequently affect the assessment and interpretation of pulmonary physiological or pathological status. In this study, for three common types of motion artifacts in chest EIT, we, for the first time, proposed to utilize the DWT as a universal framework to remove them. The method was evaluated with both simulated and real patient data. Reduction of ∼90% errors in most of the tested scenarios suggested that the proposed method would be potentially applicable and helpful in clinical practice.

The underlying reason for the DWT having a promise to detect and remove these body movement interferences in thoracic EIT is that the motion artifacts may have distinct features in amplitude and duration from the normal ventilation EIT signal. This difference is further highlighted in the wavelet domain due to the inherent localization property of the DWT. When performing DWT to decompose a specific channel of EIT signal into sublevels, a segment of approximation wavelet coefficients (corresponding to lower frequency signals) and several segments of detail wavelet coefficients (corresponding to higher frequency signals) were finally obtained. Furthermore, it was shown that those three types of motion artifacts were on the different sublevels. Namely, those motion artifacts could be portrayed and rebuilt using the related sublevels of wavelet coefficients. Therefore, we may attenuate them efficiently by suppressing the corresponding wavelet coefficients or abandoning them after detecting them. In fact, due to DWT's inherent advantages, it had not only been suggested for removing the motion artifacts for brain EIT (18) but also for other biosignals like functional near-infrared spectroscopy (11), cardiac electrophysiology (19), magnetocardiography (14), etc.

Theoretically, those motion interferences may change the external pressure exerted on the EIT electrodes and affect both the current injection and voltage measurement through these electrodes. It would eventually lead to changes in electrode-skin contact impedance. Currently, there are two directions of methods addressing this issue.

Several researchers attempted to improve EIT imaging algorithms using complete electrode models. Their ideas are to separate contact impedance changes from image reconstruction and reduce their effects on specific elements in the finite element models (20–22). These proposed methods to eliminate contact impedance artifacts might also improve clinical data quality affected by body movements. Also, some researchers may consider updating the EIT reference data when motion artifacts occur. They used synthetic reference data to replace the actual EIT reference state to cancel those artifacts to a certain extent (23).

Another direction to solve the issue is signal processing methods on biosignals, which is the path we chose in this study. The reason for choosing the DWT method in this study is that DWT can portray three different body motion artifact signals simultaneously in different wavelet domains; by one discrete wavelet transform, the characteristics of three types of motion

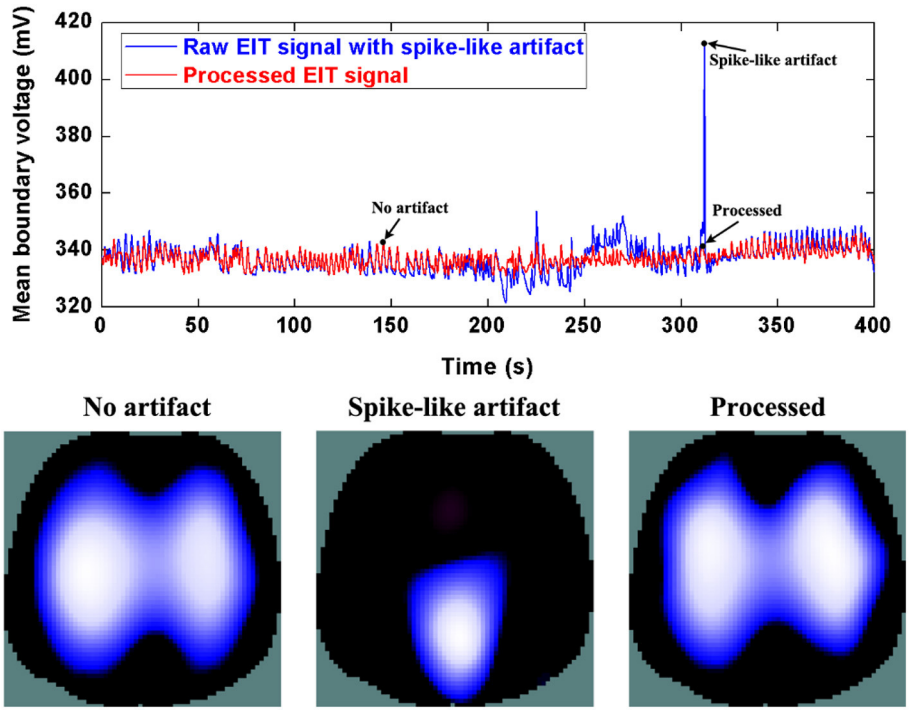

FIGURE 7 | The DWT processing results for spike-like artifact removal in patient data. The first row shows the DWT processing result in EIT measured data. The blue line represents the spike-like artifact in typical patient data, the red line the corrected data without the spike-like artifact. The second row includes EIT images without the artifact, with the artifact, and after being processed.

artifact signals can be presented simultaneously; furthermore, by attenuating these wavelet coefficients that respond to those artifacts and reconstructing the original signal, the effects of those artifact signals can be reduced simultaneously. In short, one DWT can filter out three kinds of motion artifacts at the same time. Besides the wavelet-based approaches, Wiener filtering has also been suggested for removing motion artifacts in fNIRS if prior knowledge of the original signal's power spectrum is known (24). Kalman filtering has also been applied to fNIRS and photoplethysmography with a prior assumption on the distribution of noise that models the artifacts (25). Scholkmann et al. also proposed an *ad hoc* algorithm in fNIRS, in which the moving standard deviation scheme was used to detect motion artifacts and spline interpolation was used to model and correct them (16). Specifically, the signal processing method based on sparse and redundancy representation, e.g., robust PCA, might be a new direction to address the issue if we can model the measured data as a low-rank matrix (26).

This study has several limitations. First, real-time processing by DWT was not considered, and all the analyses were performed offline. The reason is that the purpose of this preliminary study mainly focused on the feasibility of DWT to detect and remove the motion artifacts. From the present results, we would continue this work in an attempt to perform DWT in real-time. Second, in this study, we dealt with only one type of movement artifact at a time. Therefore, it is necessary to confirm whether the DWT method could simultaneously detect and attenuate or remove three types of movement artifacts. Third, except for the pulsating mattress, the sources of interference from other nursing and monitoring devices were not considered, e.g., impedance pneumography, continuous cardiac output monitor. Therefore, we need to determine whether these interferences could be reduced or removed using the DWT in future studies.

TABLE 2 | The evaluation parameters before and after being processed in the patient data validation.

		Error	Correlation
Baseline drifting	Data w. vs. w/o artifacts	1.58	0.45
	Data w/o artifact vs. DWT	0.17	0.99
Step-like artifacts	Data w. vs. w/o artifacts	0.94	0.23
	Data w/o artifact vs. DWT	0.10	0.99
Spike-like artifacts	Data w. vs. w/o artifacts	11.57	0.09
	Data w/o artifact vs. DWT	0.25	0.96

CONCLUSION

Thoracic EIT in clinical practices may often be disturbed by different body movements. The typical artifacts caused by body movements include baseline drifting (by a pulsating mattress), step-like and spike-like impedance signals. This study found that DWT is a universal and effective tool to detect and remove or

attenuate these motion artifacts. In future studies, simultaneous processing of those three types of motion artifacts in real-time needs further consideration.

DATA AVAILABILITY STATEMENT

The original contributions presented in the study are included in the article/**Supplementary Material**, further inquiries can be directed to the corresponding authors.

ETHICS STATEMENT

The studies involving human participants were reviewed and approved by the Human Research Ethics Committee of Xijing Hosptical, The Fourth Military Medical University. The patients/participants provided their written informed consent to participate in this study.

AUTHOR CONTRIBUTIONS

All authors listed have made a substantial, direct, and intellectual contribution to the work and approved it for publication.

FUNDING

The work was supported in part by the National Natural Science Foundation of China (61901478, 52077216, 62001421, and 51837011), the Medical Program of AFMU (2018HKTS10, 2019ZTC01), the Equipment Program of PLA (KJ2018-2019C132), Xijing Hospital Promoting Project (XJZT21CM13) and the Everest Program of AFMU (2019ZFB002).

SUPPLEMENTARY MATERIAL

The Supplementary Material for this article can be found online at: https://www.frontiersin.org/articles/10.3389/fmed.2022.817590/full#supplementary-material

REFERENCES

1. Kobylianskii J, Murray A, Brace D, Goligher E, Fan E. Electrical impedance tomography in adult patients undergoing mechanical ventilation: a systematic review. *J Crit Care.* (2016) 35:33–50. doi: 10.1016/j.jcrc.2016.04.028
2. Bachmann M C, Morais C, Bugedo G, Bruhn A, Morales A, Borges J B, et al. Electrical impedance tomography in acute respiratory distress syndrome. *Crit Care.* (2018) 22:263. doi: 10.1186/s13054-018-2195-6
3. Li H T, Cao L, Xu C H, Yang B, Dai M, Shi X T, et al. Evaluating and reducing the influence of scalp dehydration in the monitoring of intracranial dehydration using electrical impedance tomography. *IEEE Access.* (2020) 8:105047–54. doi: 10.1109/ACCESS.2020.2996028
4. Li J, Ji Z Y, Liu B Y, Shi X T, Dong X Z. Influence of the measuring probe structure on the electric-field edge effect in electrical impedance scanning. *J Med Imag Health In.* (2019) 9:47–52. doi: 10.1166/jmihi.2019.2538
5. Shono A, Kotani T. Clinical implication of monitoring regional ventilation using electrical impedance tomography. *J Intensive Care.* (2019) 7:4. doi: 10.1186/s40560-019-0358-4
6. Zhao Z, Fu F, Frerichs I. Thoracic electrical impedance tomography in Chinese hospitals: a review of clinical research and daily applications. *Physiol Meas.* (2020) 41:04TR01. doi: 10.1088/1361-6579/ab81df
7. Frerichs I, Amato M B, van Kaam A H, Tingay D G, Zhao Z, Grychtol B, et al. Chest electrical impedance tomography examination, data analysis, terminology, clinical use and recommendations: consensus statement of the TRanslational EIT developmeNt stuDy group. *Thorax.* (2017) 72:83–93. doi: 10.1136/thoraxjnl-2016-208357
8. Lozano A, Rosell J, Pallas-Areny R. Errors in prolonged electrical impedance measurements due to electrode repositioning and postural changes. *Physiol Meas.* (1995) 16:121–30. doi: 10.1088/0967-3334/16/2/004
9. Frerichs I, Pulletz S, Elke G, Gawelczyk B, Frerichs A, Weiler N. Patient examinations using electrical impedance tomography–sources of interference in the intensive care unit. *Physiol Meas.* (2011) 32:L1–10. doi: 10.1088/0967-3334/32/12/F01
10. Liu D, Smyl D, Du J. A parametric level set-based approach to difference imaging in electrical impedance tomography. *IEEE Trans Med Imaging.* (2019) 38:145–55. doi: 10.1109/TMI.2018.2857839
11. Molavi B, Dumont G A. Wavelet-based motion artifact removal for functional near-infrared spectroscopy. *Physiol Meas.* (2012) 33:259–70. doi: 10.1088/0967-3334/33/2/259
12. Marques V G, Rodrigo M, Guillem M S, Salinet J. A robust wavelet-based approach for dominant frequency analysis of atrial fibrillation in body surface signals. *Physiol Meas.* (2020) 41:075004. doi: 10.1088/1361-6579/ab97c1
13. Zhang G, Li W, Ma H, Liu X, Dai M, Xu C, et al. An on-line processing strategy for head movement interferences removal of dynamic brain electrical impedance tomography based on wavelet decomposition. *Biomed Eng Online.* (2019) 18:55. doi: 10.1186/s12938-019-0668-8
14. Schmidt A, Witte R, Swiderski L, Zollkau J, Schneider U, Hoyer D. Advanced automatic detection of fetal body movements from multichannel magnetocardiographic signals. *Physiol Meas.* (2019) 40:085005. doi: 10.1088/1361-6579/ab3c96
15. Martínez-Iniesta M, Ródenas J, Rieta J J, Alcaraz R. The stationary wavelet transform as an efficient reductor of powerline interference for atrial bipolar electrograms in cardiac electrophysiology. *Physiol Meas.* (2019) 40:075003. doi: 10.1088/1361-6579/ab2cb8
16. Scholkmann F, Spichtig S, Muehlemann T, Wolf M. How to detect and reduce movement artifacts in near-infrared imaging using moving standard deviation and spline interpolation. *Physiol Meas.* (2010) 31:649–62. doi: 10.1088/0967-3334/31/5/004
17. Adler A, Arnold J H, Bayford R, Borsic A, Brown B, Dixon P, et al. GREIT: a unified approach to 2D linear EIT reconstruction of lung images. *Physiol Meas.* (2009) 30:S35–55. doi: 10.1088/0967-3334/30/6/S03
18. Zhang G, Dai M, Yang L, Li W, Li H, Xu C, et al. Fast detection and data compensation for electrodes disconnection in long-term monitoring of dynamic brain electrical impedance tomography. *Biomed Eng Online.* (2017) 16:7. doi: 10.1186/s12938-016-0294-7
19. Tang M, Xia P, He Z, Zhao Z, Chen X, Yang T, et al. Wavelet-based real-time calculation of multiple physiological parameters on an embedded platform. *Physiol Meas.* (2020) 41:025010. doi: 10.1088/1361-6579/ab6f52
20. Vilhunen T, Kaipio J P, Vauhkonen P J, Savolainen T, Vauhkonen M. Simultaneous reconstruction of electrode contact impedances and internal electrical properties: I. Theory. *Meas Sci Technol.* (2002) 13:1848–54. doi: 10.1088/0957-0233/13/12/307
21. Heikkinen L M, Vilhunen T, West R M, Vauhkonen M. Simultaneous reconstruction of electrode contact impedances and internal electrical properties: II. Laboratory experiments. *Meas Sci Technol.* (2002) 13:1855–61. doi: 10.1088/0957-0233/13/12/308
22. Boverman G, Isaacson D, Newell J C, Saulnier G J, Kao T J, Amm B C, et al. Efficient simultaneous reconstruction of time-varying images and electrode contact impedances in electrical impedance tomography. *IEEE Trans Biomed Eng.* (2017) 64:795–806. doi: 10.1109/TBME.2016.2578646
23. Liu D, Smyl D, Gu D, Du J. Shape-driven difference electrical impedance tomography. *IEEE Trans Med Imaging.* (2020) 39:3801–12. doi: 10.1109/TMI.2020.3004806

24. Izzetoglu M, Devaraj A, Bunce S, Onaral B. Motion artifact cancellation in NIR spectroscopy using Wiener filtering. *IEEE Trans Biomed Eng.* (2005) 52:934–8. doi: 10.1109/TBME.2005.845243
25. Izzetoglu M, Chitrapu P, Bunce S, Onaral B. Motion artifact cancellation in NIR spectroscopy using discrete Kalman filtering. *Biomed Eng Online*. (2010) 9:16. doi: 10.1186/1475-925X-9-16
26. Giryes R, Elad M. Sparsity-based Poisson denoising with dictionary learning. *IEEE Trans Image Process.* (2014) 23:5057–69. doi: 10.1109/TIP.2014.2362057

Conflict of Interest: The authors declare that the research was conducted in the absence of any commercial or financial relationships that could be construed as a potential conflict of interest.

Publisher's Note: All claims expressed in this article are solely those of the authors and do not necessarily represent those of their affiliated organizations, or those of the publisher, the editors and the reviewers. Any product that may be evaluated in this article, or claim that may be made by its manufacturer, is not guaranteed or endorsed by the publisher.

frontiers in Medicine

ORIGINAL RESEARCH
published: 15 February 2022
doi: 10.3389/fmed.2022.803124

The Improved Catheterization Is Associated With the Deeper Radial Arteries in Ultrasound-Guided Dynamic Needle Tip Positioning Technique

Yuan Tian[1†], *Bing Bai*[1†], *Yuelun Zhang*[2†], *Lu Che*[1], *Jin Wang*[1], *Yi Wang*[1], *Chunhua Yu*[1*] *and Yuguang Huang*[1]

[1] *Department of Anaesthesiology, Peking Union Medical College Hospital, Chinese Academy of Medical Sciences and Peking Union Medical College, Beijing, China,* [2] *Medical Research Center, Peking Union Medical College Hospital, Chinese Academy of Medical Sciences and Peking Union Medical College, Beijing, China*

OPEN ACCESS

Edited by:
Zhanqi Zhao,
Furtwangen University, Germany

Reviewed by:
Lei Zhao,
Capital Medical University, China
Knut Moeller,
Furtwangen University, Germany

***Correspondence:**
Chunhua Yu
yu.chunhua@aliyun.com

[†]These authors have contributed equally to this work and share first authorship

Specialty section:
This article was submitted to Intensive Care Medicine and Anesthesiology, a section of the journal Frontiers in Medicine

Received: *27 October 2021*
Accepted: *07 January 2022*
Published: *15 February 2022*

Citation:
Tian Y, Bai B, Zhang Y, Che L, Wang J, Wang Y, Yu C and Huang Y (2022) The Improved Catheterization Is Associated With the Deeper Radial Arteries in Ultrasound-Guided Dynamic Needle Tip Positioning Technique. Front. Med. 9:803124. doi: 10.3389/fmed.2022.803124

Objective: This study aimed to determine the associations between the first-attempt success and arterial depth in ultrasound-guided radial artery catheterization (RAC) with dynamic needle tip positioning (DNTP) technique. This study also aimed to further explore the cut-off depth correlated to improved first-attempt success catheterization in less time.

Methods: The cases undertaken by RAC within the DNTP technique between March 2019 and July 2020 were extracted from our institutional cohort database. Relevant variables were collected, including patients' demographics and catheterized information. Univariable and multivariable logistic regression analyses were performed to determine the association. The receiver operating characteristic (ROC) curve and the Youden index were used to explore the cut-off values of the arterial depth. Categorized cases according to the cut-off values, the Kaplan-Meier analysis, and the log-rank test were used to determine the difference of first-attempt success with limited catheterized time between groups.

Results: In this study, 119 patients were enrolled and 98 achieved first-attempt success. The first-attempt success catheterization was observed to be correlated to arterial depth ($p < 0.01$, odds ratio 6.47). An optimal cut-off depth of 2.25 mm was found using the Youden index (0.53) by ROC curve (area under curve 0.77). Arterial depth of more than 2.25 mm was correlated to improved first-attempt success catheterization in less time (log-rank $p < 0.01$).

Conclusion: To achieve first-attempt success catheterization using the DNTP technique, an arterial depth of more than 2.25 mm was associated with less catheterized time.

Keywords: ultrasonography, radial artery, catheterization, dynamic needle tip positioning, depth

INTRODUCTION

In anesthesia, intensive care, and emergent medicine, radial artery catheterization (RAC) is a significant procedure, that allows real-time blood pressure administration and provides convenient blood sampling when needed. The ultrasound-guided catheterization has been widely accepted for the superiority of enhancing the success rate and reducing requirements for attempts and time (1–5), especially encountered the patients with hemodynamic unstable, obesity, edema, or with the artery of small size, tortuous, or spasm (6, 7). Nevertheless, further improvements remain moving forward to wrestle with complex circumstances and ensure consistency in outcomes.

Among the growing applications of ultrasound-guided techniques, the dynamic needle tip positioning (DNTP) technique was first reported using in RAC in 2012 (8). The DNTP technique is a modified short-axis, out-of-plane, ultrasound-guided technique. It focuses on discriminating the needle tip during artery puncturing until the tip of the catheter be inserted into the center of the artery (8–10). As mentioned in the meta-analysis of 12 randomized control studies enrolled 2,432 adult participants, which suggests ultrasound-guided DNTP technique and long-axis view performed better than conventional short-axis technique in improving first-attempt success (7). Though both the DNTP technique and long-axis view are committed to discriminating the needle tip, using the DNTP technique hardly worry about the time-consumption of vascular imaging (11) and losing target because of thickness artifacts (12).

Notably, the success rates of ultrasound-guided catheterization varied between studies, and the associating factors remained uncertain (13–21). Though few operators identify the arterial depth before catheterization, it was considered as associated with the performance of ultrasound-guided RAC. In pediatric patients, the arterial depth was observed to be associated with the success rates of the ultrasound-guided short-axis RAC (22). The secondary analysis of our previous randomized controlled trial demonstrated the associations of the arterial depth and complications of DNTP or conventional short-axis ultrasound-guided RAC in adults (23). Hence, it hasn't been well-established if the arterial depth is associated with the first-attempt success of DNTP-guided RAC in adults and its optimal cut-off value. Therefore, we retrospective reviewed the records of the DNTP-guided RAC to determine the association of the arterial depth and the first-attempt success, and further explore the cut-off depth associated with improved first-attempt success in less time.

METHODS

Study Design and Participants

A retrospective cohort study was conducted in Peking Union Medical College Hospital, a tertiary comprehensive hospital. This study was approved by the Institutional Review Board and Ethics Committee (S-K1366, September 11, 2020), and the need for informed consent was waived. Adult patients undergoing elective surgery who required RAC and were fulfilled by a certain anesthesiologist using the DNTP technique during March 2019 and July 2020 were involved. The anesthesiologist who performed all the cases was experienced in radial arterial catheterization and fulfilled more than 50 DNTP-guided catheterizations under supervision.

Data Collection

Data clinically relative to the first-attempt success catheterization were collected. Data were obtained from the institutional specialized cohort database of recording ultrasound-guided vascular catheterization (Hospital Clinical Research Database; Beijing Huiren Technology Development Co., Ltd., Beijing, China). The cohort database is currently used for recording the clinical practices, which was first built for our previous randomized controlled study that compared the efficiency of different methods for RAC (16).

Variables and Outcomes

Patient demographics and arterial characteristics were collected, including sex, age, body mass index (BMI), history of coronary artery disease (CAD), systolic blood pressure (SBP), diastolic blood pressure (DBP), American Society of Anesthesiologists (ASA) physical status grade, and arterial diameter and depth. The diameter and depth of the artery were measured twice at the site of puncturing before catheterization, and the mean of measurements was recorded. The diameter was defined as the distance between the anterior and posterior walls of the artery. The depth was defined as the distance between the transducer and the anterior wall of the artery.

The primary outcome is the first-attempt success, defined as successful catheterization at the first attempt without withdrawing the needle out of the skin. The secondary outcome is the catheterized time, calculated between the needle puncturing into the skin and fulfilled the catheterization with no more than five attempts or 10 min.

Statistical Analysis

As a retrospective study, we estimated the statistical power using the available sample size of 119 patients with 98 first-attempt successes. With mean values of 2.8 and 2.195 of depth in the success and failure groups and an *SD* value of 0.599 (median of 0.68 and 0.517), statistical power was 98.6%.

Variables considered as clinically significant were included in multiple logistic regression analysis with forwarding selection and results were performed as odds ratio (OR), 95% CI, and *p*-value. By using the receiver-operating characteristic (ROC) analysis, the Youden index was calculated to define the cut-off value. Patients were further categorized based on the cut-off value and the Kaplan-Meier curve and log-rank test were used to compare the first-attempt success rates with limited operation time. Statistical analysis was conducted using SPSS version 22 (IBM Corp, IL, USA). A two-sided P-value < 0.05 was considered statistically significant.

RESULTS

Overall, 119 patients were recruited, in which 98 (82.35%) of them were fulfilled at the first attempt. Demographic characteristics and catheterized information are shown in **Table 1**. The results of binary logistic regression analysis are shown in **Table 2**. Age, history of CAD, arterial diameter, and depth were independently correlated to the first-attempt success of RAC. After adjustment with age, history of CAD, and arterial diameter, the depth remained significant effect on first-attempt success (OR 6.47, 95% CI 2.16–19.41). The Hosmer-Lemeshow goodness-of-fit statistic ($P = 0.82$) indicated that the model was well-calibrated.

The cut-off value was analyzed by the ROC curve (**Figure 1**). According to the criterion of maximizing the Youden index (0.53), the optimal cut-off value for first-attempt success has corresponded to the arterial depth of 2.25 mm.

TABLE 1 | Demographic characteristics and catheterized information.

Parameters	Values (min-max)
Age (years)	60.21 (21–82)
Sex (male/female)	71/48
BMI (Kg/m^2)	23.9 (15.4–36.7)
CAD (yes/no)	58/61
SBP (mmHg)	130 (84–174)
DBP (mmHg)	76 (45–127)
ASA grade (I/II/III/IV)	0/2/117/0
Diameter (mm)	2.49(1.3–3.5)
Depth (mm)	2.69(1.6–4.3)
First-attempt success (yes/no)	98/21
Overall success (yes/no)	115/4
Catheterization time (s)	110 (12–600)

BMI, body mass index; CAD, coronary artery disease; SBP, systolic blood pressure; DBP, diastolic blood pressure; ASA grade, American Society of Anesthesiologists physical status grade.

TABLE 2 | Factors associated with the first-attempt success of DNTP guided RAC with multiple logistic regression analysis.

Dependent variable=first-attempt success catheterization or not			
	OR	**95% CI**	***P***
Age (years)	0.94	0.89–1.00	0.03*
Sex (male/female)	-	-	0.87
BMI (Kg/m^2)	-	-	0.75
CAD (yes/no)	3.58	1.04–12.32	0.04*
SBP (mmHg)	-	-	0.82
DBP (mmHg)	-	-	0.87
ASA grade (II/III)	-	-	0.92
Diameter (mm)	4.17	1.23–14.17	0.02*
Depth (mm)	6.47	2.16–19.41	<0.01*

OR, odds ratio.
**Statistically significant.*

As shown in **Figure 2**, to achieve first-attempt success, a significantly shorter catheterized time was required for the deeper artery group compared with the shallow group (log-rank $P < 0.01$).

DISCUSSION

The current study determined the association between the depth and the success rates of DNTP-guided RAC in adults. The previous study among pediatrics has reported the association between the increased depth and the improved success of catheterization using the conventional ultrasound-guided short-axis technique (22). The reason was that the needle tip can be well-adjusted to puncture into the center when there was enough distance from the anterior arterial wall. In addition, the key to the success of DNTP is identifying the needle tip, hence, it's less likely to distinguish the hyperechoic needle tip from the similar subcutaneous tissues when they are close to each other. These factors probably explained why the depth associated with the catheterization success of the DNTP technique.

According to the current study, it was estimated an optimal depth of more than 2.25 mm was associated with an improved first-attempt success rate of DNTP-guided catheterization. It was demonstrated that the depth of 2–4 mm improved the success rates of conventional short-axis ultrasound-guided RAC in children younger than 3 years old (22). We considered that the difference might be due to differences in methods

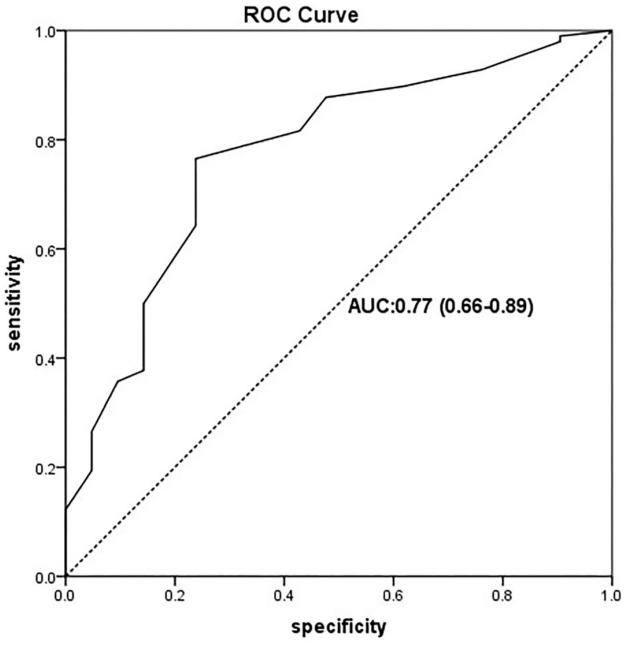

FIGURE 1 | ROC curve of the predictive model for the first-attempt success of radial artery catheterization (RAC) by the arterial depth. ROC curve with an AUC value of 0.77 (95% CI: 0.66–0.89). ROC, receiver-operating characteristic ROC; AUC, area under the ROC curve.

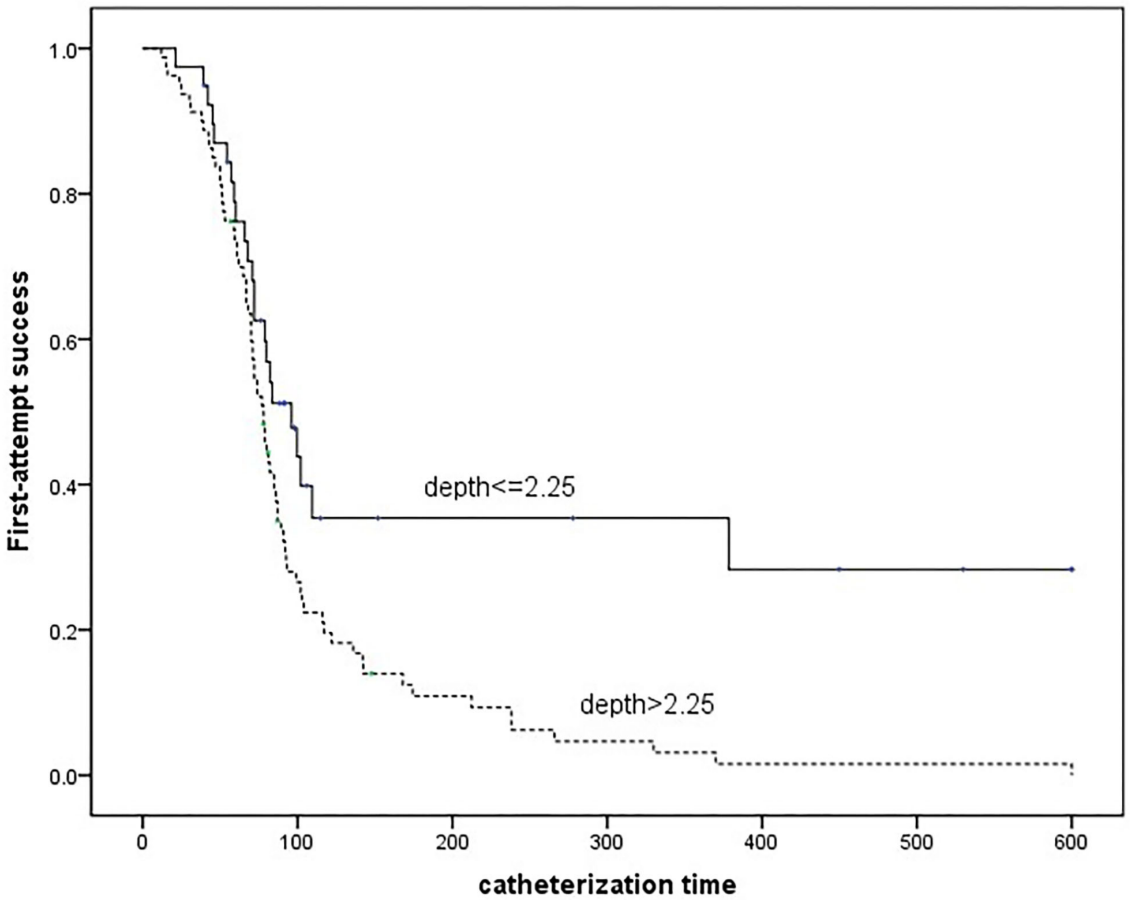

FIGURE 2 | Kaplan-Meier curve estimates the differences of time required for the first-attempt success grouped by the arterial depth.

used for catheterization, as a 95% success rate of DNTP-guided RAC was reported in arteries deeper than 4 mm (18). In patients with a deep artery, the success rates of conventional short-axis ultrasound-guided RAC might be low. The visualization of the needle tip was slashed because a steeper puncture angle was required to achieve the deep artery with constant ultrasonography. The DNTP technique enables positioning the needle tip by moving the transducer, therefore the puncture angle can be adjusted according to the visualization of the ultrasonography instead of the advancement trajectory. On the other hand, to our minds, distinguishing the needle tip in a routine procedure using a catheter with an outer diameter of 1.1 mm is not easy. Because it means that similar hyperechoic images of the arterial anterior wall and the needle tip are required to be distinguished within a distance of 0.6 mm. As the result has not previously been described, further research on the current topic is recommended.

The current study also indicated that to achieve first-attempt catheterization, the deeper arteries required less time. The previous study of the DNTP technique in neonates demonstrated trainees could achieve a higher success rate taking less time by increasing depth with saline injection (21). The reason is supposed, though a deeper artery associated with a potential longer catheterized trajectory, clear identification of needle tip saved the time.

Several limitations of this study should be underlined. First, the same operator, who was sufficiently experienced in ultrasound-guided arterial catheterization of the DNTP technique, performed all the procedures. This limited the external validity of the results. Since the objective of the current study was to determine the association between arterial depth and success catheterization, the different experiences of the operators should be controlled. Interestingly, the consistent results were demonstrated in trainee anesthesiologists that can achieve higher success rates by increasing the arterial depth (21). Second, as a retrospective study, we admitted that confounders other than the finally included factors were not well-controlled in the analysis. Future studies are needed to further investigate this subject.

In conclusion, the current study demonstrated associations between the arterial depth and the first-attempt success of ultrasound-guided RAC using the DNTP technique. An arterial

depth of more than 2.25 mm is associated with less time required to achieve first-attempt success.

DATA AVAILABILITY STATEMENT

The data used in this study are available on request to the corresponding author.

ETHICS STATEMENT

The studies involving human participants were reviewed and approved by the Institutional Review Board and Ethics Committee of Peking Union Medical College Hospital. Written informed consent for participation was not required for this study in accordance with the national legislation and the institutional requirements.

AUTHOR CONTRIBUTIONS

YT and BB contributed to the design of the study, administration of the study, data collection, data analysis, and manuscript preparation. YZ contributed to data analysis and critical manuscript review. LC, JW, and YW contributed to the design and data collection. YH contributed to the design of this study and the administration of the study. All authors read and approved the final manuscript. All authors contributed to the article and approved the submitted version.

FUNDING

The current research is supported by the CAMS Innovation Fund for Medical Sciences (CIFMS) (2021-I2M-C&T-B-020).

REFERENCES

1. Ailon J, Mourad O, Chien V, Saun T, Dev SP. Videos in clinical medicine. Ultrasound-guided insertion of a radial arterial catheter. *N Engl J Med.* (2014) 371:e21. doi: 10.1056/NEJMvcm1213181
2. Varga EQ, Candiotti KA, Saltzman B, Gayer S, Giquel J, Castillo-Pedraza C, et al. Evaluation of distal radial artery cross-sectional internal diameter in pediatric patients using ultrasound. *Paediatr Anaesth.* (2013) 23:460–2. doi: 10.1111/pan.12151
3. Schmidt GA, Blaivas M, Conrad SA, Corradi F, Koenig S, Lamperti M, et al. Ultrasound-guided vascular catheterization in critical illness. *Intensive Care Med.* (2019) 45:434–46. doi: 10.1007/s00134-019-05564-7
4. Burad J, Date R, Kodange S, Al Hashim AH, Nollain K. Comparison of conventional and ultrasound guided techniques of radial artery cannulation in different haemodynamic subsets: a randomised controlled study. *Intensive Care Med.* (2017) 43:140–1. doi: 10.1007/s00134-016-4569-z
5. Lamperti M, Biasucci DG, Disma N, Pittiruti M, Breschan C, Vailati D, et al. European Society of Anaesthesiology guidelines on perioperative use of ultrasound-guided for vascular catheterization (PERSEUS vascular catheterization). *Eur J Anaesthesiol.* (2020) 37:344–76. doi: 10.1097/EJA.0000000000001180
6. Zhang W, Li K, Xu H, Luo D, Ji C, Yang K, et al. Efficacy of ultrasound-guided technique for radial artery catheterization in pediatric populations: a systematic review and meta-analysis of randomized controlled trials. *Crit Care.* (2020) 24:197. doi: 10.1186/s13054-020-02920-8
7. Moussa Pacha H, Alahdab F, Al-Khadra Y, Idris A, Rabbat F, Darmoch F, et al. Ultrasoundguided versus palpation-guided radial artery catheterization in adult population: a systematic review and meta-analysis of randomized controlled trials. *Am Heart J.* (2018) 204:1–8. doi: 10.1016/j.ahj.2018.06.007
8. Clemmesen L, Knudsen L, Sloth E, Bendtsen T. Dynamic needle tip positioning - ultrasound guidance for peripheral vascular catheterization. A randomized, controlled and blinded study in phantoms performed by ultrasound novices. *Ultraschall Med.* (2012) 33:E321–5. doi: 10.1055/s-0032-1312824
9. Wei P, Li J, Huang J, Zhang T, Tang W. Radial artery catheterisation pressure monitoring with a closed intravascular catheter system and ultrasound-guided dynamic needle tip positioning technique. *Br J Anaesth.* (2021) 126:e144–6. doi: 10.1016/j.bja.2020.12.033
10. Takeshita J, Tachibana K, Nakayama Y, Nakajima Y, Hamaba H, Yamashita T, et al. Ultrasound-guided dynamic needle tip positioning versus conventional palpation approach for catheterisation of posterior tibial or dorsalis pedis artery in infants and small children. *Br J Anaesth.* (2021) 126:e140–2. doi: 10.1016/j.bja.2020.11.033
11. Song IK, Choi JY, Lee JH, Kim EH, Kim HJ, Kim HS, et al. Short-axis/out-of-plane or long-axis/in-plane ultrasound-guided arterial cannulation in children: a randomised controlled trial. *Eur J Anaesthesiol.* (2016) 33:522–7. doi: 10.1097/EJA.0000000000000453
12. Reusz G, Sarkany P, Gal J, Csomos A. Needle-related ultrasound artifacts and their importance in anaesthetic practice. *Br J Anaesth.* (2014) 112:794–802. doi: 10.1093/bja/aet585
13. Kiberenge RK, Ueda K, Rosauer B. Ultrasound-guided dynamic needle tip positioning technique versus palpation technique for radial arterial cannulation in adult surgical patients: a randomized controlled trial. *Anesth Analg.* (2018) 126:120–6. doi: 10.1213/ANE.0000000000002261
14. Liu L, Tan Y, Li S, Tian J. "Modified dynamic needle tip positioning" short-axis, out-of-plane, ultrasound-guided radial artery cannulation in neonates: a randomized controlled trial. *Anesth Analg.* (2019) 129:178–83. doi: 10.1213/ANE.0000000000003445
15. Nam K, Jeon Y, Yoon S, Kwon SM, Kang P, Cho YJ, et al. Ultrasound-guided radial artery cannulation using dynamic needle tip positioning versus conventional long-axis in-plane techniques in cardiac surgery patients: a randomized, controlled trial. *Minerva Anestesiol.* (2020) 86:30–7. doi: 10.23736/S0375-9393.19.13646-2
16. Bai B, Tian Y, Zhang Y, Yu C, Huang Y. Dynamic needle tip positioning versus the angle-distance technique for ultrasound-guided radial artery cannulation in adults: a randomized controlled trial. *BMC Anesthesiol.* (2020) 20:231. doi: 10.1186/s12871-020-01152-1
17. Oh EJ, Lee JH, Kwon EJ, Min JJ. Simulation-based training using a vessel phantom effectively improved first attempt success and dynamic needle-tip positioning ability for ultrasound-guided radial artery cannulation in real patients: an assessor-blinded randomized controlled study. *PLoS ONE.* (2020) 15:e0234567. doi: 10.1371/journal.pone.0234567
18. Takeshita J, Yoshida T, Nakajima Y, Nakayama Y, Nishiyama K, Ito Y, et al. Dynamic needle tip positioning for ultrasound-guided arterial catheterization in infants and small children with deep arteries: a randomized controlled trial. *J Cardiothorac Vasc Anesth.* (2019) 33:1919–25. doi: 10.1053/j.jvca.2018.12.002
19. Kim SY, Kim KN, Jeong MA, Lee BS, Lim HJ. Ultrasound-guided dynamic needle tip positioning technique for radial artery cannulation in elderly patients: a prospective randomized controlled study. *PLoS ONE.* (2021) 16:e0251712. doi: 10.1371/journal.pone.0251712
20. Xiao Q, Xu D, Zhuang S. Effect of wrist dorsiflexion on ultrasound-guided radial artery catheterisation using dynamic needle tip positioning technique in adult patients: a randomised controlled clinical trial. *Emerg Med J.* (2021) 38:524–8. doi: 10.1136/emermed-2020-209504
21. Ye P, Tan Y, Ye M, Li S, Bai L, Liu L, et al. novel method for ultrasound-guided radial artery cannulation in neonates by trainee anaesthesiologists: a randomised controlled trial. *Eur*

J Anaesthesiol. (2020) 37:91–7. doi: 10.1097/EJA.0000000000001089

22. Nakayama Y, Nakajima Y, Sessler DI, Ishii S, Shibasaki M, Ogawa S, et al. A novel method for ultrasound-guided radial arterial catheterization in pediatric patients. *Anesth Analg.* (2014) 118:1019–26. doi: 10.1213/ANE.0000000000000164
23. Bai B, Tian Y, Zhang YL Yu CH, Huang YG. Factors contributing successful ultrasound-guided radial artery cannulation and its complications when using the short-axis out-of-plane procedure. *Zhongguo Yi Xue Ke Xue Yuan Xue Bao.* (2020) 42:86–90. doi: 10.3881/j.issn.1000-503X.11617

Conflict of Interest: The authors declare that the research was conducted in the absence of any commercial or financial relationships that could be construed as a potential conflict of interest.

Publisher's Note: All claims expressed in this article are solely those of the authors and do not necessarily represent those of their affiliated organizations, or those of the publisher, the editors and the reviewers. Any product that may be evaluated in this article, or claim that may be made by its manufacturer, is not guaranteed or endorsed by the publisher.

frontiers | Frontiers in Medicine

ORIGINAL RESEARCH
published: 23 May 2022
doi: 10.3389/fmed.2022.805680

Comparison of Global and Regional Compliance-Guided Positive End-Expiratory Pressure Titration on Regional Lung Ventilation in Moderate-to-Severe Pediatric Acute Respiratory Distress Syndrome

Hong Ren[1†], Li Xie[2†], Zhulin Wang[1], Xiaoliao Tang[1], Botao Ning[1], Teng Teng[1], Juan Qian[1], Ying Wang[1], Lijun Fu[3], Zhanqi Zhao[4,5]* and Long Xiang[1,6]**

[1] Department of Critical Care Medicine, Shanghai Children's Medical Center, School of Medicine, Shanghai Jiao Tong University, Shanghai, China, [2] Clinical Research Institute, School of Medicine, Shanghai Jiao Tong University, Shanghai, China, [3] Department of Cardiology, Shanghai Children's Medical Center, School of Medicine, Shanghai Jiao Tong University, Shanghai, China, [4] Department of Biomedical Engineering, Fourth Military Medical University, Xi'an, China, [5] Institute of Technical Medicine, Furtwangen University, Villingen-Schwenningen, Germany, [6] Department of Neonatal, Second People's Hospital of Kashgar, Xinjiang, China

Purpose: To investigate the difference in the positive end-expiratory pressure (PEEP) selected with chest electrical impedance tomography (EIT) and with global dynamic respiratory system compliance (C_{rs}) in moderate-to-severe pediatric acute respiratory distress syndrome (pARDS).

Methods: Patients with moderate-to-severe pARDS (PaO_2/FiO_2 < 200 mmHg) were retrospectively included. On the day of pARDS diagnosis, two PEEP levels were determined during the decremental PEEP titration for each individual using the best compliance ($PEEP_C$) and EIT-based regional compliance ($PEEP_{EIT}$) methods. The differences of global and regional compliance (for both gravity-dependent and non-dependent regions) under the two PEEP conditions were compared. In addition, the EIT-based global inhomogeneity index (GI), the center of ventilation (CoV), and standard deviation of regional delayed ventilation (RVD_{SD}) were also calculated and compared.

Results: A total of 12 children with pARDS (5 with severe and 7 with moderate pARDS) were included. $PEEP_C$ and $PEEP_{EIT}$ were identical in 6 patients. In others, the differences were only ± 2 cm H_2O (one PEEP step). There were no statistical differences in global compliance at $PEEP_C$ and $PEEP_{EIT}$ [28.7 (2.84–33.15) vs. 29.74 (2.84–33.47) ml/cm H_2O median (IQR), $p = 0.028$ (the significant level after adjusted for multiple comparison was 0.017)]. Furthermore, no differences were found in regional compliances and other EIT-based parameters measuring spatial and temporal ventilation distributions.

OPEN ACCESS

Edited by:
Yeong Shiong Chiew, Monash University Malaysia, Malaysia

Reviewed by:
Thomas Stueber, Hannover Medical School, Germany
Andress Waldmann, University of Rostock, Germany

***Correspondence:**
Lijun Fu
fulijun@scmc.com.cn
Zhanqi Zhao
zhanqi.zhao@hs-furtwangen.de
Long Xiang
xloix@126.com

[†]These authors share first authorship

Specialty section:
This article was submitted to Intensive Care Medicine and Anesthesiology, a section of the journal Frontiers in Medicine

Received: *30 October 2021*
Accepted: *07 March 2022*
Published: *23 May 2022*

Citation:
Ren H, Xie L, Wang Z, Tang X, Ning B, Teng T, Qian J, Wang Y, Fu L, Zhao Z and Xiang L (2022) Comparison of Global and Regional Compliance-Guided Positive End-Expiratory Pressure Titration on Regional Lung Ventilation in Moderate-to-Severe Pediatric Acute Respiratory Distress Syndrome. Front. Med. 9:805680. doi: 10.3389/fmed.2022.805680

Conclusion: Although EIT provided information on ventilation distribution, PEEP selected with the best C_{rs} might be non-inferior to EIT-guided regional ventilation in moderate-to-severe pARDS. Further study with a large sample size is required to confirm the finding.

Keywords: acute respiratory distress syndrome, lung protective ventilation, electrical impedance tomography, pediatrics, respiratory compliance

INTRODUCTION

Pediatric acute respiratory distress syndrome (pARDS) was proposed by the 2015 Pediatric Acute Lung Injury Consensus Conference (PALICC) (1). The multinational survey data of the pediatric acute lung injury and sepsis investigators (PALISI) have shown that the mortality of pARDS is about 22–40% and the mortality related to pARDS can reach more than 30% in a pediatric intensive care unit (PICU) (2).

Similar to adult ARDS, the pathophysiological characteristics of pARDS include the heterogeneity of lung lesions and the formation of regional collapse in gravity-dependent areas. At present, mechanical ventilation is still the main life-supporting method for the treatment of ARDS. During mechanical ventilation, unreasonable positive end-expiratory pressure (PEEP) setting could cause excessive alveolar expansion and periodic collapse–opening and release of inflammatory mediators, resulting in ventilator-induced lung injury (VILI). It may also lead to hemodynamic instability secondary to right ventricular dysfunction (3, 4). PALICC recommends lung recruitment and titration of the optimal PEEP in pARDS (1). The optimal PEEP keeps alveolar from derecruitment in gravity-dependent areas and introduces only limited alveolar overdistension in non-gravity-dependent areas. In pARDS, the question of how to titrate PEEP is still under debate.

Electrical impedance tomography (EIT) is an advanced non-invasive ventilation monitoring technology at the bedside (5, 6). It can directly visualize whether the collapsed lung areas can be opened after the lung recruitment maneuver, guide the ventilator parameter settings, and minimize VILI. Several recent reviews have summarized the applications of EIT in the treatment of adult ARDS (7, 8). Two randomized controlled studies indicated that EIT-guided PEEP titration may reduce ARDS mortality (9, 10). In terms of children, Rosemeier et al. reported that during lung recruitment and PEEP titration, EIT could help to minimize regional alveolar overdistension and collapse and improve oxygenation (11). However, EIT is not widely used in PICU. We hypothesized that the traditional PEEP titration method using dynamic respiratory system compliance (C_{rs}) could lead to similar PEEP and regional ventilation for lung protection in pARDS.

MATERIALS AND METHODS

Study Design

This study was retrospective observational and was conducted in the PICU of Shanghai Children's Medical Center from 1 January 2020 to 31 December 2020. The Ethics Committee of Shanghai Children's Medical Center approved this study (SCMCIRB-Y20200087). For all of the included children, written informed consent was obtained from their legal guardians.

Patients

Children with moderate and severe pARDS diagnosed in accordance with the 2015 PALICC (1) and treated with invasive endotracheal intubation and lung protective ventilation were included. The exclusion criteria were as follows: (1) age > 18 years or weight < 7 kg; (2) uncorrected hemodynamic instability or decompensated shock; (3) serious lesions and trauma of the thorax and spine, surgical incision, and lesions of the relevant parts of the skin, serious deformity of the thorax, and inability to fix EIT bandage; (4) severe obesity and Body Mass Index > 50; (5) implanted intrathoracic devices, such as a cardiac pacemaker, cardiac defibrillator, or any other surgical implant; (6) ongoing cardiac defibrillation; (7) congenital heart disease, congenital diaphragmatic hernia, and severe airway obstructive diseases; (8) sildenafil or inhaled nitric oxide used to treat pulmonary hypertension for various reasons; (9) severe craniocerebral injury, intracranial pressure monitoring, or extraventricular drainage; and (10) high-frequency ventilation.

All of the children continued to receive midazolam, fentanyl sedation, analgesia, and rocuronium neuromuscular block, without spontaneous breathing. The choice of drugs, dosage, and time of administration was determined by PICU attending physicians. All of the patients were treated with low tidal volume lung protection ventilation in the supine position. Pressure control mode was adopted for mechanical ventilation, with a targeted tidal volume of 4–6 ml/predicted body weight, and FiO_2 was titrated to obtain peripheral blood oxygen saturation between 92 and 100%.

Electrical Impedance Tomography Monitoring

Electrical impedance tomography measurement was performed to monitor ventilation distribution at the bedside (Pulmovita 500, Dräger Medical, Lübeck, Germany). A belt with sixteen electrodes was placed on the transverse section around the patient's chest. A reference electrode was placed on the abdomen. The EIT image was continuously recorded and stored at 20 Hz. The respiratory data of the ventilator were transmitted to the EIT device and recorded through the MEDIBUS connection. The tidal ventilation image was divided into ventral and dorsal regions.

Positive End-Expiratory Pressure Titration Procedures

The positive end-expiratory pressure titration was performed within 6 h of pARDS diagnosis. No lung recruitment maneuver was performed before the PEEP titration. The initial PEEP was set at 15 cm H_2O. The PEEP was reduced by a step of 2 cm H_2O and a length of 2 min until the PEEP reached 5 cm H_2O.

"Optimal" PEEP was determined with EIT ($PEEP_{EIT}$) and C_{rs} ($PEEP_C$). $PEEP_{EIT}$ was selected to minimize regional overdistention and collapsed based on regional compliance (12). $PEEP_C$ was selected when C_{rs} reached its maximum during the decremental PEEP trial (13) (**Figure 1**).

Tidal relative impedance changes were normalized to tidal volume in milliliters. Regional C_{rs} for ventral and dorsal regions were calculated as tidal impedance changes in ventral and dorsal regions over driving pressure, respectively. Several EIT-based parameters were calculated to assess the spatial and temporal regional ventilation distribution. They were global inhomogeneity (GI) index (14), center of ventilation (CoV), (15) and the standard deviation of regional ventilation delayed ventilation (RVD_{SD}) (16).

Data reconstruction was conducted using the Draeger reconstruction method *via* Draeger EIT Data Analysis Tool (version 63, Dräger Medical, Lübeck, Germany), and the data were analyzed using a customized software using Matlab (The Math-Works, Natick, MA, United States).

Statistical Analysis

The data complying with normal distribution were presented as mean ± SD. The monitoring parameters between the two methods were compared with a paired-sample *t*-test. Non-normally distributed data were represented by median (interquartile range) and were compared with Wilcoxon signed-rank test. SPSS 24.0 software package (SPSS, Chicago, Illinois, United States) and MedCalc 11.4.3.0 software (Mariakel, Belgium) were used for statistical analysis. The *p*-values lower than 0.05 were considered to be statistically significant. The Holm-Bonferroni method was used to adjust the significant levels for multiple comparisons.

RESULTS

In 2020, there were 312 pediatric patients ventilated in our department. Among them, only 54 patients were pARDS and only 17 were moderate-to-severe. We illustrated the patient enrollment process with the following flowchart (**Figure 2**).

We included a total of 12 children with pARDS, including 5 with severe pARDS and 7 with moderate pARDS. The clinical characteristics of the 12 children are shown in **Table 1**.

There was no differences in global compliance at $PEEP_C$ and that at $PEEP_{EIT}$ [28.7 (2.84–33.15) vs. 29.74 (2.84–33.47)] ml/cm H_2O, $p = 0.028$ (the Holm-Bonferroni method adjusted significant level was 0.017). No differences were found in non-dependent area ($p = 0.028$ adjusted level 0.025) and gravity-dependent area ($p = 0.207$) (**Table 2**).

No differences were found in $RVD_{SD,}$ GI, and CoV between $PEEP_{EIT}$ and $PEEP_C$ (RVD_{SD}: 2.33 ± 3.65 vs. 2.75 ± 3.67, $p = 0.435$; GI: 0.378 ± 0.693 vs. 0.384 ± 0.663, $p = 0.522$; CoV: 48.75 ± 6.09 vs. 48.67 ± 6.45, $p = 0.723$) (**Figure 3**).

DISCUSSION

In the present study, we compared the PEEP selected with maximum global C_{rs} and the EIT-based regional C_{rs} methods in pARDS. The PEEP levels selected with these two methods did not differ. Both global and regional C_{rs} and spatial and temporal ventilation distribution were comparable. PEEP selected with best C_{rs} might be non-inferior to EIT-guided one with respect to regional ventilation. When regional C_{rs} is unavailable, global C_{rs} could be a practical surrogate to guide PEEP titration.

The traditional method of titrating PEEP is based on the parameters of global parameters, including P-V curve inflection points in the P-V loop and optimal results of blood gas analysis (PaO_2, $PaCO_2$, and dead space fraction) (13, 17). The computed tomography scanning method could provide regional information (18) but it is impractical due to the need for transportation and radiation exposure. PEEP titration with transesophageal pulmonary pressure titration could be promising. However, in a study of 200 patients with moderate-to-severe ARDS, Beitler et al. (19) found that, when compared

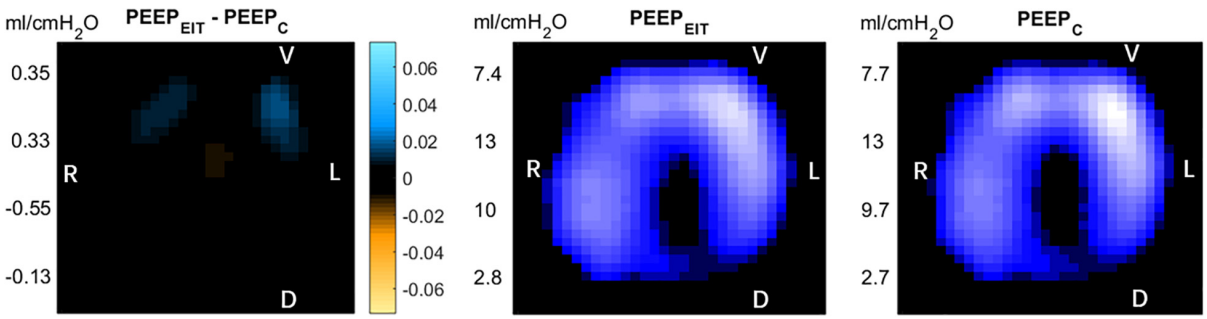

FIGURE 1 | Left: After the positive end-expiratory pressure (PEEP) titration by the two methods, the difference of electrical impedance is displayed on the electrical impedance tomography (EIT) diagram. Blue: compliance gain; Orange: compliance loss. Middle: PEEP titrated according to the regional compliance method. Right: PEEP titrated according to global dynamic respiratory system compliance. R, right; L, left V, Ventral D, dorsal.

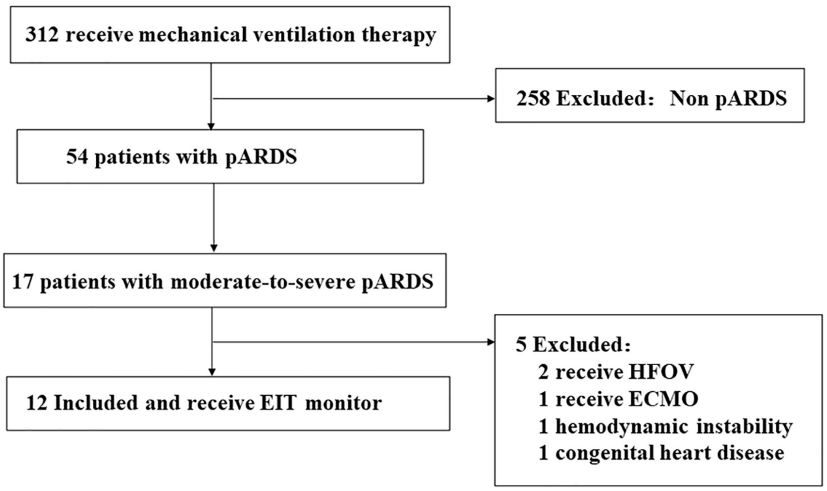

FIGURE 2 | Flowchart of patient enrollment in this study. HFOV, High frequency oscillation ventilation; ECMO, Extracorporeal membrane oxygenation.

TABLE 1 | The clinical characteristics of 12 included children with Pards.

Patients	Age (month)	Gender	Weight (kg)	PaO_2/FiO_2	FiO_2	PEEP	Sputum etiology	Blood etiology	Underling diseases	Outcome
1	16	Female	10	72.33	0.6	7	*Enterobacter aerogenes*	Methicillin-resistant staphylococcus	Post liver transplantation	Survived
2	36	Female	17	76.22	0.9	9	Parainfluenza virus *Streptococcus pneumoniae*	Human staphylococcus	Acute lymphoblastic leukemia	Survived
3	108	Female	41	88.42	0.95	13	None	*Staphylococcus epidermidis*	Acute lymphoblastic leukemia	Deceased
4	35	Male	13	88.43	0.7	9	Parainfluenza virus	Epstein-Barr virus	Lymphoma	Survived
5	13	Male	9	91.25	0.8	9	*None*	None	High IgM immunodeficiency disease	Deceased
6	5	Male	8.5	125.8	0.5	6	*Candida albicans*	None	Rhabdomyosarcoma	Survived
7	48	Male	18.3	141.83	0.6	9	*Escherichia coli* (CRE)	None	Acute lymphoblastic leukemia	Survived
8	65	Male	20	143.33	0.6	10	*Pneumocystis carinii*	None	Acute lymphoblastic leukemia	Survived
9	5	Male	8	143.33	0.6	6	*Acinetobacter baumannii, Klebsiella pneumoniae*	None	Post liver transplantation	Survived
10	84	Male	14.5	168.33	0.6	8	*Pneumocystis carinii*	None	Congenital hypogammaglobulinemia	Survived
11	144	Male	40	175.11	0.6	9	*Pneumocystis carinii*	None	Acute lymphoblastic leukemia	Survived
12	72	Female	23	181.67	0.6	7	*Mycoplasma pneumoniae*	None	None	Survived

TABLE 2 | The comparison between the global compliance and regional compliance at $PEEP_{EIT}$ and $PEEP_C$.

	OD/CL	Global dynamic respiratory system compliance	*P*
PEEP	9.83 ± 2.17	10.05 ± 2.43	0.104
Global compliance $_T$	28.7 (2.84–33.15)	29.74 (2.84–33.47)	0.028[#]
Non-gravity-dependent area compliance	12.2 (1.34–17.11)	12.46 (1.34–18.41)	0.028[##]
Gravity-dependent area compliance	13.82 (1.58–17.11)	14.93 (1.58–18.28)	0.207

[#] *The Holm-Bonferroni method adjusted significant level was 0.017.*
[##] *The Holm-Bonferroni method adjusted significant level was 0.025.*

with the empirical PEEP-FiO_2 method, the optimal PEEP by transesophageal pulmonary pressure titration did not improve the prognosis (p = 0.88) and mechanical ventilation time (p = 0.85). This study showed that due to the heterogeneity of ARDS lesions, the parameters reflecting only global lung ventilation may not represent the regional lung lesions. The optimal PEEP value is different not only before and after lung injury but also between dorsal and ventral regions. Therefore, it is necessary to monitor the compliance of different regions. EIT provides information on regional ventilation at the bedside. Costa et al. (12) and Meier et al. (20) reported that EIT can be used to monitor regional compliance. Lowhagen et al. (21) proposed a so-called "intra tidal gas distribution," which divides regional tidal impact into eight isovolume parts, to identify tidal changes and overdistension in the lung regions. Zhao et al. (22) reported better compliance value and oxygenation index (PaO_2/FiO_2) in patients with ARDS in whom PEEP was titrated according to the OD/CL method than those titrated with PEEP using P-V curve. They also concluded that if the study population doubled and the intergroup mortality remained unchanged, the mortality of the PEEP group titrated according to the regional compliance would be significantly lower. Recently, Hsu et al. (9) and He et al. (10) reported that PEEP titrated by the regional C_{rs} method can reduce mortality when compared with traditional methods in adult patients with ARDS.

Although pARDS and adult ARDS share the same pathological and pathophysiological characteristics, the data of adult ARDS clinical studies are not always applicable to the pARDS. The pediatric and adult patients are different at least in the following aspects: (1)the definition of pARDS in the PALICC is different from adults ARDS in Berlin definition:(a) the definition of pARDS eliminates the requirement of bilateral infiltration in chest imaging; (b) use oxygen index (OI) and Oxygen saturation index (OSI) instead of PaO_2/FiO_2 ratio with minimum PEEP level; (c) pARDS is defined for special children with chronic lung disease or cyanotic congenital heart disease (23). (2) Compared with adults ARDS, the definition pARDS have lower requirements for respiratory mechanical parameters. Taking compliance as an example, the elasticity of the chest wall in children is significantly reduced, and the elastin and collagen components of the lung change with age (24). In addition, the respiratory system compliance cannot be accurately calculated because the tidal volume delivered to lungs is not accurately measured in children:(a) there is serious air leakage around the endotracheal tube, which may be minimized in patients with severe pARDS because of the cuffed endotracheal tubes; (b) the ideal weight measurement of children is more complex, especially those with severe scoliosis; (c) the device and location of the device (proximal airway vs. at the ventilator) to measure tidal volume may result in different values for tidal volume, based on the type of ventilator, circuit tubing used, compliance of the patient, compliance of the tubing, and size of the patient. For these reasons, PALICC does not recommend the use of compliance in the definition of pARDS. (3) There are few prospective studies on the optimal PEEP level of pARDS, resulting in no unified recommended method for PEEP titration in the treatment of pARDS with mechanical ventilation. The risk of high PEEP may be related to the adverse results of cardiopulmonary interaction caused by low chest wall elasticity in children or newborns (25, 26). Khemani et al. (27) reported that the PEEP setting lower than the recommended PEEP setting of ARDSNet will increase the mortality of pARDS. The study from Khemani et al. confirmed that PEEP was independently related to the mortality of pARDS, and clearly pointed out the necessity of prospective study on optimizing the PEEP in pARDS.

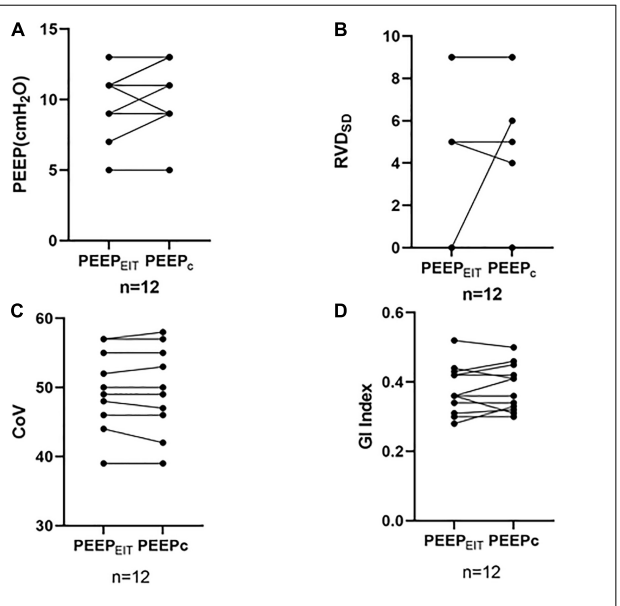

FIGURE 3 | (A) No differences were found in the PEEP between $PEEP_{EIT}$ and $PEEP_C$. **(B)** No differences were found in the standard deviation of regional delayed ventilation (RVD_{SD}) between $PEEP_{EIT}$ and $PEEP_C$. **(C)** No differences were found in CoV between $PEEP_{EIT}$ and $PEEP_C$. and **(D)** No differences were found in GI Index between $PEEP_{EIT}$ and $PEEP_C$.

Due to the uniqueness of children and the limitations of monitoring tools, the above-mentioned findings in adult ARDS might not be directly applicable to pARDS. EIT pediatric electrodes are still in development. Since global C_{rs} is monitored throughout the entire period of mechanical ventilation, it could be used for PEEP titration in the absence of EIT.

It should be noted that the global dynamic respiratory compliance used in our study could be different from the static compliance measured during volume controlled and with inspiratory hold. Stahl et al. (28) suggested that the application of dynamic respiratory mechanics as a diagnostic tool in ventilated patients should be more appropriate than using static lung mechanics.

Several studies have reported that there is a correlation between the OD/CL method and the global respiratory system compliance method. Su et al. (29) showed in 18 patients with ARDS that during the decline of PEEP, PEEP titrated by the OD/CL method correlated with PEEP selected for the best compliance of the respiratory system. In an animal study, Bikker et al. (30) found a correlation between the optimal PEEP based on the EIT regional compliance and PEEP titrated according to the global compliance in eight porcine ALI models induced by oleic acid. In addition, Puel et al. (31) reported that in patients with severe ARDS undergoing venous-venous extracorporeal

membrane oxygenation (V-V ECMO), the OD/CL was consistent with PEEP compliance (PEEPcomp) titrated according to global compliance. However, based on the fact that OD is more harmful to patients than CL, some researchers revised the OD/CL balance scheme and proposed "OD/CL15" that allows 15% CL. The ratio definition minimizes the alveolar OD (32, 33). OD/CL15 leads to the reduction of the optimal PEEP and increases the risk of lung collapse. Franchineau et al. (34) examined 15 patients with ARDS and found that the optimal PEEP set according to OD/CL15 was different from the PEEP estimated by the optimal compliance of the lung. It showed that the PEEP titration based on EIT considered not only the global compliance but also the balance between overdistension and collapse in different regions, whereas the PEEP titrated according to the global optimal compliance may not represent the optimal ventilator ventilation parameters.

In the present study, we evaluated three EIT-based parameters to assess the spatial and regional ventilation distributions, namely the GI, CoV, and RVD_{SD} indices. Frerichs et al. (35) reported that in neonatal respiratory distress syndrome (NRDS) the use of pulmonary surfactant can transfer the CoV of children from a non-gravity-dependent area to a gravity-dependent area. Another study showed a significant difference between PEEP measured according to GI and the value recommended by ARDSnet guidelines, and PEEP value did not correlate with PaO_2/FiO_2 (36). RVD may reveal the degree of tidal recruitment if the PEEP is inadequate (16). It may also be used to evaluate the diaphragm activities during spontaneous breathing tests (37).

In the present study, no significant differences in CoV, GI, or RVD_{SD} between $PEEP_{EIT}$ and $PEEP_C$ were found, which indicates that the ventilation heterogeneity of pARDS may not be as large as that of adult ARDS.

This study has several limitations. First, the very small sample size limited the conclusions. The huge variation in age (from 5 to 144 months) and therefore body height might be another major limitation of this study. Karsten et al. (38) showed that the clinical availability and rationality of EIT measurement depend on appropriate belt position, impedance visualization, correct analysis, and data interpretation. When EIT is used to estimate global parameters, such as tidal volume or end expiratory lung volume changes, the optimal electrode plane is between the 4th and 5th intercostal spaces. In our study, due to the various age and weights of children, the EIT belt was uniformly placed at the connecting line at the nipple level. Brabant et al. (39) show that the volume-impedance ratio may vary depending on the PEEP levels. To ensure that the belt position was adequate and PEEP-dependent volume-impedance ratio did not significantly influence the results, we first evaluated whether the volume-impedance ratios at different PEEP were significantly different. With the adequate belt positioning, no difference in volume-impedance ratios at different PEEP levels was found. Then, the mean ratio of volume-impedance at all PEEP was used. Bikker et al. (40) showed that induced cranio-caudal shift of lung tissue may alter the proportion of the lung which is captured within the EIT sensitivity region in adult patients with ARDS. In our study, this effect of PEEP-induced cranio-caudal shifting may be even more pronounced in patients with smaller lungs (e.g., 4 months) compared to older/taller children. The small sample size and the huge variation in lung size in this cohort may have led to the non-significant result. According to the current research results, future clinical trials should focus on increasing the number of cases with pARDS, exploring the EIT on the global and regional ventilation of pARDS, and guiding the implementation of pulmonary protective ventilation strategy of pARDS.

CONCLUSION

During lung protection ventilation therapy in moderate-to-severe pARDS, although EIT provided information of ventilation distribution, PEEP selected with best C_{rs} might be non-inferior to EIT-guided one regarding regional ventilation in moderate-to-severe pARDS. EIT can monitor lung regional compliance and enrich the understanding of pARDS lung protection ventilation by monitoring GI, CoV, RVD, and other parameters. More patients should be included in future larger, possibly multicenter, clinical trials to explore the clinical efficacy of EIT for lung protective ventilation in pARDS.

DATA AVAILABILITY STATEMENT

The original contributions presented in the study are included in the article/supplementary material, further inquiries can be directed to the corresponding author/s.

ETHICS STATEMENT

The studies involving human participants were reviewed and approved by the Ethics Committee of Shanghai Children's Medical Center (SCMCIRB-Y20200087). Written informed consent to participate in this study was provided by the participants' legal guardian/next of kin. Written informed consent was obtained from the minor(s)' legal guardian/next of kin for the publication of any potentially identifiable images or data included in this article.

AUTHOR CONTRIBUTIONS

LoX, LF, ZZ, HR, and LiX were responsible for the literature search, study design, writing, and critical revision. ZW, XT, BN, TT, JQ, and YW mainly participated in data collection, data analysis, and data interpretation. All authors have read and approved the final manuscript.

FUNDING

This work was supported by the Clinical Study of Shanghai Municipal Health Commission (202040338) to LoX.

ACKNOWLEDGMENTS

We thank the resident doctors, chief residents, respiratory therapist and nurses at Shanghai Children's Medical Center, Shanghai Jiao Tong University, School of Medicine, for their caring the patient in PICU.

REFERENCES

1. Pediatric Acute Lung Injury Consensus Conference Group [PALICCG]. Pediatric acute respiratory distress syndrome: consensus recommendations from the Pediatric Acute Lung Injury Consensus Conference. *Pediatr Crit Care Med.* (2015) 16:428–39. doi: 10.1097/PCC.0000000000000350
2. Cheifetz IM. Pediatric ARDS. *Respir Care.* (2017) 62:718–31. doi: 10.4187/respcare.05591
3. Terragni PP, Rosboch G, Tealdi A, Corno E, Menaldo E, Davini O, et al. Tidal hyperinflation during low tidal volume ventilation in acute respiratory distress syndrome. *Am J Respir Crit Care Med.* (2007) 175:160–6. doi: 10.1164/rccm.200607-915OC
4. Vieillard-Baron A, Price LC, Matthay MA. Acute cor pulmonale in ARDS. *Intensive Care Med.* (2013) 39:1836–8. doi: 10.1007/s00134-013-3045-2
5. Frerichs I, Amato MB, van Kaam AH, Tingay DG, Zhao Z, Grychtol B, et al. Chest electrical impedance tomography examination, data analysis, terminology, clinical use and recommendations: consensus statement of the TRanslational EIT development study group. *Thorax.* (2017) 72:83–93. doi: 10.1136/thoraxjnl-2016-208357
6. Kobylianskii J, Murray A, Brace D, Goligher E, Fan E. Electrical impedance tomography in adult patients undergoing mechanical ventilation: a systematic review. *J Crit Care.* (2016) 35:33–50. doi: 10.1016/j.jcrc.2016.04.028
7. Maciejewski D, Putowski Z, Czok M, Krzych ŁJ. Electrical impedance tomography as a tool for monitoring mechanical ventilation. An introduction to the technique. *Adv Med Sci.* (2021) 66:388–95. doi: 10.1016/j.advms.2021.07.010
8. Bachmann MC, Morais C, Bugedo G, Bruhn A, Morales A, Borges JB, et al. Electrical impedance tomography in acute respiratory distress syndrome. *Crit Care.* (2018) 22:263. doi: 10.1186/s13054-018-2195-6
9. Hsu HJ, Chang HT, Zhao Z, Wang PH, Zhang JH, Chen YS, et al. Positive end-expiratory pressure titration with electrical impedance tomography and pressure-volume curve: a randomized trial in moderate to severe ARDS. *Physiol Meas.* (2021) 42:014002. doi: 10.1088/1361-6579/abd679
10. He H, Chi Y, Yang Y, Yuan S, Long Y, Zhao P, et al. Early individualized positive end-expiratory pressure guided by electrical impedance tomography in acute respiratory distress syndrome: a randomized controlled clinical trial. *Crit Care.* (2021) 25:230. doi: 10.1186/s13054-021-03645-y
11. Rosemeier I, Reiter K, Obermeier V, Wolf GK. Mechanical ventilation guided by electrical impedance tomography in children with acute lung injury. *Crit Care Explor.* (2019) 1:e0020. doi: 10.1097/CCE.0000000000000020
12. Costa EL, Borges JB, Melo A, Suarez-Sipmann F, Toufen C Jr., Bohm SH, et al. Bedside estimation of recruitable alveolar collapse and hyperdistension by electrical impedance tomography. *Intensive Care Med.* (2009) 35:1132–7. doi: 10.1007/s00134-009-1447-y
13. Suarez-Sipmann F, Böhm SH, Tusman G, Pesch T, Thamm O, Reissmann H, et al. Use of dynamic compliance for open lung positive end-expiratory pressure titration in an experimental study. *Crit Care Med.* (2007) 35:214–21. doi: 10.1097/01
14. Zhao Z, Möller K, Steinmann D, Frerichs I, Guttmann J. Evaluation of an electrical impedance tomography-based Global Inhomogeneity Index for pulmonary ventilation distribution. *Intensive Care Med.* (2009) 35:1900–6. doi: 10.1007/s00134-009-1589-y
15. Auer U, Schramel JP, Moens YP, Mosing M, Braun C. Monitoring perioperative changes in distribution of pulmonary ventilation by functional electrical impedance tomography. *Acta Anaesthesiol Scand.* (1998) 42:721–6. doi: 10.1111/j.1399-6576.1998.tb05308.x
16. Muders T, Luepschen H, Zinserling J, Greschus S, Fimmers R, Guenther U, et al. Tidal recruitment assessed by electrical impedance tomography and computed tomography in a porcine model of lung injury*. *Crit Care Med.* (2012) 40:903–11. doi: 10.1097/CCM.0b013e318236f452
17. Maisch S, Reissmann H, Fuellekrug B, Weismann D, Rutkowski T, Tusman G, et al. Compliance and dead space fraction indicate an optimal level of positive end-expiratory pressure after recruitment in anesthetized patients. *Anesth Analg.* (2008) 106:175–81. doi: 10.1213/01.ane.0000287684.74505.49
18. Gattinoni L, Caironi P, Cressoni M, Chiumello D, Ranieri VM, Quintel M, et al. Lung recruitment in patients with the acute respiratory distress syndrome. *N Engl J Med.* (2006) 354:1775–86. doi: 10.1056/NEJMoa052052
19. Beitler JR, Sarge T, Banner-Goodspeed VM, Gong MN, Cook D, Novack V, et al. Effect of Titrating Positive End-Expiratory Pressure (PEEP) with an esophageal pressure-guided strategy vs an empirical high PEEP-FiO_2 strategy on death and days free from mechanical ventilation among patients with acute respiratory distress syndrome: a randomized clinical trial. *JAMA.* (2019) 321:846–57. doi: 10.1001/jama.2019.0555
20. Meier T, Luepschen H, Karsten J, Leibecke T, Grossherr M, Gehring H, et al. Assessment of regional lung recruitment and derecruitment during a PEEP trial based on electrical impedance tomography. *Intensive Care Med.* (2008) 34:543–50. doi: 10.1007/s00134-007-0786-9
21. Lowhagen K, Lundin S, Stenqvist O. Regional intratidal gas distribution in acute lung injury and acute respiratory distress syndrome assessed by electric impedance tomography. *Minerva Anestesiol.* (2010) 76:1024–35.
22. Zhao Z, Chang MY, Chang MY, Gow CH, Zhang JH, Hsu YL, et al. Positive end-expiratory pressure titration with electrical impedance tomography and pressure-volume curve in severe acute respiratory distress syndrome. *Ann Intensive Care.* (2019) 9:7. doi: 10.1186/s13613-019-0484-0
23. Khemani RG, Smith LS, Zimmerman JJ, Erickson S, Pediatric Acute Lung Injury Consensus Conference Group. Pediatric acute respiratory distress syndrome: definition, incidence, and epidemiology: proceedings from the Pediatric Acute Lung Injury Consensus Conference. *Pediatr Crit Care Med.* (2015) 16:S23–40. doi: 10.1097/PCC.0000000000000432
24. Kneyber MC, Zhang H, Slutsky AS. Ventilator-induced lung injury. Similarity and differences between children and adults. *Am J Respir Crit Care Med.* (2014) 190:258–65. doi: 10.1164/rccm.201401-0168CP
25. Khemani RG, Newth CJ. The design of future pediatric mechanical ventilation trials for acute lung injury. *Am J Respir Crit Care Med.* (2010) 182:1465–74. doi: 10.1164/rccm.201004-0606CI
26. Ingaramo OA, Ngo T, Khemani RG, Newth CJ. Impact of positive end-expiratory pressure on cardiac index measured by ultrasound cardiac output monitor. *Pediatr Crit Care Med.* (2014) 15:15–20. doi: 10.1097/PCC.0b013e3182976251
27. Khemani RG, Parvathaneni K, Yehya N, Bhalla AK, Thomas NJ, Newth CJL. Positive end-expiratory pressure lower than the ARDS network protocol is associated with higher pediatric acute respiratory distress syndrome mortality. *Am J Respir Crit Care Med.* (2018) 198:77–89. doi: 10.1164/rccm.201707-1404OC
28. Stahl CA, Möller K, Schumann S, Kuhlen R, Sydow M, Putensen C, et al. Dynamic versus static respiratory mechanics in acute lung injury and acute respiratory distress syndrome. *Crit Care Med.* (2006) 34:2090–8.
29. Su PL, Lin WC, Ko YF, Su PF, Chen CW. Positive end-expiratory pressure selection based on best respiratory system compliance or collapse/hyperdistension curves in patients with acute respiratory distress syndrome: lack of correlation with alveolar recruitment. *Intensive Care Med.* (2018) 44:389–91. doi: 10.1007/s00134-017-5022-7
30. Bikker IG, Blankman P, Specht P, Bakker J, Gommers D. Global and regional parameters to visualize the 'best' PEEP during a PEEP trial in a porcine model with and without acute lung injury. *Minerva Anestesiol.* (2013) 79:983–92.
31. Puel F, Crognier L, Soulé C, Vardon-Bounes F, Ruiz S, Seguin T, et al. Assessment of electrical impedance tomography to set optimal positive end-expiratory pressure for veno-venous ECMO-treated severe ARDS patients. *J Crit Care.* (2020) 60:38–44. doi: 10.1016/j.jcrc.2020.06.017
32. Pelosi P, Rocco PRM, Gama de Abreu M. Close down the lungs and keep them resting to minimize ventilator-induced lung injury. *Crit Care.* (2018) 22:72. doi: 10.1186/s13054-018-1991-3
33. Gibot S, Conrad M, Courte G, Cravoisy A. Electrical impedance tomography for positive end-expiratory pressure titration in COVID-19-related acute respiratory distress syndrome. *Am J Respir Crit Care Med.* (2020) 202:280–4. doi: 10.1164/rccm.202003-0816LE
34. Franchineau G, Bréchot N, Lebreton G, Hekimian G, Nieszkowska A, Trouillet JL, et al. Bedside contribution of electrical impedance tomography to setting positive end-expiratory pressure for extracorporeal membrane oxygenation-treated patients with severe acute respiratory distress syndrome. *Am J Respir Crit Care Med.* (2017) 196:447–57. doi: 10.1164/rccm.201605-1055OC
35. Frerichs I, Dargaville PA, van Genderingen H, Morel DR, Rimensberger PC. Lung volume recruitment after surfactant administration modifies spatial

distribution of ventilation. *Am J Respir Crit Care Med.* (2006) 174:772–9. doi: 10.1164/rccm.200512-1942OC
36. Hochhausen N, Biener I, Rossaint R, Follmann A, Bleilevens C, Braunschweig T, et al. Optimizing PEEP by electrical impedance tomography in a porcine animal model of ARDS. *Respir Care.* (2017) 62:340–9. doi: 10.4187/respcare.05060
37. Bickenbach J, Czaplik M, Polier M, Marx G, Marx N, Dreher M. Electrical impedance tomography for predicting failure of spontaneous breathing trials in patients with prolonged weaning. *Crit Care.* (2017) 21:177. doi: 10.1186/s13054-017-1758-2
38. Karsten J, Stueber T, Voigt N, Teschner E, Heinze H. Influence of different electrode belt positions on electrical impedance tomography imaging of regional ventilation: a prospective observational study. *Crit Care.* (2016) 20:3. doi: 10.1186/s13054-015-1161-9
39. Brabant O, Crivellari B, Hosgood G, Raisis A, Waldmann AD, Auer U, et al. Effects of PEEP on the relationship between tidal volume and total impedance change measured *via* electrical impedance tomography (EIT). *J Clin Monit Comput.* (2021) 25:1–10. doi: 10.1007/s10877-021-00651-x
40. Bikker IG, Preis C, Egal M, Bakker J, Gommers D. Electrical impedance tomography measured at two thoracic levels can visualize the ventilation distribution changes at the bedside during a decremental positive end-expiratory lung pressure trial. *Crit Care.* (2011) 15:R193. doi: 10.1186/cc10354

Conflict of Interest: The authors declare that the research was conducted in the absence of any commercial or financial relationships that could be construed as a potential conflict of interest.

Publisher's Note: All claims expressed in this article are solely those of the authors and do not necessarily represent those of their affiliated organizations, or those of the publisher, the editors and the reviewers. Any product that may be evaluated in this article, or claim that may be made by its manufacturer, is not guaranteed or endorsed by the publisher.

Advantages of publishing in Frontiers

OPEN ACCESS
Articles are free to read for greatest visibility and readership

FAST PUBLICATION
Around 90 days from submission to decision

HIGH QUALITY PEER-REVIEW
Rigorous, collaborative, and constructive peer-review

TRANSPARENT PEER-REVIEW
Editors and reviewers acknowledged by name on published articles

Frontiers
Avenue du Tribunal-Fédéral 34
1005 Lausanne | Switzerland

Visit us: www.frontiersin.org
Contact us: frontiersin.org/about/contact

REPRODUCIBILITY OF RESEARCH
Support open data and methods to enhance research reproducibility

DIGITAL PUBLISHING
Articles designed for optimal readership across devices

FOLLOW US
@frontiersin

IMPACT METRICS
Advanced article metrics track visibility across digital media

EXTENSIVE PROMOTION
Marketing and promotion of impactful research

LOOP RESEARCH NETWORK
Our network increases your article's readership